Abstract

BRANNEN, CANDICE LEIGH. Donor-Acceptor Contributions to Ferromagnetic Exchange Coupling within Heterospin Biradicals. (Under the direction of David A. Shultz.)

The evaluation of new Donor-Acceptor heterospin biradicals is carried out within this thesis: SQ-Gal, SQ-Ph-Gal, SQ-E-NN, and SQ-TNN. A molecular orbital and spin density analysis is performed in order to predict the exchange coupling within these biradicals. A Valence Bond Configuration Interaction model is used to describe exchange coupling in a Donor-Acceptor-type Semiquinone-NitronylNitroxide (SQNN) biradical ligand. Within this framework, a SQ $\rightarrow$ NN charge transfer state is responsible for the experimentally determined ferromagnetic coupling in the ground state, and the intraligand exchange parameter is correlated with the single-site Coulomb repulsion integral (U), the singlet-triplet gap (2K) of the CT excited state, and the electronic coupling matrix element, H_{ab}. This charge transfer transition is observed spectroscopically, and probed using resonance Raman spectroscopy. Importantly, if the crystal structure of the Donor-Acceptor biradical is known, this H_{ab} can be directly linked to the molecular conformation determined by X-ray crystallography. We suggest how our methods could be extended to any bridge fragment for SQ-Bride-NN complexes. This model is useful for designing new strongly exchange coupled systems, for using electronic structure theory to study exchange in organic systems, and for correlating exchange coupling parameters with elements of electron transfer theory.

Donor-Acceptor Contributions to Ferromagnetic Exchange Coupling within Heterospin Biradicals

By

Candice Leigh Brannen

A dissertation submitted to the graduate faculty of North Carolina State University in partial fulfillment of the requirements for the degree of Doctor of Philosophy

Chemistry

Raleigh, North Carolina
2006

Approved by:

David A. Shultz
Chair of the Advisory Committee

T. Brent Gunnoe

Paul Maggard

Tatyana Smirnova

Marian McCord

Biography

Candice Leigh Brannen was born to Lehman and Jenniee Brannen in Savannah, GA. Where she lived and attended public schools until 1995. She began college at The University of Georgia. She completed her B.S. in Chemistry in 1999. 2 years later in 2001 she began graduate school at North Carolina State University where she earned her Ph. D. in Chemistry in September of 2006.

Acknowledgements

This journey would not have ever happened if it were not for the love and guidance of my two wonderful parents Lehman and Jenniee. My mother had the tough job of continuing my education everyday when I arrived home from school. She taught me that no one could determine my future but me. That my education was in my hands, I could make of it whatever I put into it. My dad played the role of life coach. He taught me humility, perserverance, and my work ethic. Not only did I have wonderful parents, but wonderful grandparents. “Weeble Woble” taught me how to work hard for what it was that I desired. My grandfather taught me about unconditional love.

While in school I have met a lot of wonderful people who not only were my friends but inspiration. First and foremost, Jessica and Joe Bousquet were my first friends I met at NCSU. We had great times together, but also were wonderful study buddies. Jeremy and Mike helped through Inorganic. Marty Lail was a kindred spirit. We always seemed to be in the same boat. Tashni joined our group late, but we made fast friends. If it were not for her I am sure I would not have been able to make it through this with my sanity. Our constant lab banter kept some humor in the whole situation. I also needed her encouragement. Chuck, it was a brief time together, but you are a funny character and I am glad we became friends. Nick I am glad that you visited our group, I am honored to have made you one of my friends. And finally Rob, we only just met, but it seems like we have been friends for a lifetime. I have and will continue to enjoy our friendship.

And last, but certainly not least, Ryan Fuierer, my best friend and one of the most wonderful people I have ever met. I could not have made it through it without you on my side. Thanks and I cannot wait to begin our life together. I love you!

Table of Contents

Page

List of Figures

Page

List of Tables

Page

List of Schemes

Page

Chapter 1

The importance of Exchange Coupling in Biradicals.

I. Introduction – Why Study Exchange Coupling in Biradicals?

The history of magnets and magnetism is undeniably long and impressive. People of the ancient Greek province of Magnesia in Thessaly discovered a lodestone, a naturally magnetic variety of magnetite (Fe_3O_4), 3500 years ago.[1,2] Through experiments the Chinese found that a lodestone would always point in a north-south direction if it was allowed to rotate freely, thus the birth of the compass.

Magnetism has played a crucial role in the discovery of the New World as well as in the development of science and technology. Columbus' explorations and discoveries would not have been possible without the compass. The magnetic properties of iron allowed electricity to be generated inexpensively since 1886. Since then magnetism has found applications in other industries: communications, information storage, transportation, and home appliances, to name only a few. Until recently, magnets were limited to metallurgically processed inorganic materials with little thought given to organic materials.[1,3]

The use of molecules instead of atoms expands the field of magnetism and is expected to enable (a) the control of magnetic properties through organic-synthesis, (b) the improvement of commercially useful magnetic properties, and (c) the combination of magnetic properties with other physical properties such as mechanical, electrical, and/or optical.[3,4] Magnetism however, is a bulk property of a material.[4] To understand and control the bulk magnetic properties of an organic material, the simplest systems must be synthesized and studied.

It is the interaction of the magnetic moments of the unpaired electrons that gives rise to magnetic properties that can be studied and manipulated. This interaction is called exchange coupling.[5] As such, organic biradicals are the simplest molecular systems to use in order to understand from where bulk magnetic properties arise. Organic biradicals contain two unpaired electrons. It is the focus of this work to study exchange coupling in organic biradical ligands in an effort to (1) further the understanding of the properties that govern exchange coupling, (2) relate exchange coupling to electron transfer and (3) allow the rational design of new molecular spintronic materials.

I.A. Magnetic Behavior- An Overview

Unpaired electrons are the building block of magnetism; more specifically their magnetic moment, and their relative alignment in bulk materials gives rise to different magnetic behaviors.[4] One of these electrons may not exhibit a large magnetic moment, but alignment of many in a bulk material can result in a large magnetic moment.

The result of electron-electron interactions gives rise to five main types of magnetism to be discussed (Figure I.2).[6] Electrons can be either paired or unpaired. Electrons can also be aligned either parallel, spin-up spin-up ($\alpha\alpha$), spin-down spin-down ($\beta\beta$), or antiparallel, spin-up spin-down ($\alpha\beta$) with respect to each other. Pairing of electrons results in the most common type of magnetism: diamagnetism. It is the result of core electrons aligned antiparallel, and valence electrons that pair in a bonding or non-bonding fashion. Diamagnetic materials are repelled by a magnetic field.

Paramagnetism is the phenomenon that results from randomly oriented, unpaired electrons that continuously reorient themselves in the absence of a magnetic field. The consequence of continuous reorientation is no net magnetic moment due to the

cancellation of magnetic moments. From paramagnetic materials come three other important magnetic behaviors: antiferromagnetism, ferromagnetism and ferrimagnetism.

Antiferromagnetic materials are made up of unpaired electrons interacting in an antiparallel fashion in bulk (3-D) materials. As a consequence of electrons aligning antiparallel throughout the material, no net magnetic moment exists.

Ferromagnetism is the opposite of antiferromagnetism. Unpaired electrons align parallel throughout the 3d bulk material resulting in a magnetic moment in the absence of an applied magnetic field. With an applied magnetic field, the "domains" of the material all align parallel with one another until the magnetization "saturates". Upon removal of the applied magnetic field the individual moments remain parallel. The remaining magnetic moment can also exhibit hysteresis.

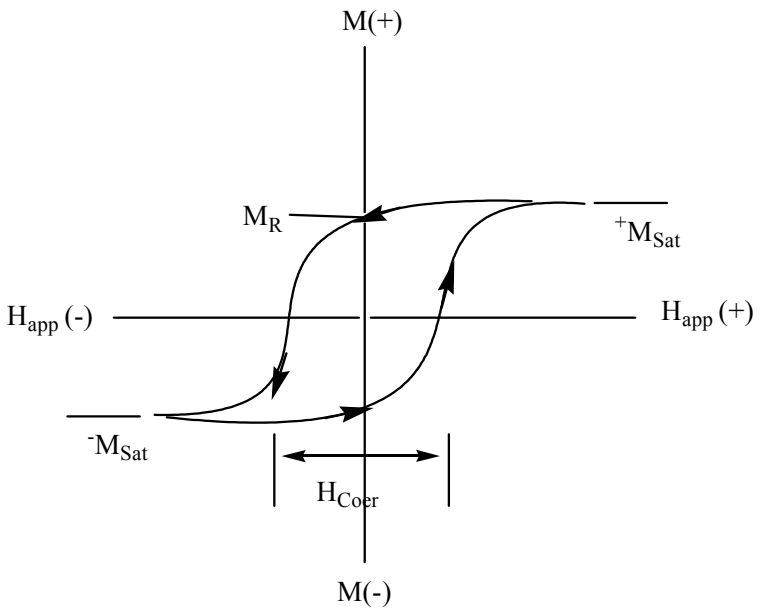

Figure I.1 Example hysteresis plot.

One of the most distinctive features of materials with bulk magnetism is hysteresis. Hysteresis is observed for ferromagnetic and ferrimagnetic materials below their critical point and arises from rearrangement of domain walls within the material. The hysteresis of a sample is determined by looking at magnetization as a function of an applied magnetic field. A typical hysteresis curve for a bulk magnetic material is shown in Figure I.1.

The hysteresis of a material is typically defined by two distinctive points; the remnant magnetization (M_R) and the coercive field (H_c). Remnant magnetization is obtained by applying and removing a large magnetic field and represents the extent to which a bulk magnetic material exhibits spontaneous magnetism. The coercive field of a sample is the magnetic field required to bring the magnetization of a sample to zero. Coercive fields from 0.01 G to 15,000 G have been observed for different materials. In general materials with low coercive fields (< 1 G) have been termed “soft” magnets, while materials with high coercive field (>500 G) have been termed “hard” magnets.

Ferrimagnetism is present when there are two different spin carrying species with unequal spin values ($S_1 \neq S_2$) that have antiparallel alignment. Because these spin values are unequal, a net magnetic moment results within a bulk material.

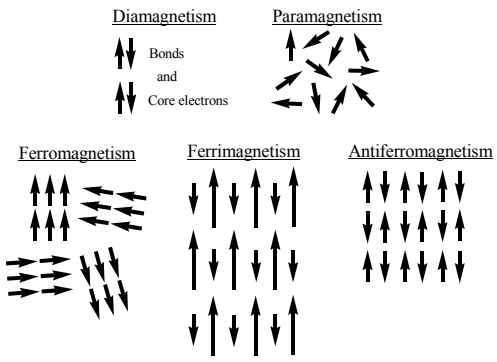

Figure I.2. Five main types of magnetic behavior.

Magnetism is typically measured by a materials' response to a magnetic field (either repulsive or attractive). This response is termed the magnetization (M) of the material. The magnetization (M) is proportional to an applied magnetic field by a constant known as magnetic susceptibility (χ_{exp}).

$$M = \chi_{exp} H \tag{1.1}$$

The magnetic susceptibility is comprised of several components: a diamagnetic contribution, a paramagnetic component, and for metals a Pauli susceptibility.[6]

$$\chi_{exp} = \chi_{dia} + \chi_{para} + \chi_{Pauli} \tag{1.2}$$

In a paramagnetic material, χ_{para} is inversely proportional to temperature according to the Curie Law, where (C) is the Curie constant and (T) is the temperature:[6]

$$\chi_{para} = \frac{C}{T} \tag{1.3}$$

However, most paramagnetic species do not follow the Curie Law; most follow a modified behavior, known as Curie-Weiss behavior where θ is the Weiss constant and has units of temperature.[6]

$$\chi_{para} = \frac{C}{T - \theta} \tag{1.4}$$

The Curie constant has been related to several other important parameters:[7]

$$\theta = \frac{zJS(S+1)}{3k_B} \tag{1.5}$$

In Equation 1.5, *z* is the number of nearest neighbors, ***J*** is proportional to the energy gap between the ground spin-state and the lowest excited spin-state, *S* is the spin quantum number, S(S+1) is the multiplicity, and k_B is Boltzmann's constant. Deviation from the Curie Law can be caused by several factors that include spin-orbit coupling, zero-field splitting, and intermolecular interactions. When θ is zero, the Curie Law is obeyed; if θ > 0, ferromagnetic interactions are possible; if θ < 0, antiferromagnetic interactions are suggested. Below are cartoons of χ vs. T plots for each material.

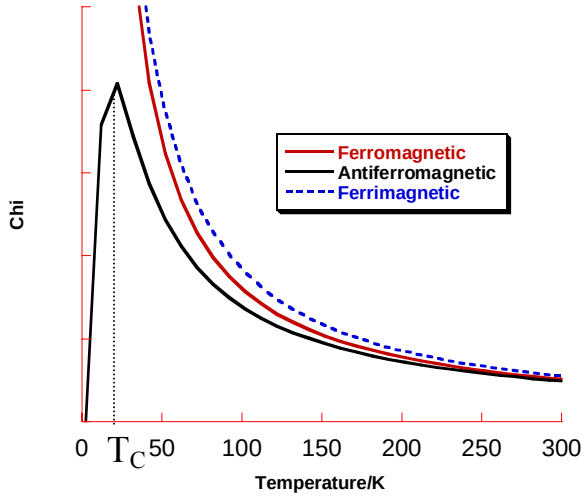

Figure I.3. χ_{Para} vs. T for (a) ferromagnetic, (b) antiferromagnetic, and (c) ferromagnetic materials, with magnetic moment alignments indicated for each case.

I.B.1. Molecular Analogs to Bulk Magnetic Properties

In the Shultz group we study molecular analogs of bulk magnetic materials. Biradical molecules, molecules with two unpaired electrons, are the molecular analogs of bulk magnets.

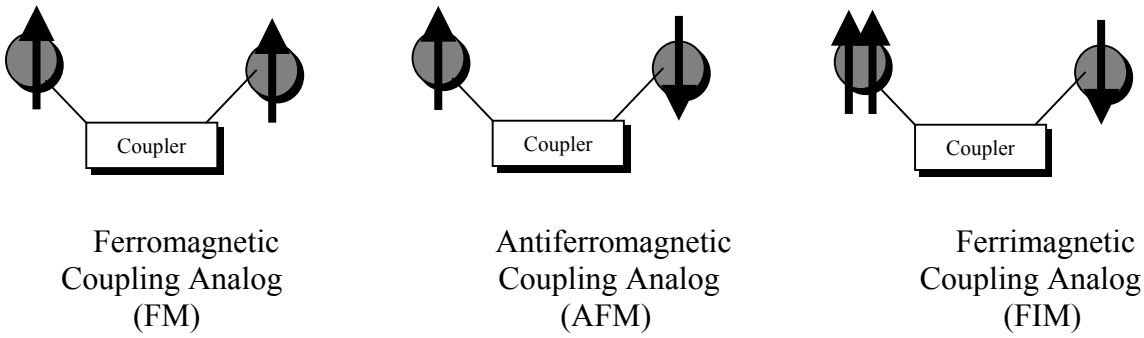

Figure I.4. Shultz Group molecular analogs.

It is the interaction of the unpaired electrons as a function of molecular structure that is important in our research. The interactions of these electrons can either be ferromagnetic or antiferromagnetic in nature, as defined above for bulk materials but in an intramolecular sense. The strength of these interactions can be measured using magnetometry. The interaction between unpaired electrons is known as the exchange parameter, J. When two unpaired electrons interact, the total exchange coupling (J_{TOT}) consists of two components, a ferromagnetic component (J_F) and an antiferromagnetic component (J_{AF}).

$$J_{TOT} = J_F + J_{AF} \tag{1.6}$$

By convention, $J_F > 0$ and $J_{AF} < 0$. If $|J_{AF}| > |J_F|, J_{TOT} < 0$ then the electrons are said to couple antiferromagnetically. If $|J_F| > |J_{AF}|, J_{TOT} > 0$ then the electrons are said to couple ferromagnetically. It can be seen that depending on which component of Equation 1.6 is dominant, the total exchange coupling is either ferromagnetic or antiferromagnetic. Thus, ferromagnetism is a bulk property of a material and the exchange coupling parameter is a molecular property. Understanding and controlling these exchange interactions within molecules is the focus of the work in the Shultz group.[8]

I.B.2. Shultz group research efforts.

A deeper understanding of exchange coupling and structure-property relationships is and has been one of the main focuses within the Shultz group. In order to make the progression toward the synthesis and design of molecules for new magnetic materials, understanding the basic interactions on a simplified model must first be accomplished. Biradicals are the simplest, multi-spin systems, and there is a great deal of information that can be learned by probing the interaction between the two unpaired electrons. One area of research within the Shultz group is to show a structure-property relationship within a series of biradicals, both bis(semiquinone)s and bis(nitroxide)s. It has been known for some time that delocalization and planarity have a significant effect on the strength and sign of exchange coupling within a high-spin molecule. [4,9-18] Seen below are a series of trimethylene methane (TMM)-linked bis(semiquinone)s and bis(nitroxide)s used to show the relationship between conformation and exchange coupling.[10,19-21]

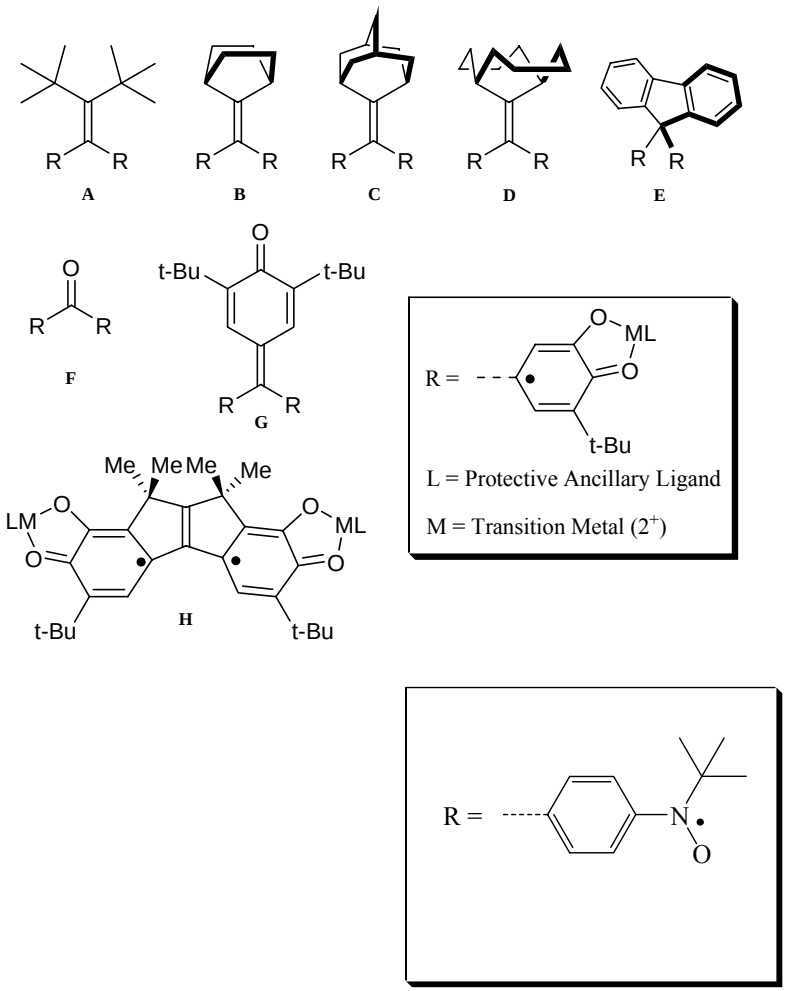

Figure I.5. Series of TMM-linked bis (semiquinones) and bis(nitroxide)s.

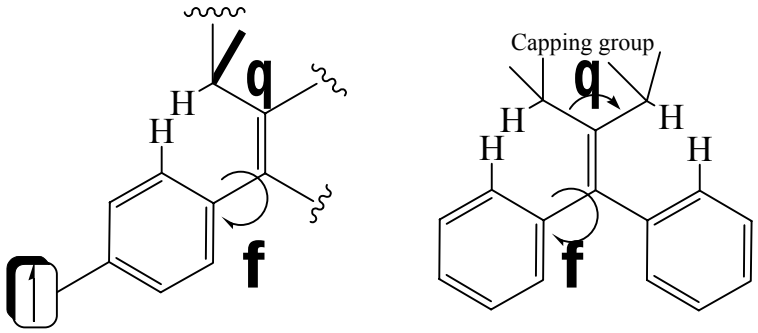

Figure I.6. Structure shows how the size of the bicyclic "cap" can vary the angle θ and thus the steric interaction between the two hydrogen atoms. That steric interaction will then affect the amount of twisting angle φ and thus affect the strength of exchange coupling within the biradical.

The theory, which is supported by experiment, is that the more the rings are twisted out of planarity in relation to the TMM coupling unit, the more the exchange coupling will be attenuated. Dr. Rosario Fico and Dr. Scot Bodnar have contributed most of the research on the bis(nitroxide) series and the bis(semiquinone) series.

Table I.1 Phenyl and Nitroxide torsion angles and ***J*** value for TMM bis(nitroxides).[20]

	Phenyl torsion	Nitroxide torsion	J value
$D(PhNit)_2$	65.92 ± 0.05 82.37 ± 0.05	40.68 ± 0.1 23.14 ± 0.1	-14.03 ± 0.12 -11.8 ± 1.2
$B(PhNit)_2$	54.3 ± 0.1 55.5 ± 0.1	9.8 ± 0.2 11.1 ± 0.2	-5.75 ± 0.31
$C(PhNit)_2$	54.73 ± 0.08 53.47 ± 0.08	11.23 ± 0.07 9.9 ± 0.1	hysteresis -5.11 ± 0.24
$B(PhNit)_2$	43.19 ± 0.11 50.84 ± 0.11	31.4 ± 0.2 31.3 ± 0.2	+6.79 ± 0.18 +6.07 ± 0.15
$A(PhNit)_2$			+5.24
$H(PhNit)_2$	1.9 ± 0.3 1.8 ± 0.3	30.1 ± 0.2 28.4 ± 0.2	+25.5 ± 1.6 +26.35 ± 1.73
$E(PhNit)_2$	39.2 ± 0.5 41.0 ± 0.5	13.5 ± 0.4 24.3 ± 0.5	-2.61 ± 0.01 -2.85 ± 0.13

Table I.2 Semiquinone ring torsion angles and ***J*** values for TMM bis(semiquinone).[19]

	Semiquinone ring torsion	J value
$D(SQ)_2$	64.10 ± 0.13 78.04 ± 0.13	-30.3 ±0.8
$C(SQ)_2$	47.51 ± 0.18 48.94 ± 0.27	+24.4 ±0.6
$B(SQ)_2$	48.37±0.29	+87.0 ±3.0
$G(SQ)_2$	50.3 ± 0.3 42.6 ± 0.8	+209.4 ±1.4
$H(SQ)_2$	4.9 ± 0.8, 9.7 ± 0.8 7.3	+163.6 ±1.6
$E(SQ)_2$	42.3 ± 0.9 52.4 ± 0.1	+0.99 ±0.06

Another area of research within the Shultz group is the use of substituents to modulate the exchange coupling in biradicals. The first example of electronic modulation of exchange coupling within an isostructural series of meta-phenylene (MPH) coupled bis(semiquinone)s with triplet ground states has recently been accomplished.[22] Substituents could affect the singlet-triplet energy gap, $\mathbf{D}E_{ST}$ in a triplet ground-state biradical in several ways. They could alter the singlet selectively, alter the triplet selectively, or alter both states simultaneously. The substituents also could easily affect higher lying closed-shell excited states, which in turn could have influences on the lower lying open-shell states. Using a meta-phenylene coupling unit, ***J***-modulation is achieved by varying the substituent in a series of groundstate triplet bis(semiquinone) complexes. Both strong electron pair donors (NMe_2) and strong electron pair withdrawers (NO2)

have been shown to attenuate exchange coupling by approximately 50% relative to a neutral t-Bu substituent. Using Hückel calculations, the attenuation can be attributed to spin-density dilution and orbital interactions that lead to the more disjoint nature of the SOMOs associated with the substituted species.

Table I.3 Exchange coupling values for substituted bis(semiquinone). [22]

	J value
4-NMe_2	+ 34.9 ± 0.7
4-t-Bu	+ 59.3 ± 1.2
4-NO_2	+ 31.0 ± 0.6

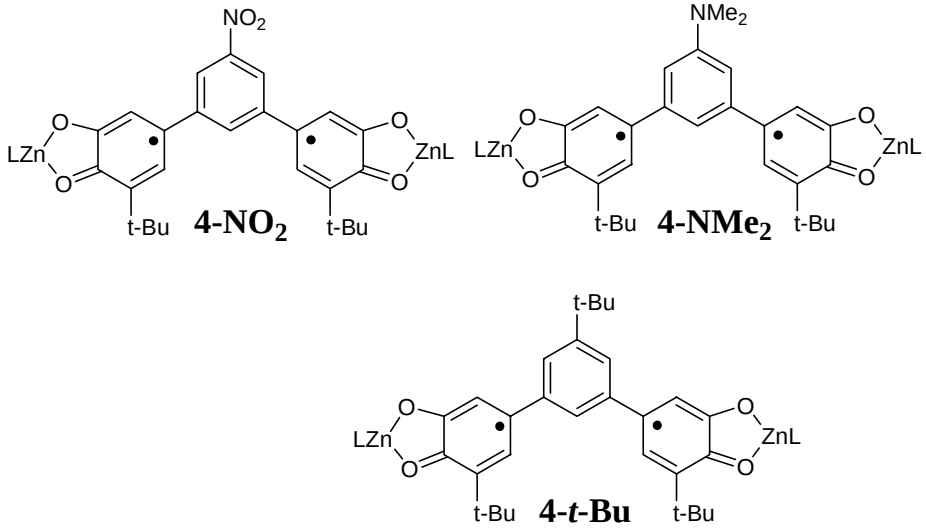

Figure I.7. meta-phenylene-type coupled bis(semiquinone)s. Note the meta substitution pattern relative to the spin-containing groups (semiquinones). Typical electron donor (NMe2), electron withdrawer (NO2), and mild donor (t-Bu).[22]

A third area of research in the Shultz group has been to develop new design principles based on mixed valency, a three-spin system featuring an inherently weak

antiferromagnetic coupler is used to do so.[23] The effects of mixed valency might be modest and difficult to observe in a strongly coupled system. Furthermore, ferromagnetic exchange coupling was desired. The first example of enhanced ferromagnetic coupling in a mixed-valent molecule that lacks an effective ***p***-type ferromagnetic coupler ([Na+][$(LZn)_3(SQ_2Cat)$]-), formed from one-electron reduction of an antiferromagnetically coupled triradical, $(LZn)_3(SQ_3)$ has been realized. It has been shown that delocalization enhances ferromagnetic coupling in a molecule that lacks an intrinsic ferromagnetic Coupler.

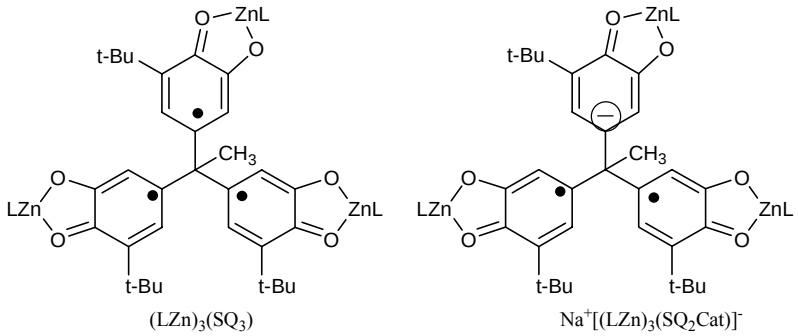

Figure I.8. Tri-radical $(LZn)_3(SQ_3)$, where J<0, and mixed valent biradical $Na^+[(LZn)_3(SQ_3Cat)]^-$, where $J \geq 0$.[23]

We have contributed an extensive amount to homospin biradical chemistry. The work in this thesis builds on this foundation. We propose that there is a third group of biradicals, we call these the heterospin Donor-Acceptor biradicals. These biradicals are an extension of our work on the $Tp^{Cum,Me}$MSQNN series of biradicals. We propose to study a group of heterospin biradicals each containing the semiquinone ligand. The second radical group in these molecules will be nitronyl nitroxide and galvinoxyl. Within the SQNN we attempt to place a bridge unit in between the SQ and NN fragments in

order to determine its effects on the exchange coupling and electronic coupling. Future work in this area will include the study of the effects of torsion of the bridge on the electronic and exchange coupling.

I.C. References

(1) Chen, C.-W. *Magnetism and Metallurgy of Soft Magnetic Materials*; Dover Publications, Inc.: Mineola, NY, 1986.

(2) Gilbert, W.; Dover Publications Inc., 1958.

(3) Turnbull, M. M., Sugimoto, Toyonari, and Thompson, Laurence K. *Molecule-Based Magnetic Materials: Theory, Techniques, and Applications*; American Chemical Society: Washinton D.C., 1996.

(4) Lahti, P. M. *Magnetic Properties of Organic Materials*; Marcel Dekker, Inc.: New York, 1999.

(5) Borden, W. T. *Diradicals*; John Wiley & Sons: New York, 1982.

(6) Hurd, C. M. *Contemp. Phys.* 1982, *23*, 469-493.

(7) Atkins, P. *Physical Chemistry*; 5th ed. ed.; W. H. Freeman and Company: New York, 1994.

(8) Rajca, A. *Chem. Rev.* 1994, *94*, 871-893.

(9) Silverman, S. K.; Dougherty, D. A. *J. Phys. Chem.* 1993, *97*, 13273-13283.

(10) Shultz, D. A.; Boal, A. K.; Lee, H.; Farmer, G. T. *J. Org. Chem.* 1999, *64*, 4386-4396.

(11) Shultz, D. A.; Boal, A. K.; Farmer, G. T. *J. Am. Chem. Soc.* 1997, *119*, 3846-3847.

(12) Okada, K.; Matsumoto, K.; Oda, M.; Murai, H.; Akiyama, K.; Ikegami, Y. *Tetrahedron Lett.* 1995, *36*, 6693-6694.

(13) Okada, K.; Imakura, T.; Oda, M.; Murai, H.; Baumgarten, M. *J. Am. Chem. Soc.* 1996, *118*, 3047-3048.

(14) Nakazono, S.; Karasawa, S.; Iwamura, H. *Angew. Chem. Int. Ed. Engl.* 1998, *37*, 1550.

(15) Matsuda, K.; Iwamura, H. *Chem. Commun.* 1996, 1131-1132.

(16) Kanno, F.; Inoue, K.; Koga, N.; Iwamura, H. *J. Am. Chem. Soc.* 1993, *115*, 847-850.

(17) Fang, S.; Lee, M.-S.; Hrovat, D. A.; Borden, W. T. *J. Am. Chem Soc.* 1995, *117*, 6727-6731.

(18) Adam, W.; van Barneveld, C.; Bottle, S. E.; Engert, H.; Hanson, G. R.; Harrer, H. M.; Heim, C.; Nau, W. M.; Wang, D. *J. Am. Chem. Soc.* 1996, *118*, 3974-3975.

(19) Shultz, D. A.; Fico, R. M., Jr.; Bodnar, S. H.; Kumar, R. K.; Vostrikova, K. E.; Kampf, J. W.; Boyle, P. D. *J. Am. Chem. Soc.* 2003, *125*, 11761-11771.

(20) Shultz, D. A., Fico,Rosario M., Lee,Hyoyoung, Kampf,Jeff W., Kirschbaum,Jeff W., Pinkerton, A. Alan, and Boyle, Paul D. *J. Am. Chem. Soc.* 2003, *125*, 15426-15432.

(21) Shultz, D. A.; Lee, H.; Fico, R. M., Jr. *Tetrahedron* 1999, *55*, 12079-12086.

(22) Andrea Caneschi, A. D., Hyoyoung Lee, David A. Shultz, and Lorenzo Sorace *Inorg. Chem* 2001, *40*, 408-411.

(23) Shultz, D. A.; Kumar, R. K. *J. Am. Chem. Soc.* 2001, *123*, 6431-6432.

Chapter 2

Exchange Coupling of Unpaired Electrons.

II. The Basis of Molecular Magnetism: Exchange Coupling of Unpaired Electrons.

The Shultz group, studies biradicals, molecules with two unpaired electrons, because they are the simplest of multi-spin molecular analogs of magnetic materials. Our research efforts are focused on showing structure-property relationships of exchange coupling within biradicals. Most of the biradicals studied to date display ferromagnetic coupling and have high-spin (S=1) ground states. These biradicals can be thought of as molecular analogs of ferromagnets. In chapter 1 examples of ferromagnetic coupling was evident in the MPH bis-SQ (t-butyl, nitro and dimethyl amine),[1] the TMM bis-nitroxides (dimethyl, "flat"),[2] and TMM bis-SQ (bicyclo[4.4.1] undecane).[3] Some of the biradicals studied display antiferromagnetic coupling and are lowspin (S=0), usually a result of conformation.[4] In chapter 1 examples of antiferromagnetic coupling was evident in the di-t-butyl TMM bis-nitroxide.[2] These biradicals can be thought of as molecular analogs of antiferromagnets. Finally, the heterospin systems studied, to be talked about later, within the group can be thought of as molecular analogs of ferrimagnets.[5,6]

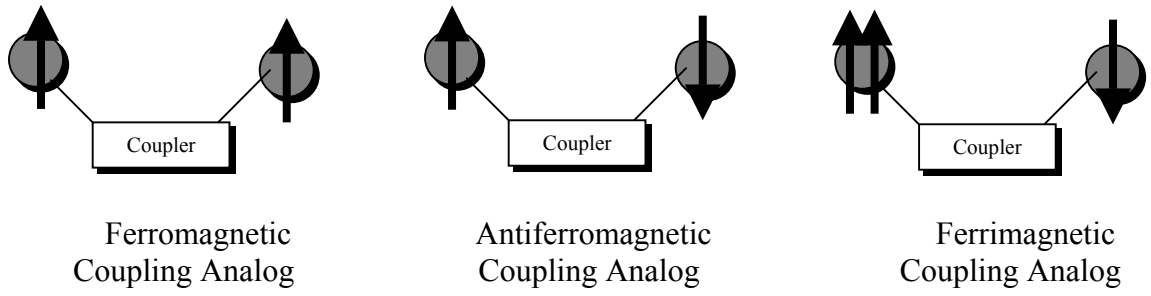

Figure II.1. Shultz Group molecular analogs of magnetic materials.

Controlling the exchange interactions within the biradical molecular analogs is the focus of the work in the Shultz group.[7] It is important to study exchange coupling for three reasons: (a) as seen in the previous section exchange coupling is the molecular

equivalent of ferromagnetism in the solid state, (b) it can be correlated with electron transfer, and (c) to further develop the fundamentals for the development of new molecular materials for molecular spintronics.

II.A. Quantum mechanical Approach: demonstrating preference of the sign of the exchange coupling.

Using a two-orbital/two-electron model with orthogonal magnetic orbitals,[7] we can demonstrate how preferences for ferromagnetic (triplet) or antiferromagnetic (singlet) states arise. The total wavefunction must be antisymmetric with respect to exchange of electron labels because electrons are by nature indistinguishable. Therefore, the wavefunction must not distinguish between the electrons. If two electrons (1 and 2) in two MOs (a and b) are considered, the spatial wavefunctions can be constructed. If we chose the wavefunction $\phi_A(1)\phi_B(2)$ this would be incorrect because switching the electron labels renders the electrons distinguishable, i.e. $[\phi_A(1)\phi_B(2)]^2 \neq [\phi_A(2)\phi_B(1)]^2$. Therefore, normalized linear combinations of the wavefunctions above are constructed:

$$\Psi_S = 0.707[\phi_A(1)\phi_B(2) + \phi_B(1)\phi_A(2)] \quad (2.1)$$

$$\Psi_A = 0.707[\phi_A(1)\phi_B(2) - \phi_B(1)\phi_A(2)] \quad (2.2)$$

The wavefunction in (2.1) is symmetric with respect to exchange because if the electrons are exchanged, wavefunction (2.1) results. The wavefunction in (2.2) is antisymmetric with respect to exchange of electrons because if the labels are exchanged, the negative of wavefunction (2.2) results. The other half of the total electronic wavefunction is comprised of the spin function. For two electrons in two spin orbitals there exists four possible combinations:

$$\chi_{\uparrow\uparrow} = \alpha(1)\alpha(2) \quad (2.3)$$

$$\chi_{\downarrow\downarrow} = \beta(1)\beta(2) \quad (2.4)$$

$$\chi_{\uparrow\downarrow} = \alpha(1)\beta(2) \quad (2.5)$$

$$\chi_{\downarrow\uparrow} = \beta(1)\alpha(2). \quad (2.6)$$

The first two are symmetric with respect to exchange, but the latter two are unacceptable because they allow for distinction between the two spin labels. Again, linear combinations must be taken. The resulting four spin functions and their symmetries with respect to exchange of electron labels are:

$$\chi_S = \alpha(1)\alpha(2) \quad (2.7)$$

$$\chi_S = \beta(1)\beta(2) \quad (2.8)$$

$$\chi_S = 0.707[\alpha(1)\beta(2) + \beta(1)\alpha(2)] \quad (2.9)$$

$$\chi_A = 0.707[\alpha(1)\beta(2) - \beta(1)\alpha(2)] \quad (2.10)$$

The first three are the triplet sublevels and the last is the singlet sublevel.

The total electronic wavefunction must be antisymmetric with respect to electron label exchange to satisfy the requirement of indistinguishability. This means that the symmetric orbital wavefunction must be combined with the antisymmetric spin function, and the antisymmetric orbital wavefunction must be combined with the symmetric spin functions. The product of the two functions (orbital × spin) gives the state wavefunction. The products are:

$$[\Psi_S = .5[[\phi_A(1)\phi_B(2) + \phi_B(1)\phi_A(2)] \times [\alpha(1)\beta(2) - \beta(1)\alpha(2)]] \quad (2.11)$$

$$[\Psi_A = .5[\phi_A(1)\phi_B(2) - \phi_B(1)\phi_A(2)]] \times [\alpha(1)\alpha(2)] \text{ and}$$

$$\times [\beta(1)\beta(2)] \text{ and}$$

$$\times [0.707[\alpha(1)\beta(2) + \beta(1)\alpha(2)] \quad (2.12)$$

The first wavefunction (2.11) describes the singlet state; whereas, the second set of equations, (2.12), describes the three microstates of the triplet.

If the two-electron two-orbital picture is considered, the preferences for ferromagnetic or antiferromagnetic states can be realized. The configurations discussed above and two closed-shell configurations of the electrons are shown below.

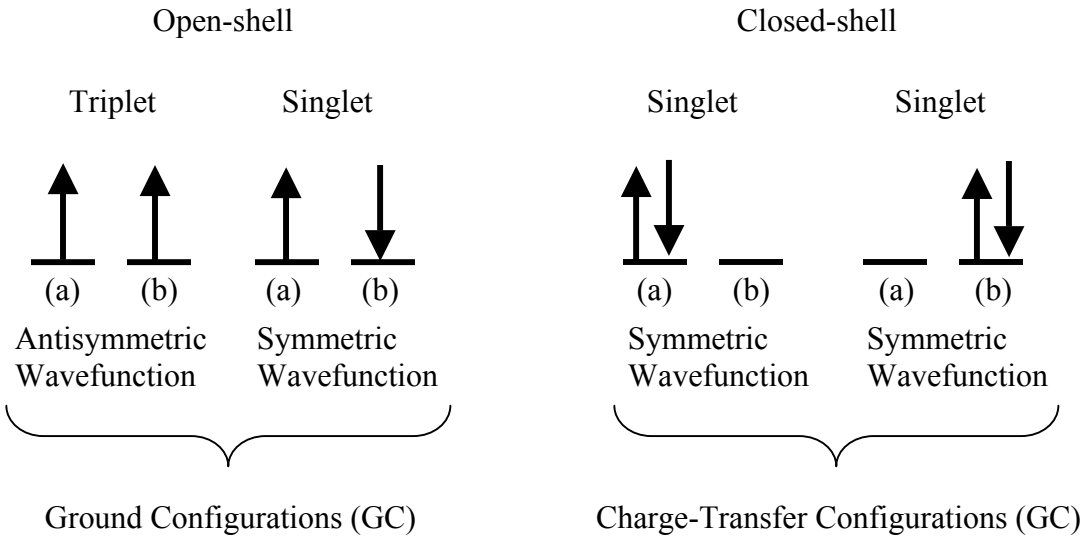

Figure II.2. Open shell (left) and closed shell (right) configurations of a two electron, two orbital system.

To determine the energies of the singlet and triplet in the absence of a magnetic field, the Hamiltonian is used. It is a simple electrostatic energy operator; therefore, only spatial portions of wavefunctions determine the energies of states. The spatial wavefunctions of the open-shell (os) triplet (T) and singlet (S) as well as the two closed-shell (cs) singlets are:

$$\varphi_{S,\,OS} = 0.707[\phi_A(1)\phi_B(2) + \phi_B(1)\phi_A(2)] \quad (2.13)$$

$$\varphi_{T,\,OS} = 0.707[\phi_A(1)\phi_B(2) - \phi_B(1)\phi_A(2)] \quad (2.14)$$

$$\varphi_{S+,\,CS} = 0.707[\phi_A(1)\phi_A(2) + \phi_B(1)\phi_B(2)] \quad (2.15)$$

$$\varphi_{S\text{-, CS}} = 0.707[\phi_A(1)\phi_A(2) - \phi_B(1)\phi_B(2)] \quad (2.16)$$

The zero-order Hamiltonian, Equation 2.17, excludes electron-electron repulsion, and is used to calculate the state energies.

$$H^0 = h(1) + h(2) \quad (2.17)$$

Energy of the triplet is:

$$E_{\text{triplet, OS}} = .5\langle\ \phi_A(1)\phi_B(2) - \phi_B(1)\phi_A(2)\ |h(1)+h(2)|\ \phi_A(1)\phi_B(2) - \phi_B(1)\phi_A(2)\ \rangle$$

$$= .5[\langle\ \phi_A(1)\phi_B(2)\ |\ h(1)+h(2)|\ \phi_A(1)\phi_B(2)\ \rangle\ -$$

$$\langle\ \phi_A(1)\phi_B(2)\ |\ h(1)+h(2)|\ \phi_B(1)\phi_A(2)\ \rangle\ -$$

$$\langle\ \phi_B(1)\phi_A(2)\ |\ h(1)+h(2)|\ \phi_A(1)\phi_B(2)\ \rangle\ +$$

$$\langle\ \phi_B(1)\phi_A(2)\ |\ h(1)+h(2)|\ \phi_B(1)\phi_A(2)\ \rangle\ ]$$

$$= .5[\langle\ \phi_B(2)|\phi_B(2)\ \rangle\ \langle\ \phi_A(1)|h(1)|\phi_A(1)\ \rangle\ +$$

$$\langle\ \phi_A(1)|\phi_A(1)\ \rangle\ \langle\ \phi_B(2)|h(2)|\phi_B(2)\ \rangle\ -$$

$$\langle\ \phi_B(2)|\phi_A(2)\ \rangle\ \langle\ \phi_A(1)|h(1)|\phi_B(1)\ \rangle\ -$$

$$\langle\ \phi_A(1)|\phi_B(1)\ \rangle\ \langle\ \phi_B(2)|h(2)|\phi_A(2)\ \rangle\ -$$

$$\langle\ \phi_A(2)|\phi_B(2)\ \rangle\ \langle\ \phi_B(1)|h(1)|\phi_A(1)\ \rangle\ -$$

$$\langle\ \phi_B(1)|\phi_A(1)\ \rangle\ \langle\ \phi_A(2)|h(2)|\phi_B(2)\ \rangle\ +$$

$$\langle\ \phi_A(2)|\phi_A(2)\ \rangle\ \langle\ \phi_B(1)|h(1)|\phi_B(1)\ \rangle\ +$$

$$\langle\ \phi_B(1)|\phi_B(1)\ \rangle\ \langle\ \phi_A(2)|h(2)|\phi_A(2)\ \rangle]$$

$$= .5\ [\boldsymbol{a} + \boldsymbol{a}\ - 0 - 0 - 0 - 0 + \boldsymbol{a} + \boldsymbol{a}] = 2\boldsymbol{a}. \quad (2.18)$$

where $\boldsymbol{a}$ is the coulomb integral ($\boldsymbol{a} = \langle\ \phi_A(1)|h(1)|\phi_A(1)\ \rangle = \langle\ \phi_B(2)|h(2)|\phi_B(2)\ \rangle$.

Energy of the open-shell singlet is :

$$E_{singlet,\,OS} = .5\langle\ \phi_A(1)\phi_B(2) + \phi_B(1)\phi_A(2)\ |h(1)+h(2)|\ \phi_A(1)\phi_B(2) + \phi_B(1)\phi_A(2)\ \rangle$$

$$= .5[\langle\ \phi_A(1)\phi_B(2)\ |\ h(1)+h(2)|\phi_A(1)\phi_B(2)\ \rangle\ +$$

$$\langle\ \phi_A(1)\phi_B(2)\ |\ h(1)+h(2)|\phi_B(1)\phi_A(2)\ \rangle +$$

$$\langle\ \phi_B(1)\phi_A(2)\ |\ h(1)+h(2)|\phi_A(1)\phi_B(2)\ \rangle +$$

$$\langle\ \phi_B(1)\phi_A(2)\ |\ h(1)+h(2)|\phi_B(1)\phi_A(2)\ \rangle\ ]$$

$$= .5[\langle\ \phi_B(2)|\phi_B(2)\ \rangle\ \langle\ \phi_A(1)|h(1)|\phi_A(1)\ \rangle\ +$$

$$\langle\ \phi_A(1)|\phi_A(1)\ \rangle\ \langle\ \phi_B(2)|h(2)|\phi_B(2)\ \rangle\ -+$$

$$\langle\ \phi_B(2)|\phi_A(2)\ \rangle\ \langle\ \phi_A(1)|h(1)|\phi_B(1)\ \rangle\ +$$

$$\langle\ \phi_A(1)|\phi_B(1)\ \rangle\ \langle\ \phi_B(2)|h(2)|\phi_A(2)\ \rangle +$$

$$\langle\ \phi_A(2)|\phi_B(2)\ \rangle\ \langle\ \phi_B(1)|h(1)|\phi_A(1)\ \rangle +$$

$$\langle\ \phi_B(1)|\phi_A(1)\ \rangle\ \langle\ \phi_A(2)|h(2)|\phi_B(2)\ \rangle +$$

$$\langle\ \phi_A(2)|\phi_A(2)\ \rangle\ \langle\ \phi_B(1)|h(1)|\phi_B(1)\ \rangle +$$

$$\langle\ \phi_B(1)|\phi_B(1)\ \rangle\ \langle\ \phi_A(2)|h(2)|\phi_A(2)\ \rangle]$$

$$= .5\ [\boldsymbol{a} + \boldsymbol{a} + 0 + 0 + 0 + 0 + \boldsymbol{a} + \boldsymbol{a}] = 2\boldsymbol{a}. \qquad (2.19)$$

Energy of the first closed-shell singlet is:

$$E_{singlet,\,CS} = .5\langle\ \phi_A(1)\phi_B(2) + \phi_B(1)\phi_A(2)\ |h(1)+h(2)|\ \phi_A(1)\phi_B(2) + \phi_B(1)\phi_A(2)\ \rangle$$

$$= .5[\langle\ \phi_A(1)\phi_B(2)\ |\ h(1)+h(2)|\phi_A(1)\phi_B(2)\ \rangle\ +$$

$$\langle\ \phi_A(1)\phi_B(2)\ |\ h(1)+h(2)|\phi_B(1)\phi_A(2)\ \rangle +$$

$$\langle\ \phi_B(1)\phi_A(2)\ |\ h(1)+h(2)\ |\phi_A(1)\phi_B(2)\ \rangle +$$

$$\langle\ \phi_B(1)\phi_A(2)\ |\ h(1)+h(2)\ |\phi_B(1)\phi_A(2)\ \rangle\ ]$$

$$= .5[\langle\ \phi_B(2)\,|\,\phi_B(2)\ \rangle\ \langle\ \phi_A(1)\,|\,h(1)\,|\,\phi_A(1)\ \rangle\ +$$

$$\langle\ \phi_A(1)\,|\,\phi_A(1)\ \rangle\ \langle\ \phi_B(2)\,|\,h(2)\,|\,\phi_B(2)\ \rangle\ -+$$

$$\langle\ \phi_B(2)\,|\,\phi_A(2)\ \rangle\ \langle\ \phi_A(1)\,|\,h(1)\,|\,\phi_B(1)\ \rangle\ +$$

$$\langle\ \phi_A(1)\,|\,\phi_B(1)\ \rangle\ \langle\ \phi_B(2)\,|\,h(2)\,|\,\phi_A(2)\ \rangle +$$

$$\langle\ \phi_A(2)\,|\,\phi_B(2)\ \rangle\ \langle\ \phi_B(1)\,|\,h(1)\,|\,\phi_A(1)\ \rangle +$$

$$\langle\ \phi_B(1)\,|\,\phi_A(1)\ \rangle\ \langle\ \phi_A(2)\,|\,h(2)\,|\,\phi_B(2)\ \rangle +$$

$$\langle\ \phi_A(2)\,|\,\phi_A(2)\ \rangle\ \langle\ \phi_B(1)\,|\,h(1)\,|\,\phi_B(1)\ \rangle +$$

$$\langle\ \phi_B(1)\,|\,\phi_B(1)\ \rangle\ \langle\ \phi_A(2)\,|\,h(2)\,|\,\phi_A(2)\ \rangle]$$

$$= .5\ [\boldsymbol{a} + \boldsymbol{a} + 0 + 0 + 0 + 0 + \boldsymbol{a} + \boldsymbol{a}] = 2\boldsymbol{a} \qquad .(2.20)$$

Energy of the second closed-shell singlet is:

$$E_{singlet,\,CS} = .5\langle\ \phi_A(1)\phi_B(2) - \phi_B(1)\phi_A(2)\ |\,h(1)+h(2)\,|\,\phi_A(1)\phi_B(2) - \phi_B(1)\phi_A(2)\ \rangle$$

$$= .5[\langle\ \phi_A(1)\phi_B(2)\ |\ h(1)+h(2)\,|\,\phi_A(1)\phi_B(2)\ \rangle\ -$$

$$\langle\ \phi_A(1)\phi_B(2)\ |\ h(1)+h(2)\,|\,\phi_B(1)\phi_A(2)\ \rangle\ -$$

$$\langle\ \phi_B(1)\phi_A(2)\ |\ h(1)+h(2)\,|\,\phi_A(1)\phi_B(2)\ \rangle\ +$$

$$\langle\ \phi_B(1)\phi_A(2)\ |\ h(1)+h(2)\,|\,\phi_B(1)\phi_A(2)\ \rangle\ ]$$

$$= .5[\langle\ \phi_B(2)\,|\,\phi_B(2)\ \rangle\ \langle\ \phi_A(1)\,|\,h(1)\,|\,\phi_A(1)\ \rangle\ +$$

$$\langle\ \phi_A(1)\,|\,\phi_A(1)\ \rangle\ \langle\ \phi_B(2)\,|\,h(2)\,|\,\phi_B(2)\ \rangle\ -$$

$$\langle\ \phi_B(2)\,|\,\phi_A(2)\ \rangle\ \langle\ \phi_A(1)\,|\,h(1)\,|\,\phi_B(1)\ \rangle\ -$$

$$\langle\ \phi_A(1)\,|\,\phi_B(1)\ \rangle\ \langle\ \phi_B(2)\,|\,h(2)\,|\,\phi_A(2)\ \rangle\ -$$

$$\langle\ \phi_A(2)\,|\,\phi_B(2)\ \rangle\ \langle\ \phi_B(1)\,|\,h(1)\,|\,\phi_A(1)\ \rangle\ -$$

$$\langle\ \phi_B(1)\,|\,\phi_A(1)\ \rangle\ \langle\ \phi_A(2)\,|\,h(2)\,|\,\phi_B(2)\ \rangle\ +$$

$$\langle\ \phi_A(2)\,|\,\phi_A(2)\ \rangle\ \langle\ \phi_B(1)\,|\,h(1)\,|\,\phi_B(1)\ \rangle\ +$$

$$\langle\ \phi_B(1)\,|\,\phi_B(1)\ \rangle\ \langle\ \phi_A(2)\,|\,h(2)\,|\,\phi_A(2)\ \rangle]$$

$$= .5\ [\boldsymbol{a} + \boldsymbol{a}\ - 0 - 0 - 0 - 0 + \boldsymbol{a} + \boldsymbol{a}] = 2\boldsymbol{a}. \qquad (2.21)$$

All of the energies when calculated to zero-order come out to be $2\boldsymbol{a}$, where $\boldsymbol{a}$ = the Hückel $\boldsymbol{a}$ value, which is the energy of the electron within a single orbital. Therefore, to zero-order, regardless of the orientation of the electrons, the energy will be the same as long as the electrons occupy identical orbitals. This is, of course, neglecting electron-electron repulsion. Electron-electron repulsions for the four states can be calculated by using a first-order Hamiltonian that accounts for electron-electron repulsions,

$$H^1 = h(1) + h(2) + e^2/r_{12} \qquad (2.22)$$

The energies of the open-shell singlet have been abbreviated earlier and the triplet states become:

$$E_{singlet,\,OS} = 0.707\langle\ \phi_A(1)\phi_B(2) + \phi_B(1)\phi_A(2)\ |\,e^2/r_{12}\,|\,\phi_A(1)\phi_B(2) + \phi_B(1)\phi_A(2)\ \rangle$$

$$= 0.707[\langle\ \phi_A(1)\phi_B(2)\ |\,e^2/r_{12}\,|\,\phi_A(1)\phi_B(2)\ \rangle\ +$$

$$\langle\ \phi_A(1)\phi_B(2)\ |\,e^2/r_{12}\,|\,\phi_B(1)\phi_A(2)\ \rangle + \langle\ \phi_B(1)\phi_A(2)\ |\,e^2/r_{12}\,|\,\phi_A(1)\phi_B(2)\ \rangle +$$

$$\langle\ \phi_B(1)\phi_A(2)\ |\,e^2/r_{12}\,|\,\phi_B(1)\phi_A(2)\ \rangle\ ]$$

$$= 0.707[\langle\ \phi_A(1)\phi_A(1)\ |\,e^2/r_{12}\,|\,\phi_B(2)\phi_B(2)\ \rangle\ +$$

$$\langle\ \phi_A(1)\phi_B(1)\ |e^2/r_{12}|\ \phi_A(2)\phi_B(2)\ \rangle + \langle\ \phi_B(1)\phi_A(1)\ |e^2/r_{12}|\ \phi_A(2)\phi_B(2)\ \rangle +$$

$$\langle\ \phi_B(1)\phi_B(1)\ |e^2/r_{12}|\ \phi_A(2)\phi_A(2)\ \rangle]$$

$$= 0.707\,[j + k\ + k + j]$$

$$= j + k \qquad (2.23)$$

$$E_{triplet} = 0.707\langle\ \phi_A(1)\phi_B(2) - \phi_B(1)\phi_A(2)\ |e^2/r_{12}|\ \phi_A(1)\phi_B(2) - \phi_B(1)\phi_A(2)\ \rangle$$

$$= 0.707[\langle\ \phi_A(1)\phi_B(2)\ |e^2/r_{12}|\ \phi_A(1)\phi_B(2)\ \rangle -$$

$$\langle\ \phi_A(1)\phi_B(2)\ |e^2/r_{12}|\ \phi_B(1)\phi_A(2)\ \rangle -$$

$$\langle\ \phi_B(1)\phi_A(2)\ |e^2/r_{12}|\ \phi_A(1)\phi_B(2)\ \rangle + \langle\ \phi_B(1)\phi_A(2)\ |e^2/r_{12}|\ \phi_B(1)\phi_A(2)\ \rangle\ ]$$

$$= 0.707[\langle\ \phi_A(1)\phi_A(1)\ |e^2/r_{12}|\ \phi_B(2)\phi_B(2)\ \rangle -$$

$$\langle\ \phi_A(1)\phi_B(1)\ |e^2/r_{12}|\ \phi_A(2)\phi_B(2)\ \rangle -$$

$$\langle\ \phi_B(1)\phi_A(1)\ |e^2/r_{12}|\ \phi_A(2)\phi_B(2)\ \rangle + \langle\ \phi_B(1)\phi_B(1)\ |e^2/r_{12}|\ \phi_A(2)\phi_A(2)\ \rangle\ ]$$

$$= 0.707\,[j - k\ - k + j]$$

$$= j - k \qquad (2.24)$$

Energy of the first closed-shell singlet:

$$E_{S+,\,CS} = 0.707\langle\ \phi_A(1)\phi_A(2) + \phi_B(1)\phi_B(2)\ |e^2/r_{12}|\ \phi_A(1)\phi_A(2) + \phi_B(1)\phi_B(2)\ \rangle$$

$$= 0.707[\langle\ \phi_A(1)\phi_A(2)\ |e^2/r_{12}|\ \phi_A(1)\phi_A(2)\ \rangle +$$

$$\langle\ \phi_A(1)\phi_A(2)\ |e^2/r_{12}|\ \phi_B(1)\phi_B(2)\ \rangle$$

$$+ \langle\ \phi_B(1)\phi_B(2)\ |e^2/r_{12}|\ \phi_A(1)\phi_A(2)\ \rangle + \langle\ \phi_B(1)\phi_B(2)\ |e^2/r_{12}|\ \phi_B(1)\phi_B(2)\ \rangle\ ]$$

$$= 0.707[\langle\ \phi_A(1)\phi_A(1)\ |e^2/r_{12}|\ \phi_B(2)\phi_B(2) +$$

$$\langle\ \phi_A(1)\phi_B(1)\ |e^2/r_{12}|\ \phi_A(2)\phi_B(2)\ \rangle$$

$$+ \langle\ \phi_B(1)\phi_A(1)\ |e^2/r_{12}|\ \phi_A(2)\phi_B(2)\ \rangle + \langle\ \phi_B(1)\phi_B(1)\ |e^2/r_{12}|\ \phi_B(2)\phi_B(2)\ \rangle\ ]$$

$$= 0.707\ [j^\circ + k\ + k + j^\circ\ ]$$

$$= j^\circ + k \tag{2.25}$$

Energy of the second closed-shell singlet:

$$E_{S\text{-}, CS} = 0.707 \langle\ \phi_A(1)\phi_A(2) - \phi_B(1)\phi_B(2)\ |e^2/r_{12}|\ \phi_A(1)\phi_A(2) - \phi_B(1)\phi_B(2)\ \rangle$$

$$= 0.707[\langle\ \phi_A(1)\phi_A(2)\ |e^2/r_{12}|\ \phi_A(1)\phi_A(2)\ \rangle -$$

$$\langle\ \phi_A(1)\phi_A(2)\ |e^2/r_{12}|\ \phi_B(1)\phi_B(2)\ \rangle$$

$$- \langle\ \phi_B(1)\phi_B(2)\ |e^2/r_{12}|\ \phi_A(1)\phi_A(2)\ \rangle + \langle\ \phi_B(1)\phi_B(2)\ |e^2/r_{12}|\ \phi_B(1)\phi_B(2)\ \rangle\ ]$$

$$= 0.707[\langle\ \phi_A(1)\phi_A(1)\ |e^2/r_{12}|\ \phi_B(2)\phi_B(2)\ \rangle -$$

$$\langle\ \phi_A(1)\phi_B(1)\ |e^2/r_{12}|\ \phi_A(2)\phi_B(2)\ \rangle$$

$$+ \langle\ \phi_B(1)\phi_A(1)\ |e^2/r_{12}|\ \phi_A(2)\phi_B(2)\ \rangle + \langle\ \phi_B(1)\phi_B(1)\ |e^2/r_{12}|\ \phi_B(2)\phi_B(2)\ \rangle\ ]$$

$$= 0.707\ [j^\circ - k\ - k + j^\circ\ ]$$

$$= j^\circ - k \tag{2.26}$$

Within Equations 2.23 through 2.26, $j = \langle\ \phi_A(1)\phi_B(2)\ |e^2/r_{12}|\ \phi_A(1)\phi_B(2)\ \rangle$ is a two-center coulomb integral, the electron-electron repulsion felt between two electrons in different orbitals, $k = \langle\ \phi_A(1)\phi_B(1)\ |e^2/r_{12}|\ \phi_A(2)\phi_B(2)\ \rangle$ is a two-center exchange integral, the electron-electron repulsion felt between two electrons within the overlap region of two orbitals, and $j^\circ = \langle\ \phi_A(1)\phi_A(1)\ |e^2/r_{12}|\ \phi_B(2)\phi_B(2)\ \rangle$ is the one-center coulomb integral, electron-electron repulsion felt between two electrons in the same

orbital. Usually, j° is significantly larger than j. A cartoon of the orbitals can be seen in Figure II.3.

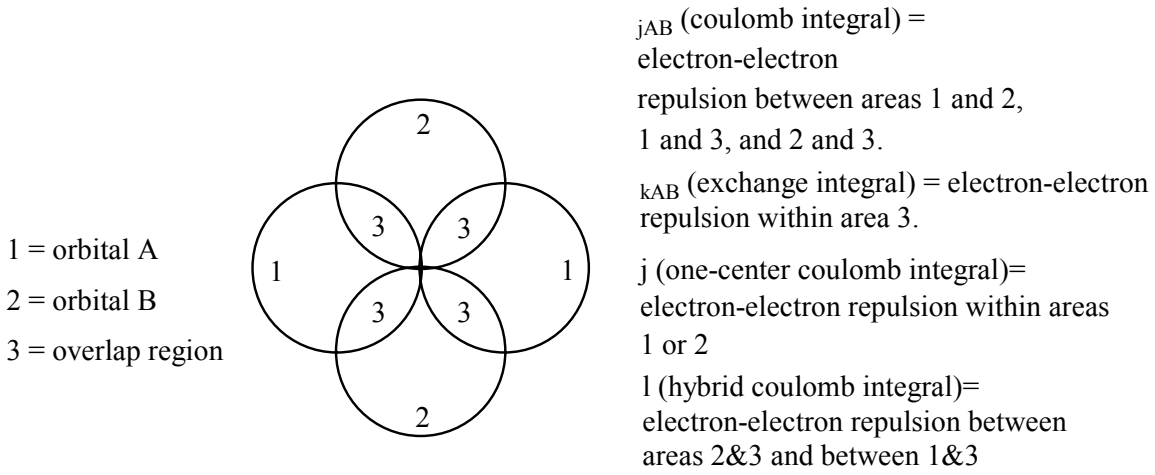

Figure II.3. Pictorial representation of electron-electron repulsion from Equations 2.23 - 2.26 using two orthogonal p-orbitals.

Thus far, the energy of the states (Equations 2.18-2.21) in terms of the energy of the electron in a single orbital (zero-order Hamiltonian, H^0) and the energy of the electron-electron repulsions in two orbitals (first-order Hamiltonian, H^1) has been described. Figure II.4 is a pictorial representation of the energy of the states and the terms describing them. We should also notice that the lowest energy state is a triplet and that energy gap between the triplet and the lowest-lying singlet is $\Delta E_{S\text{-}T} = 2\boldsymbol{J}_{Tot} = 2k$.

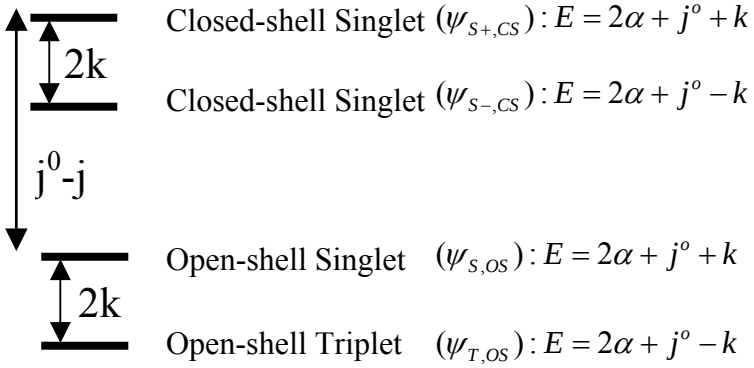

Figure II.4. Relative energy states of a two-electron, two-orbital system including the energy from the electron in a single orbital (H^0), and electron-electron repulsions (H^1). Notice that without second-order contributions (configuration interaction) the triplet state is lower in energy by 2*k* compared to that of the open-shell singlet.

This would be the end of the story if we did not consider configuration interaction, which occur when higher lying states mix into lower lying states with the stipulation that the symmetries are identical. To do this a second order correction is needed.

$$E_i^{(2)} = \frac{\left\langle \Psi_i \left| H^{(1)} \right| \Psi_j \right\rangle^2}{E_i - E_j} \tag{2.27}$$

Highest closed-shell singlet mixing into the open-shell singlet:

$$\left\langle \ \Psi_{s,OS} \ \middle| \ h(1) + h(2) + 1/r_{12} \middle| \Psi_{s+,CS} \ \right\rangle^2$$

$$= \left\langle 1/\sqrt{2}\,[\phi_A(1)\phi_B(2) + \phi_B(1)\phi_A(2)] \middle| \ h(1) + h(2) + 1/r_{12} \middle| [\phi_A(1)\phi_A(2) + \phi_B(1)\phi_B(2)] \ \right\rangle^2$$

$$= \{[0.5\left\langle \ \phi_A(1)\phi_B(2) + \phi_B(1)\phi_A(2) \ \middle| h(1) \middle| \phi_A(1)\phi_A(2) + \phi_B(1)\phi_B(2) \ \right\rangle +$$

$$\left\langle \ \phi_A(1)\phi_B(2) + \phi_B(1)\phi_A(2) \middle| \ h(2) \middle| \phi_A(1)\phi_A(2) + \phi_B(1)\phi_B(2) \ \right\rangle +$$

$$\left\langle \ \phi_A(1)\phi_B(2) + \phi_B(1)\phi_A(2) \middle| \ 1/r_{12} \middle| \phi_A(1)\phi_A(2) + \phi_B(1)\phi_B(2) \ \right\rangle \ ]\}^2$$

$$= \{[0.5\langle\ \phi_A(1)\phi_B(2)\ |h(1)|\ \phi_A(1)\phi_A(2)\ \rangle + \langle\ \phi_A(1)\phi_B(2)\ |h(1)|\ \phi_B(1)\phi_B(2)\ \rangle$$

$$+\langle\ \phi_B(1)\phi_A(2)\ |h(1)|\ \phi_A(1)\phi_A(2)\ \rangle + \langle\ \phi_B(1)\phi_A(2)\ |h(1)|\ \phi_B(1)\phi_B(2)\ \rangle +$$

$$\langle\ \phi_A(1)\phi_B(2)\ |h(2)|\ \phi_A(1)\phi_A(2)\ \rangle + \langle\ \phi_A(1)\phi_B(2)\ |h(2)|\ \phi_B(1)\phi_B(2)\ \rangle + \langle\ \phi_B(1)\phi_A(2)$$

$$|h(2)|\ \phi_A(1)\phi_A(2)\ \rangle + \langle\ \phi_B(1)\phi_A(2)\ |h(2)|\ \phi_B(1)\phi_B(2)\ \rangle + \langle\ \phi_A(1)\phi_B(2)$$

$$|\ 1/r_{12}|\ \phi_A(1)\phi_A(2)\ \rangle + \langle\ \phi_A(1)\phi_B(2)\ |\ 1/r_{12}|\ \phi_B(1)\phi_B(2)\ \rangle + \langle\ \phi_B(1)\phi_A(2)$$

$$|\ 1/r_{12}|\ \phi_A(1)\phi_A(2)\ \rangle + \langle\ \phi_B(1)\phi_A(2)\ |\ 1/r_{12}|\ \phi_B(1)\phi_B(2)\ \rangle]\}^2$$

$$= \{[0.5\langle\ \phi_B(2)|\ \phi_A(2)\ \rangle\ \langle\ \phi_A(1)|h(1)|\ \phi_A(1)\ \rangle + \langle\ \phi_B(2)|\ \phi_B(2)\ \rangle$$

$$\langle\ \phi_A(1)|h(1)|\ \phi_B(1)\ \rangle + \langle\ \phi_A(2)|\ \phi_A(2)\ \rangle\ \langle\ \phi_B(1)|h(1)|\ \phi_A(1)\ \rangle + \langle\ \phi_A(2)|\ \phi_B(2)\ \rangle$$

$$\langle\ \phi_B(1)|h(1)|\ \phi_B(2)\ \rangle + \langle\ \phi_A(1)|\ \phi_A(1)\ \rangle\ \langle\ \phi_B(2)|h(2)|\ \phi_A(2)\ \rangle + \langle\ \phi_A(1)|\ \phi_B(1)\ \rangle$$

$$\langle\ \phi_B(2)|h(2)|\ \phi_B(2)\ \rangle + \langle\ \phi_B(1)|\ \phi_A(1)\ \rangle\ \langle\ \phi_A(2)|h(2)|\ \phi_A(2)\ \rangle +$$

$$\langle\ \phi_B(1)|\ \phi_B(1)\ \rangle\ \langle\ \phi_A(2)|h(2)|\ \phi_B(2)\ \rangle + \langle\ \phi_A(1)\phi_A(1)\ |\ 1/r_{12}|\ \phi_A(2)\phi_B(2)\ \rangle +$$

$$\langle\ \phi_A(1)\phi_B(2)\ |\ 1/r_{12}|\ \phi_B(2)\phi_B(2)\ \rangle + \langle\ \phi_B(1)\phi_A(1)\ |\ 1/r_{12}|\ \phi_A(2)\phi_A(2)\ \rangle +$$

$$\langle\ \phi_B(1)\phi_B(2)\ |\ 1/r_{12}|\ \phi_A(2)\phi_B(2)\ \rangle]\}^2$$

$$=\{[0.5[0+\beta+\beta+0+\beta+0+0+\beta+l+l+l+l]\}^2 =\{[0.5\ [4\beta+4l]\}^2$$

$$= 4(\beta+l)^2 \qquad (2.28)$$

The energy of the two mixed states now contains a correction when calculated with configuration interaction. The correction becomes:

$$E = \frac{4(\beta + l)^2}{j - j^\circ} \qquad (2.29)$$

The lower closed-shell singlet mixing into the open-shell singlet:

$$\langle\ \Psi_{s,OS}\ |\ h(1)+h(2)+1/r_{12}\,|\,\Psi_{s\text{-},CS}\ \rangle^2$$

$$=\left\langle 1/\sqrt{2}\,[\phi_A(1)\phi_B(2)+\phi_B(1)\phi_A(2)]\,|\ h(1)+h(2)+1/r_{12}\,|\,[\phi_A(1)\phi_A(2)-\phi_B(1)\phi_B(2)]\ \right\rangle^2$$

$$=\{[0.5\langle\ \phi_A(1)\phi_B(2)+\phi_B(1)\phi_A(2)\ |h(1)|\,\phi_A(1)\phi_A(2)-\phi_B(1)\phi_B(2)\ \rangle+$$

$$\langle\ \phi_A(1)\phi_B(2)+\phi_B(1)\phi_A(2)|\ h(2)|\,\phi_A(1)\phi_A(2)-\phi_B(1)\phi_B(2)\ \rangle+$$

$$\langle\ \phi_A(1)\phi_B(2)+\phi_B(1)\phi_A(2)|\ 1/r_{12}|\,\phi_A(1)\phi_A(2)-\phi_B(1)\phi_B(2)\ \rangle\ ]\}^2$$

$$=\{[0.5\langle\ \phi_A(1)\phi_B(2)\ |h(1)|\,\phi_A(1)\phi_A(2)\ \rangle-\langle\ \phi_A(1)\phi_B(2)\ |h(1)|\,\phi_B(1)\phi_B(2)\ \rangle$$

$$+\langle\ \phi_B(1)\phi_A(2)\ |h(1)|\,\phi_A(1)\phi_A(2)\ \rangle-\langle\ \phi_B(1)\phi_A(2)\ |h(1)|\,\phi_B(1)\phi_B(2)\ \rangle+\langle\ \phi_A(1)\phi_B(2)$$

$$|h(2)|\,\phi_A(1)\phi_A(2)\ \rangle-\langle\ \phi_A(1)\phi_B(2)\ |h(2)|\,\phi_B(1)\phi_B(2)\ \rangle+\langle\ \phi_B(1)\phi_A(2)$$

$$|h(2)|\,\phi_A(1)\phi_A(2)\ \rangle-\langle\ \phi_B(1)\phi_A(2)\ |h(2)|\,\phi_B(1)\phi_B(2)\ \rangle+\langle\ \phi_A(1)\phi_B(2)$$

$$|1/r_{12}|\,\phi_A(1)\phi_A(2)\ \rangle-\langle\ \phi_A(1)\phi_B(2)\ |1/r_{12}|\,\phi_B(1)\phi_B(2)\ \rangle+\langle\ \phi_B(1)\phi_A(2)$$

$$|1/r_{12}|\,\phi_A(1)\phi_A(2)\ \rangle-\langle\ \phi_B(1)\phi_A(2)\ |1/r_{12}|\,\phi_B(1)\phi_B(2)\ \rangle\ ]\}^2$$

$$=\{[0.5\langle\ \phi_B(2)|\phi_A(2)\ \rangle\langle\ \phi_A(1)|h(1)|\phi_A(1)\ \rangle+\langle\ \phi_B(2)|\phi_B(2)\ \rangle$$

$$\langle\ \phi_A(1)|h(1)|\phi_B(1)\ \rangle-\langle\ \phi_A(2)|\phi_A(2)\ \rangle\langle\ \phi_B(1)|h(1)|\phi_A(1)\ \rangle+\langle\ \phi_A(2)|\phi_B(2)\ \rangle$$

$$\langle\ \phi_B(1)|h(1)|\phi_B(2)\ \rangle-\langle\ \phi_A(1)|\phi_A(1)\ \rangle\langle\ \phi_B(2)|h(2)|\phi_A(2)\ \rangle+\langle\ \phi_A(1)|\phi_B(1)\ \rangle$$

$$\langle\ \phi_B(2)|h(2)|\phi_B(2)\ \rangle-\langle\ \phi_B(1)|\phi_A(1)\ \rangle\langle\ \phi_A(2)|h(2)|\phi_A(2)\ \rangle+\langle\ \phi_B(1)|\phi_B(1)\ \rangle$$

$$\langle\ \phi_A(2)|h(2)|\phi_B(2)\ \rangle-\langle\ \phi_A(1)\phi_A(1)\ |1/r_{12}|\,\phi_A(2)\phi_B(2)\ \rangle+$$

$$\langle\ \phi_A(1)\phi_B(2)\ |1/r_{12}|\,\phi_B(2)\phi_B(2)\ \rangle-\langle\ \phi_B(1)\phi_A(1)\ |1/r_{12}|\,\phi_A(2)\phi_A(2)\ \rangle+$$

$$\langle\ \phi_B(1)\phi_B(2)\ |1/r_{12}|\,\phi_A(2)\phi_B(2)\ \rangle\ ]\}^2$$

$$=\{[0.5[0\text{-}\beta+\beta\text{-}0+\beta\text{-}0+0\text{-}\beta+l\text{-}l+l\text{-}l]\}^2=\{[0.5\ [0]\}^2$$

$$= 0 \tag{2.30}$$

The energy remains the same as found above:

$$E = j^{\circ} - k. \tag{2.31}$$

There will not be a correction to the triplet state energy, E_T.

In Equations 2.28-2.30, **b** is the resonance integral ($\mathbf{b} = \langle\ \phi_A(1)\,|\,h(1)\,|\,\phi_B(1)\ \rangle$), and l is the hybrid two-center coulomb integral ($l = \langle\ \phi_A(1)\phi_A(1)\ |\ 1/r_{12}\,|\,\phi_A(2)\phi_B(2)\ \rangle$). Based on these equations, configuration interactions only occur within the singlet manifold. The two higher-lying singlets cannot mix with the triplet state since their symmetries are different.

The relative energies of the two electron two orbital system are represented pictorially in Figure II.5. On the left is the energy of the states in the absence of configuration interaction. As the first-order Hamiltonian predicted, the triplet is lower than the singlet; such a case would represent ferromagnetic coupling. The result of the second-order correction (configuration interaction),shows mixing the higher-lying closed-shell singlet with the lower open-shell singlet lowers the singlet state, or contributes to the antiferromagnetic coupling (right).

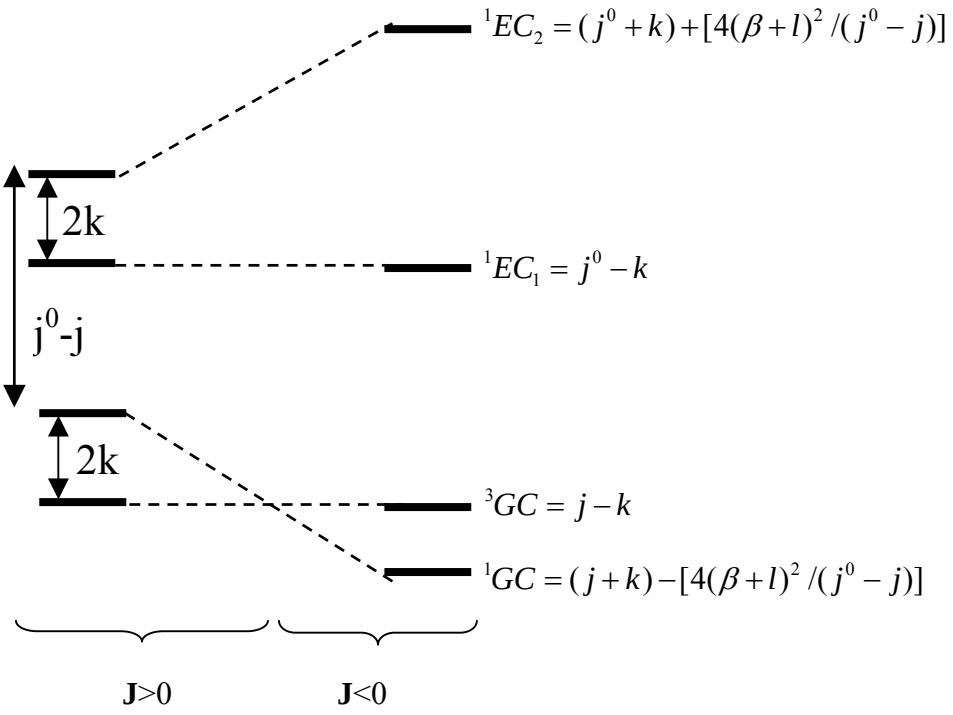

Figure II.5. Energy states of the two electron two orbital system. Ground configuration (left) and Ground configuration with configuration interaction (right).

The exchange coupling parameter is a measure of the energy difference between the triplet state and the singlet state. Through the above calculations the simplistic equation of the total exchange coupling in Equation 2.1 becomes:

$$\boldsymbol{J}_{\mathrm{TOT}} = \boldsymbol{J}_{\mathrm{F}} + \boldsymbol{J}_{\mathrm{AF}} = 2k - \frac{4(\beta + l)^2}{j^{\circ} - j} \qquad (2.32)$$

Where 2*k* is now the ferromagnetic contribution to the exchange coupling, $\boldsymbol{J_F}$, and $4(\beta+l)^2/(j^{\circ} - j)$ is the antiferromagnetic contribution to the exchange coupling, $\boldsymbol{J_{AF}}$. Also, from the above equations, it can now be seen quantitatively why the triplet is said to be lower in energy than the singlet. In fact it can now be calculated that the triplet is $2K_{ab}$ lower than the singlet.

$$E_{singlet} = j_{ab} + k_{ab} \quad (2.33)$$

$$E_{triplet} = j_{ab} - k_{ab} \quad (2.34)$$

$$E_{singlet} - E_{triplet} = 2k_{ab} \quad (2.35)$$

So the more overlap density between the two orbitals, the stronger the ferromagnetic contribution to ***J***.

II.B. Qualitative approaches for determining extent of exchange coupling in biradicals.

II.B.1. Hund's rule as it applies to molecules.

Another way to describe $\boldsymbol{J_F}$ and the overlap region is Hund's Rule. Hund's rule states that an atom in its ground state has electrons that are placed into degenerate orbitals so as to maximize m_s.[8] Hund's rule can be understood if two electrons filling orthogonal p-orbitals of the carbon atom are considered. If the electrons align in a parallel fashion the spins have a tendency to stay apart; therefore repelling each other less. Whereas if they align antiparallel they are attracted and the repulsion energy becomes greater than the spin aligned configuration. The quantum mechanical basis for this is explained above. It is found that the triplet state is lower than the singlet state in energy by $2k_{ab}$, where k_{ab} is the exchange integral, $k = \langle \ \phi_A(1)\phi_B(1) \mid e^2/r_{12} \mid \phi_A(2)\phi_B(2) \ \rangle$. In other words, k is the energy that the atom "saves" by avoiding the overlap region between the two orbitals. The size of k_{ab} depends on the overlap density of the two orbitals. The more overlap of the two orbitals, the larger k_{ab} and the preference for a triplet state, Figure II.6.

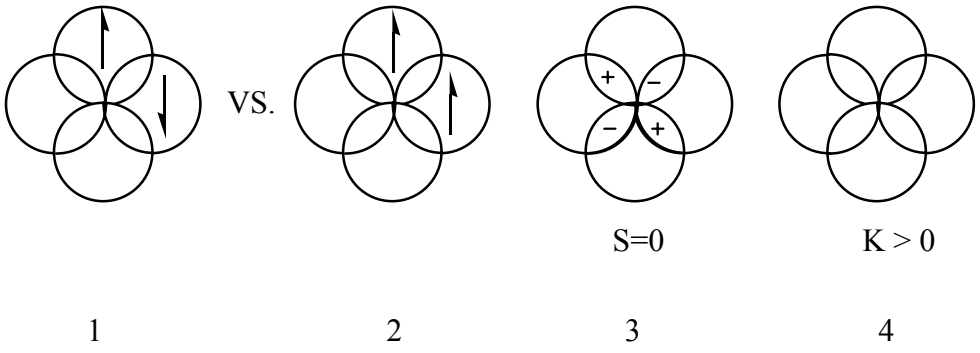

Figure II.6. Antiferromagnetic (1) vs. Ferromagnetic (2) interaction in a simplified orthogonal p-orbital system. (3) shows that the overlap integral (S) is equal to zero as the values of the overlap regions cancel each other. (4) shows that the exchange integral (K) is significant (overlap is substantial disregarding sign).

Hund's Rule can also be applied to molecules. Unpaired electrons in biradicals reside within the singly occupied molecular orbitals (SOMOs).[4,9] Figure II.6 can also be used to describe molecules. The electrons can align either antiparallel, antiferromagnetic, or parallel, ferromagnetic. As stated above, the preference for ferromagnetic or antiferromagnetic alignment of the electrons within the SOMOs depends on k_{ab}. The size of k_{ab}, in biradicals, depends on the overlap density of the SOMOs. This means that k_{ab} depends on the spin density (coefficients) on the common atoms of the overlapping orbitals. Thus, orthogonal SOMOs, by virtue of Hund's Rule, tend to give rise to a high-spin ferromagnetic state.[10,11,7]

II.B.2. Topology rules of biradicals.

The molecular version of Hund's Rule utilizes the fragment orbitals (FOs) of biradicals to predict how the unpaired electrons align just as the atomic version uses atomic orbitals (AOs). There are also topology rules that can be applied to predict the alignment of unpaired electrons in certain open-shell molecules. Longuet-Higgins proposed a method commonly known as the "star, non-star rule".[12] It only works for even alternant π-systems. To predict the ground state spin, first mark the atoms with stars (*)

and non-stars such that no two stars or non-stars are adjacent. The number of stars should also be maximized this allows for the greatest delocalization. The ground state (GS) spin then becomes S = (N*- N•)/2.

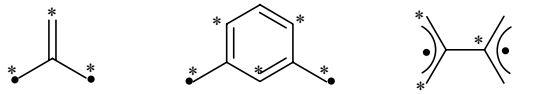

TMM	M-Xylylene	TME
(Triplet)	(Triplet)	(Singlet)
(3-1)/2 = 1	(5-3)/2 = 1	(3-3)/2 = 0

Figure II.7. Pictorial representation of the star-nonstar method.

Prediction of the ground state spin is also nicely explained using Hückel molecular orbitals (MOs) and quantum mechanics. Hückel Theory can be used to calculate the wavefunctions of a given π-system. The coefficients of the atoms in the FOs are then squared to give the spin density on each atom. Spin density can be represented using spheres of differing sizes (Figure II.8). If the fragment orbitals (FOs) contain atoms with overlapping spin density these are considered non-disjoint.[13] But if the atoms in the FOs lack common spin density they are considered to be disjoint.[13]

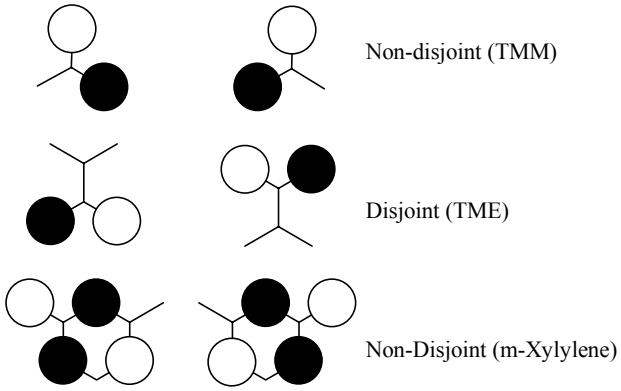

Figure II.8. Fragment Orbitals of Disjoint (TME) and Nondisjoint (TMM, m-Xylyene).

According to the Pauli Exclusion Principle, two electrons with the same spin are not allowed to occupy the same space. Electrons of the same spin avoid the common region of space and thus avoid the electron-electron repulsion associated with that space. Electrons of opposite spin are not prohibited to occupy a common region of space and therefore experience the repulsion associated with it. This results in a higher singlet state energy compared to that of the triplet. For a disjoint molecule such as tetramethylene ethane (TME) two electrons would not simultaneously occupy the same AOs. This causes the singlet state and triplet state to have the same energy. In a non-disjoint molecule such as trimethylene methane (TMM) the two electrons could possibly occupy the same AOs simultaneously. This would cause the electron-electron repulsion energy to be increased. As a result of these two cases the energy of the triplet state, E_t, will be larger than the energy for the singlet state, E_s.[7]

Both disjoint and non-disjoint molecules are also non-Kekulé hydrocarbons. Ref A non-Kekulé hydrocarbon is a molecule with a resonance structure that has as many **p**-bonds as possible, but at least two atoms that are not included in a **p**-bond.[14] In other words, regardless of what resonance structure is drawn, there will always be two unpaired

electrons in the biradical. Non-disjoint molecules are also called cross-conjugated. The Valence Bond (VB) model works for the determination of the ground state spin for a non-Kekulé molecule, while MO theory works for the estimation of the size of the singlet triplet energy gap, ΔE_{st}. Together the two approaches can be used to estimate the size of ΔE_{st} of the ground configuration in a disjoint or non-disjoint molecule.Ref But Hückel theory does have limitations in describing SOMOs. The coefficients cannot account for geometric configurations or different symmetries of biradical molecules.[13] Often the Hückel FOs that ”work” are chosen from many possible FOs.[13]

Another method for predicting whether a system is disjoint or non-disjoint is based on the connectivity of fragments and the coefficients of these fragments as opposed to the overall MO picture.[13] If the allyl radical is considered, it can be seen that there are two types of atoms: active (A, having spin density), and inactive (I, no spin density), Figure II.9. The active atoms are the two atoms on both ends. The inactive atom is the middle carbon atom. If one attaches an active atom of a radical (•CH2) to an inactive atom of a radical (Case1, A – I), a non-disjoint system TMM, is formed (triplet ground state). If an active atom ($\bullet CH_2$) is attached to another active atom (Case 2, A – A), a bond is formed. Finally if two inactive atoms are attached (Case 3, I – I), a disjoint system TME, is formed.

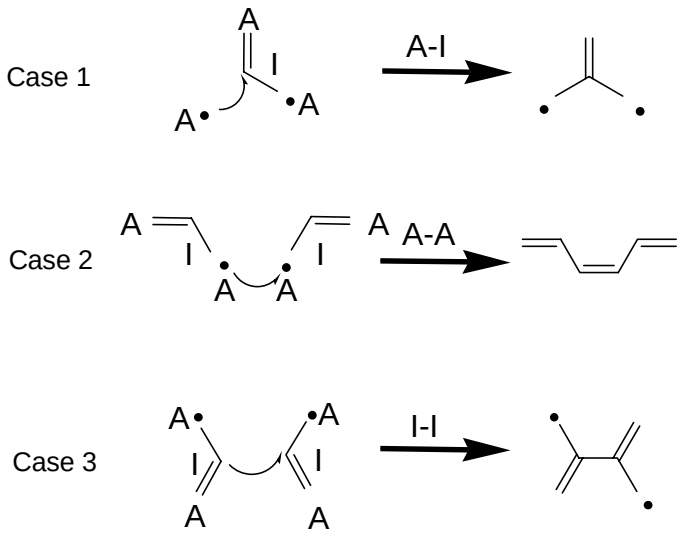

Figure II.9. Three examples of using fragments to determine if a molecule is disjoint or non-disjoint. Case 1: active to inactive leads to non-disjoint (high spin); Case 2: active to active leads to bond formation; Case 3: inactive to inactive leads to disjoint.

II. C. Molecular Design - How to make a High-Spin Biradical.

Biradical molecules in the Shultz group are prepared by connecting two spin-containing units via an exchange-coupling unit. The design is pictured in Figure II.10.

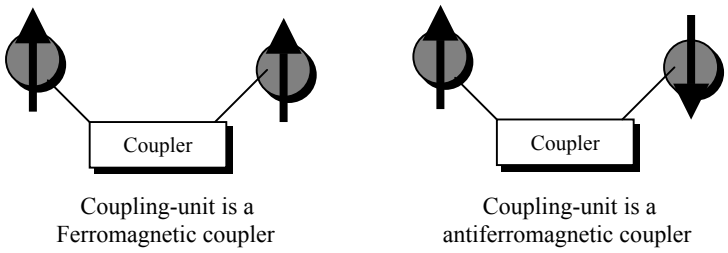

Figure II.10. Left, Ferromagnetic coupling-unit. Right, Antiferromagnetic coupling-unit.

The π-topology and conformation of biradicals are essential in understanding whether a biradical is a triplet (above left) or a singlet (above right). The design above involves

attaching paramagnetic functional groups via a coupling unit, usually a π-system. The goal of this attachment is to achieve a cross conjugated π-topology.[7] This design gives non-disjoint FOs that make high-spin ground states with substantial exchange integrals possible.[13] There are two commonly used ferromagnetic coupling units: ethenylidene and meta-phenylene. These coupling units have been used to synthesize the two most common homospin biradicals trimethylenemethane (TMM) and m-Xylyene.

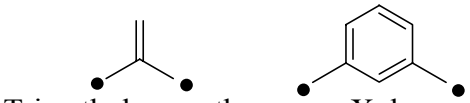

Figure II.11. TMM and m-Xylyene biradicals. Examples of the use of ethenylidene and m-Phenylene as coupling units.

The ferromagnetic coupling ability of the ethenylidene unit was confirmed through the study of the TMM biradical.[13,15-18] TMM was determined to have a singlet-triplet gap of ΔE_{st} = 14 kcal/mol.[19] It was Berson, Migirdicyan, and Platz that determined the ferromagnetic coupling ability of the meta-phenylene unit through the biradical meta-Xylyene (mX).[18,20,21,22] m-Xylyene was found to have a singlet-triplet gap of ΔE_{st} = 10 kcal/mol.

When two spins are exchange coupled, states are created with different multiplicities. These higher lying states are sometimes thermally accessible. The Heisenberg- Dirac-Van Vleck (HDVV) Hamiltonian is used to describe exchange coupled spins,

$$\hat{H}_{ab} = -2J_{ab}\hat{S}_a\hat{S}_b \tag{2.36}$$

This empirical Hamiltonian describes the spin angular momentum operators ($\hat{S}_a$and $\hat{S}_b$) and the magnitude of this interaction depends on $\boldsymbol{J}_{\mathrm{Tot}}$, the isotropic exchange parameter.

The product of the spin operators can be expressed in terms of the component spin operators and the total spin operator.

$$\hat{S}_{Tot} = \hat{S}_a + \hat{S}_b \tag{2.37}$$

$$\hat{S}_{Tot}^2 - (\hat{S}_s + \hat{S}_b)^2 = \hat{S}_a^2 + \hat{S}_b^2 + 2\hat{S}_a\hat{S}_b \tag{2.38}$$

$$\hat{S}_a\hat{S}_b = \frac{1}{2}(\hat{S}_{Tot}^2 - \hat{S}_a^2 - \hat{S}_b^2) \tag{2.39}$$

Since the eigenvalue of S^2 is S(S+1), the energy of the state can easily be determined by substituting in the appropriate terms.

$$E_{Tot} = -J_{ab}[S_{Tot}(S_{Tot}+1) - S_a(S_a+1) - S_b(S_b+1)] \tag{2.40}$$

Since the final two terms are constants Equation 2.40 reduces to Equation 2.41.

$$E_{Tot} = -J_{ab}[S_{Tot}(S_{Tot}+1)] \tag{2.41}$$

Thus, the energy of the singlet state, triplet state and the energy gap between them can be determined

$$E_{Triplet} = -J[1(1+1)] = -2J \tag{2.42}$$

$$E_{Singlet} = -J[0(0+1)] = 0 \tag{2.43}$$

The singlet-triplet energy gap is then just 2***J***.

$$\Delta E_{ST} = E_S - E_T = 2J - 0 = 2J \tag{2.44}$$

By the convention used above, $\boldsymbol{J}_{\mathrm{Tot}} > 0$ describes ferromagnetic coupling and $\boldsymbol{J}_{\mathrm{Tot}} < 0$ describes antiferromagnetic coupling. The exchange coupling parameter, $\boldsymbol{J}_{\mathrm{Tot}}$, can be determined experimentally by either Electron Paramagnetic Resonance (EPR) or by magnetometry.

In EPR spectroscopy, the double integrated $\mathbf{D}m_s=2$ signal is typically used.

Temperature dependence of this signal can be used to determine $\boldsymbol{J}_{\mathrm{Tot}}$ through the expression, Equation 2.45.[23]

$$I = \frac{C}{T}\left(\frac{3e^{\left(-2J_{Tot}/k_BT\right)}}{1+3e^{\left(-2J_{Tot}/k_BT\right)}}\right) \tag{2.45}$$

When $\boldsymbol{J} < 0$ the magnitude can be determined. When $\boldsymbol{J} > 0$ only a linear plot will result. For molecules with very small magnetic moments a Super Conducting Quantum Interference Device (SQUID) is typically used. The temperature dependence of the magnetic susceptibility for an S=1 system is given by the HDVV equation, Equation 2.46.[11]

$$\chi = \frac{2Ng^2\beta^2}{k_BT}\frac{e^{\left(-2J/k_BT\right)}}{1+3e^{\left(-2J/k_BT\right)}} \tag{2.46}$$

Both instruments, EPR and SQUID magnetometry, are described in detail in Chapter 3.

The Shultz group investigates two classes of biradicals: homo- and heterospin. Homospin biradicals consist of spin carriers that have equal spin values, $S_1 = S_2$. Whereas, heterospin biradicals consist of spin carries that have unequal spin values $S_1 \neq S_2$. Heterospin biradicals can be further divided into two categories, those with donor-donor spin carriers and those with donor-acceptor spin carriers. Each of these will be explained further in the following two sections.

II.D.1. Homo- and Heterospin Biradicals.

Homospin biradicals can be prepared if (1) the two paramagnetic functional groups attached via the coupling unit are equal in spin values, i.e. $S_1 = S_2$ and (2) if the

SOMOs of the paramagnetic groups are non-disjoint. To achieve non-disjoint systems in homospin biradicals, an atom of positive spin density in one paramagnetic group is attached to an atom with negative spin positive in the second paramagnetic group. Also to achieve non-disjoint SOMOs, the SOMOs must contain atoms that have common spin density. Below are the Huckel SOMOs of a TMM type bis-semiquinone (SQ) to illustrate the nondisjoint SOMOs that contain common spin density.

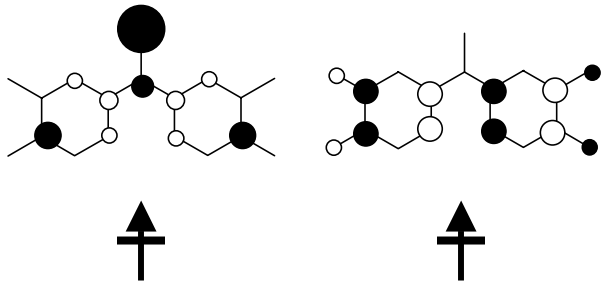

Figure II.12. Huckel SOMOs of a TMM type bis-SQ.

II.D.1.A. Previously Studied Homospin and Heterospin Biradicals.

Iwamura, as well as the Shultz group have both done extensive work with the TMM type homospin biradicals. [24-27,3,6] There have been a variety of paramagnetic functional groups used. Some are the semiquinone, nitroxide, phenoxy, nitrene, and carbene. Figure II.13 is an example of just four of these molecules.

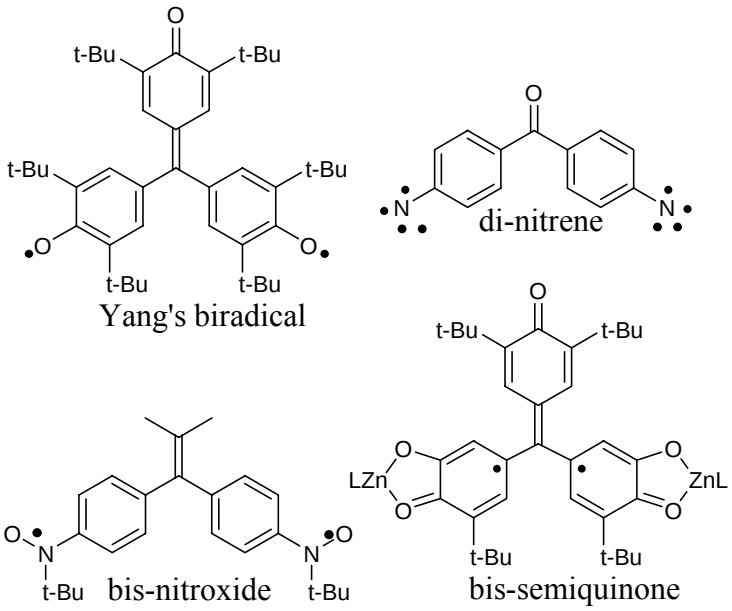

Figure II.13. Examples of TMM type biradicals.

As discussed in chapter 1, there has also been work in the Shultz group and in other groups on the m-phenylene type biradicals. [25-26]

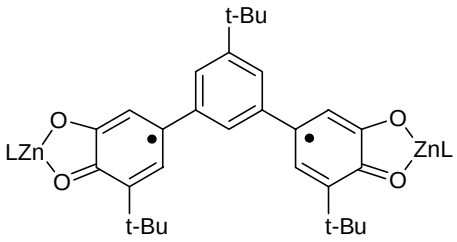

4-*t*-Bu

Figure II.14. Example of MPH coupled biradical: meta-phenylene bis(semiquinone).

Heterospin biradicals can also be prepared using the same non-disjoint requirement laid out above. But in the case of the heterospin biradicals the two spin carriers have unequal spin values, $S_1 \neq S_2$. There have been several groups to work on

these types of biradicals, but many have not measured the exchange coupling parameter.[25,27,1,26]

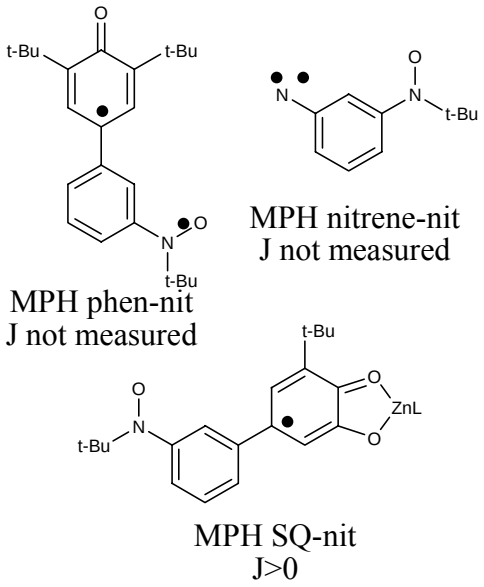

Figure II.15. Examples of heterospin MPH coupled biradicals. From top left to bottom: MPH phenoxy-nitroxide, MPH nitrene-nitroxide, and MPH nitroxide-semiquinone. [25,27,1,26]

Table II.1 Table of biradicals with calculated (left) and measured J-values (right).

Biradical	Calculated J (cm^{-1})	Biradical	Measured J (cm^{-1})
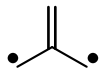	+6143.8[a17]	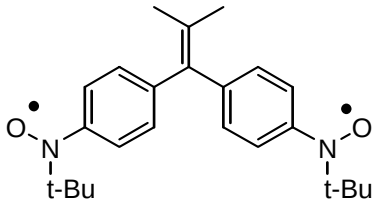	+5.3[28]
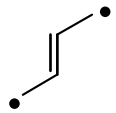	26,540[a7]		
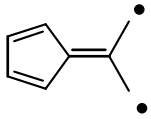	*b*29	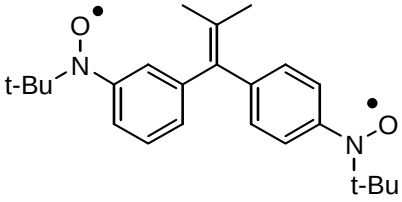	-1.7[28]
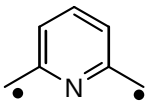	+3000[a30]		
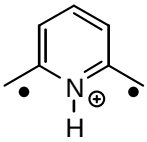	-643[a30]	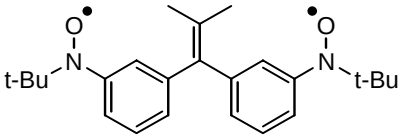	-0.9[28]
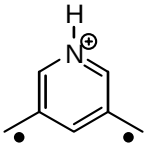	+2286[a30]	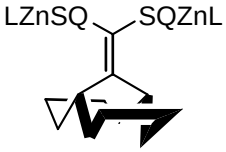	-30.3± 0.8[31]
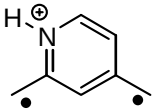	-250[a30]	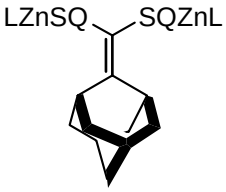	+24.4± 0.6[31]
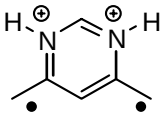	-7787[a30]		
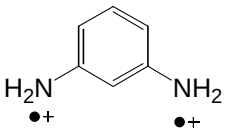	-3822[a]	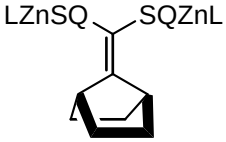	+87.0± 3.0[31]
	-232.2[32]	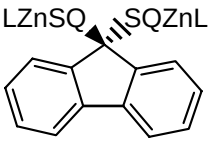	+0.99± 0.06[31]

Table II.1. Continued Table of biradicals with calculated (left) and measured J-values (right).

Biradical	Calculated J (cm^{-1})	Biradical	Measured J (cm^{-1})
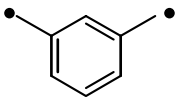	+3572[32]	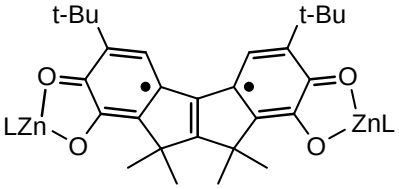	163.6 ±1.6[31]
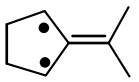	+2679[32]		
	+607.2[32]	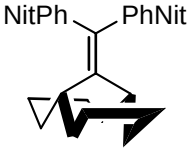	-14.03 ±0.12[33] -11.8±1.2[e33]
	+324.1[32]		
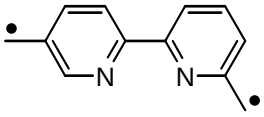	+3571.62[c34]	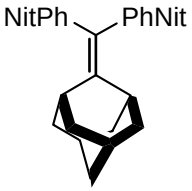	-5.11± 0.24[e33]
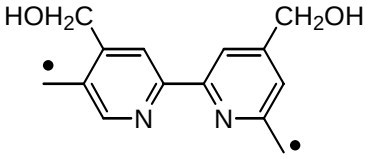	+3562.77[c34]	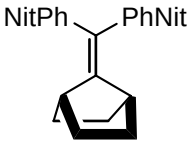	+6.79±0.18[33] +6.07±0.15[e33]
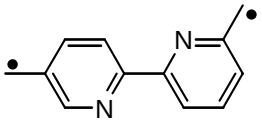	+3277.32[c34]	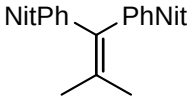	+5.24[33]
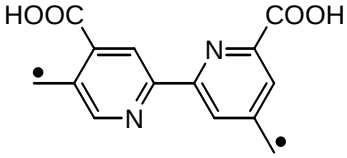	+3219.81[c34]	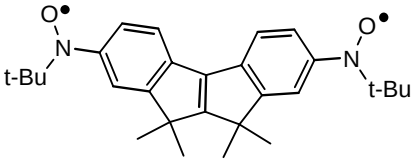	+25.5±1.6[33] +26.35± +1.73[e33]

Table II.1. Continued Table of biradicals with calculated (left) and measured J-values (right).

Biradical	Calculated J (cm^{-1})	Biradical	Measured J (cm^{-1})
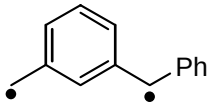	+0.0131[c35]	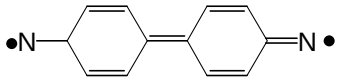	+214.3
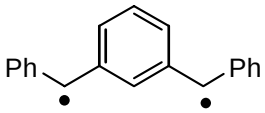	+0.00929[c35]	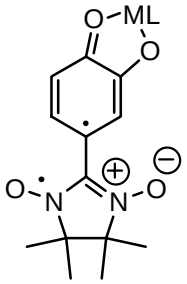 M=Mn M=Ni M=(OMe)Cu M=Zn	-41.3±0.5[6] -87.8±4.0[6] 75.6±1.0[6] >300[6]
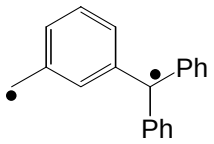	+1114[c]		
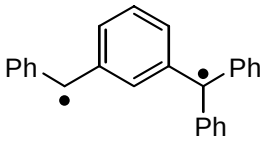	+0.0066[c35]		
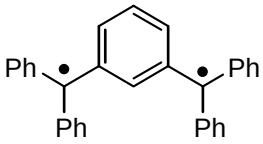	0.0044[c35]	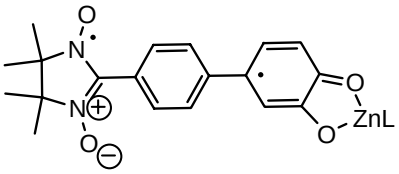	100.1±3.2[6]
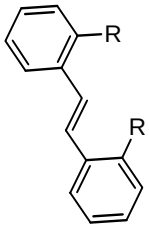 R=CH_2 • R=O • R=HNO• R=t-Bu-NO•	-964.4[d36] -2500[d36] -428.6[d36] -71.4[d36]	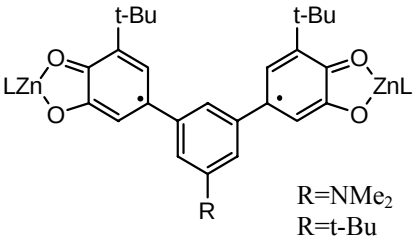 R=NMe_2 R=t-Bu R=NO_2	34.9±0.7[37] 59.3±1.2[37] 31.0±0.6[37]

Table II.1. Continued Table of biradicals with calculated (left) and measured J-values (right).

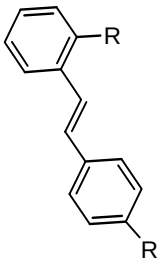	R=CH_2 • R=O • R=HNO • R=t-Bu-NO •	-1321.6[d36] -4465[d36] -500[d36] -214.3[d36]	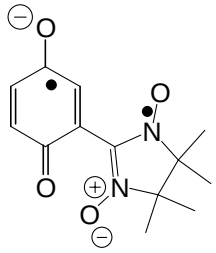	>0
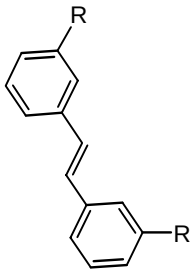	R=CH_2 • R=O • R=HNO • R=t-Bu-NO •	-285.8[d36] -321.5[d36] -214.3[d36] -178.6[d36]	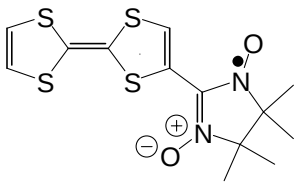	69.5
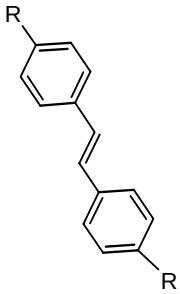	R=CH_2 • R=O • R=HNO • R=t-Bu-NO •	-1607.4[c36] -2857.6[c36] -643[c36] -428.6[c36]	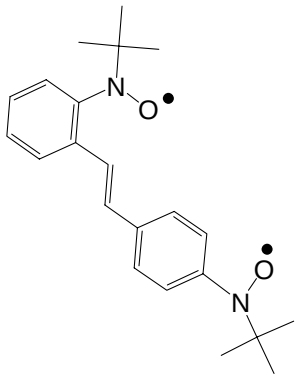	41.8±1
			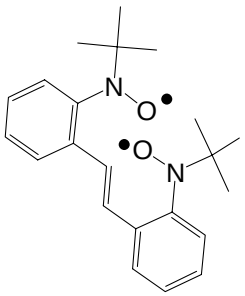	-9.6<J<0

[a]ab initio calculations. [b]UHF calculations. [c]UB3LYP method. [d]PVC film sample analysis. †SQZnL denotes semiquinone zinc trispyrazolylborate ligand (see chapter 3 for structure of L ligand). ‡PhNit denotes phenylnitroxide radical. Measured values of J-values by SQUID magnetometry.

II.D.2. Heterospin Donor-Acceptor Biradicals

The design of heterospin donor-acceptor biradicals differs from the homospin and heterospin biradicals, that were discussed above, in (1) paramagnetic functional groups carry different spin values ($S_1 \neq S_2$), (2) there is not a coupler and (3) atoms of positive spin density are attached to atoms of negative spin density. In heterospin biradicals it is the interaction of the SOMO of one spin carrier, for now we will call this the donor, with the LUMO of the other spin carrier, we will call this the acceptor. This is because in heterospin systems if just the two SOMOs of the functional groups were considered they would be disjoint and would be predicted to not form a high-spin ground state.

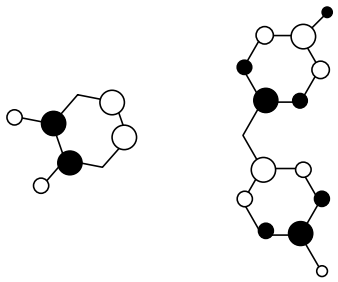

(a) (b)

Figure II.16. Hückel SOMOs of (a) SQ and (b) galvinoxyl (Gal).

In this instance, the SOMO of the donor mixes with the LUMO of the acceptor to create a new SOMO that is non-disjoint with the SOMO of the donor. A donor radical is defined as a paramagnetic functional group having positive spin density at the point of attachment; whereas the acceptor radical is defined as a paramagnetic functional group having negative spin density at the point of attachment.

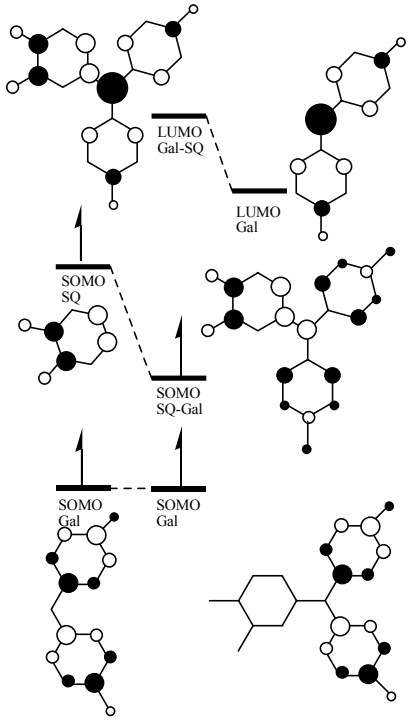

Figure II.17. (SQ)$SOMO_{donor}$-(Gal)$LUMO_{acceptor}$ interaction that creates non-disjoint heterospin biradical SOMOs.

II.D.2.A. Previously studied Heterospin Donor-Acceptor Biradicals.

Of the few donor-acceptor heterospin biradicals synthesized most contain some type of nitroxide species. Iwamura has produced several of these biradicals: carbene/nitrene,[38] and nitronylnitroxide/nitroxide.[38-40].

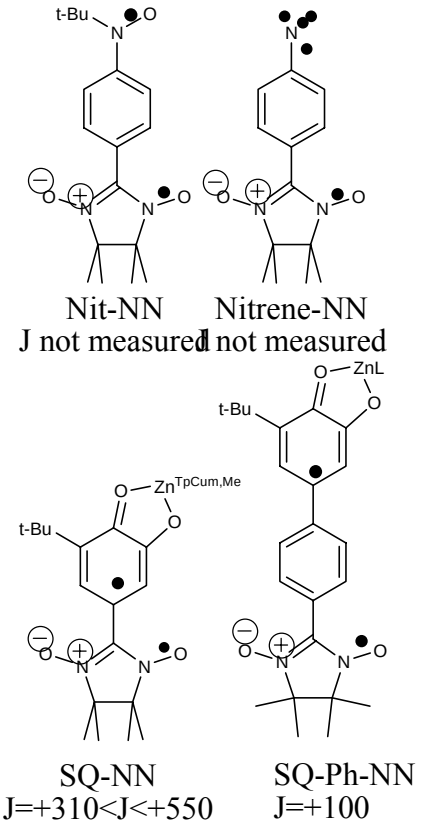

Figure II.18. Examples of heterospin biradicals and exchange coupling values.

Lahti has produced nitrene/nitroxide.[41] Sugawara has reported the nitronyl nitroxide/radical anion/cation.[42] Finally, the Shultz group has reported the synthesis of four donor-acceptor type heterospin biradicals. These include nitroxide/semiquinone,[43] nitronyl nitroxide/ semiquinone,[6] and nitroxide/galvinoxyl.[44,45]

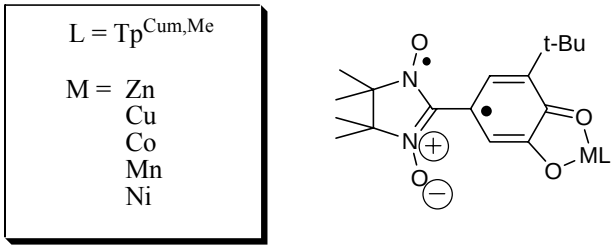

Figure II.19. Semiquinone-Nitronyl nitroxide with M = Zn, Cu, Co, Mn, and Ni, and L = $Tp^{Cum.Me}$.

In the Shultz group, a series of semiquinone- nitronyl nitroxide biradicals were prepared to investigate the donor-acceptor heterospin biradicals, Figure II.19. Several other interesting complexes were made as well. For example, a six-coordinate Ni complex was prepared using a tetradentate ligand in place of the tridentate TpCum,Me ligand. This resulted in a change from antiferromagnetic interaction in the nitronyl nitroxide-semiquinone Ni complex (**NN-SQNiL**) between the Ni metal ion and the semiquinone portion, to a ferromagnetic interaction in the (**NN-SQNiL**$^{\text{¢}}$) complex. Also, a phenyl spacing unit was put in place between the nitronyl nitroxide and the semiquinone to determine its effect on the strength of coupling as well as open up the possibility for coordination polymers.

The magnetic data of **(NNSQ)ZnL** is important because it gives the nature of the NN-SQ exchange interaction without the further complication of a paramagnetic metal ion. Because no significant loss in value for χT is seen as the temperature is increased to 300 K, this suggests that even at 300 K, the triplet ground-state is the only state that is being populated. Because the magnetic data for the Zn complex is a straight line, only a lower limit of $\boldsymbol{J}$NN-SQ = +310 cm^{-1} can be placed on the exchange parameter. Because of this extremely strong intraligand exchange coupling, the NN-SQ is treated as an S = 1 species rather than two independent S = ½ species. $\boldsymbol{J}$ is the exchange interaction between the paramagnetic metal and the strongly coupled NN-SQ ligand, $\hat{S}_1$ is the spin operator for the NN-SQ ligand (SNN-SQ = 1), and $\hat{S}_2$ is the spin operator for the metal ion. This approach has been used before for other high-spin organic molecules in previous work.[46]

Because only a lower limit could be placed on the ***J***-value for **(NNSQ)ZnL**, complex **(NN-PhSQ)ZnL** was also studied to see how an phenyl-spacer would attenuate the exchange coupling. For the phenyl-spaced derivative **(NN-PhSQ)ZnL** the intraligand exchange was determined to be $\boldsymbol{J}$ = +100 cm^{-1}. The reduction of the exchange parameter is caused by the addition of additional atoms between the two radical species, as well as the additional torsions associated with the phenyl-spacer. However, a $\boldsymbol{J}$ = 100 cm^{-1} is still quite large.

The magnetic data for **[NNSQ(OMe)]CuL** is consistent with the unpaired electron associated with the Cu ion being ferromagnetically coupled to the NN-SQ ligand. The room temperature χT value of 1.67 emu·K/mol is greater than both three uncorrelated spins (χT = 1.125 emu·K/mol) and an uncorrelated S = 1 and S = ½ species (χT = 1.375 emu·K/mol), which suggests there is both strong intraligand ferromagnetic coupling as well as ferromagnetic metal-ligand coupling. The fit for **[NNSQ(OMe)]CuL** was achieved with $J_{SQ\text{-}Cu}$ = +75.6 cm^{-1}. The χT data for the Mn complex clearly shows an antiferromagnetic interaction, which yields an S = 3/2 ground-state. The five parallel spins associated with the Mn(II) ion are coupled to the NNSQ ligand (two spins) antiferromagnetically, a value of $\boldsymbol{J}$ = -41.3 cm^{-1} was determined.

The χT vs. T data for **(NNSQ)NiL** shows a strong antiferromagnetic interaction between the S_{Ni} = 1 and the $S_{NN\text{-}SQ}$ = 1 spin centers leading ultimately to a S = 0, diamagnetic ground-state. This is clearly seen by the decreasing value of χT in going from 300 K towards lower temperatures and eventually approaching a value of zero, which is expected for a S = 0 state. A Curie tail can be seen in the χ vs. T plot for **(NNSQ)NiL** at low temperatures. Taking into account this impurity, the susceptibility

data for **(NNSQ)NiL** were initially fit with a model that takes into account a paramagnetic impurity term. The best-fit to the susceptibility data yielded a J = -91 cm^{-1}, with less than 1% of an S = 1 impurity.

The six-coordinate Ni complex **(NNSQ)NiL'** data was found to have χT product that is consistent with ferromagnetic coupling between the Ni metal ion and the NN-SQ spins. The best-fit to the susceptibility data yielded $\boldsymbol{J}$ = +79.9 cm^{-1}.

The susceptibility data for **(NN-SQ)CoL** could not be fit using simple spin-only susceptibility expressions. This is likely due to the large spin-orbit coupling effects within the CoII parent ground state.

It is clear that these heterospin donor-acceptor biradicals exhibit large ferromagnetic exchange coupling. Enhanced ferromagnetic exchange coupling could be evidence that in the calculation of $\boldsymbol{J_{TOT}}$ there exist other contributions to the ferromagnetic term that could arise from excited states. When the exchange coupling values for heterospin and homospin biradicals are considered, it seems clear that heterospin biradicals might have inherently stronger ferromagnetic coupling than their counterparts, homospin biradicals. This is the impetus for the research presented within this document.

II.E. References

(1) Shultz, D. A.; Bodnar, S. H.; Lee, H.; Kampf, J. W.; Incarvito, C. D.; Rheingold, A. L. *J. Am. Chem. Soc.* **2002**, *124*, 10054-10061.

(2) Shultz, D. A.; Boal, A. K.; Lee, H.; Farmer, G. T. *J. Org. Chem.* **1999**, *64*, 4386-4396.

(3) Shultz, D. A.; Fico, R. M., Jr.; Bodnar, S. H.; Kumar, R. K.; Vostrikova, K. E.; Kampf, J. W.; Boyle, P. D. *J. Am. Chem. Soc.* **2003**, *125*, 11761-11771.

(4) Lahti, P. M. *Magnetic Properties of Organic Materials*; Marcel Dekker, Inc.: New York, 1999.

(5) Shultz, D. A. *Polyhedron* **2003**, *22*, 2423-2426.

(6) Shultz, D. A.; Vostrikova, K. E.; Bodnar, S. H.; Koo, H. J.; Whangbo, M. H.; Kirk, M. L.; Depperman, E. C.; Kampf, J. W. *J. Am. Chem. Soc.* **2003**, *125*, 1607-1617.

(7) Rajca, A. *Chem. Rev.* **1994**, *94*, 871-893.

(8) Atkins, P. *Physical Chemistry*; 5th ed. ed.; W. H. Freeman and Company: New York, 1994.

(9) Borden, W. T. In *Magnetic Properties of Organic Materials*; Lahti, P. M., Ed.; Marcel Dekker: New York, 1999, p Chapter 5.

(10) Borden, W. T. *Diradicals*; John Wiley & Sons: New York, 1982.

(11) Kahn, O. *Molecular Magnetism*; VCH: New York, 1993.

(12) Longuett Higgins, H. C. *J. Chem. Phys.* **1950**, *18*, 265.

(13) Borden, W. T.; Davidson, E. R. *J. Am. Chem. Soc.* **1977**, *99*, 4587-4594.

(14) Dougherty, D. A. *Acc. Chem. Res.* **1991**, *24*, 88-94.

(15) Dowd, P. *J. Am. Chem. Soc.* **1966**, *88*, 2587.

(16) Dowd, P. *Acc. Chem. Res.* **1972**, *5*, 242.

(17) Dixon, D. A.; Dunning, T. H., Jr. ; Eades, R. A.; Kleier, D. A. *J. Am. Chem. Soc.* **1981**, *103*, 2878.

(18) Berson, J. A. *Acc. Chem. Res.* **1978**, *11*, 446.

(19) Wenthold, P. G.; Hu, J.; Squires, R. R.; Lineberger, W. C. *J. Am. Chem. Soc.* **1996**, *118*, 475-476.

(20) Platz, M. S. In *Diradicals*; Borden, W. T., Ed.; Wiley: New York, 1982, p 195.

(21) Berson, J. A. *Diradicals*; Wiley: New York, 1982.

(22) Migirdicyan, E. B. *J. Am. Chem. Soc.* **1975**, *97*, 7400.

(23) Berson, J. A., Ed. *The Chemistry of the Quinonoid Compounds, Vol. II*; John Wiley & Sons: New York, 1988.

(24) Depperman, E.; Bodnar, S. H.; Vostrikova, K. E.; Shultz, D. A.; Kirk, M. L. *J. Am. Chem. Soc.* **2001**, *123*, 3133-3134.

(25) Shultz, D. A.; Bodnar, S. H. *Inorg. Chem.* **1999**, *38*, 591-594.

(26) Iwamura, H.; Koga, N. *Acc. Chem. Res.* **1993**, *26*, 346.

(27) Mukai, K. *Bull. Chem. Soc. Jpn.* **1975**, *48*, 2405.

(28) Matsumoto, T.; Koga, N.; Iwamura, H. *J. Am. Chem. Soc.* **1992**, *114*, 5448-5449.

(29) Li, S.; Ma, J.; Jiang, Y. *J. Phys. Chem.* **1996**, *100*, 4775-4780.

(30) West, A. P., Jr. ; Silverman, S. K.; Dougherty, D. A. *J. Am. Chem. Soc.* **1996**, *118*, 1452-1463.

(31) Shultz, D. A.; Vostrikova, K. E.; Bodnar, S. H.; Koo, H.-J.; Whangbo, M.-H.; Kirk, M. L.; Depperman, E. C.; Kampf, J. W. *J. Am. Chem. Soc.* **2003**, *125*, 1607-1617.

(32) Jacobs, S. J.; Shultz, D. A.; Jain, R.; Novak, J.; Dougherty, D. A. *J. Am. Chem. Soc.* **1993**, *115*, 1744-1753.

(33) Shultz, D. A.; Fico, R. M.; Lee, H.; Kampf, J. W.; Kirschbaum, K.; Pinkerton, A. A.; Boyle, P. D. *JACS* **2003**, *125*, 15426-15432.

(34) Duan, H. X.; Su, Z. M.; Qiu, Y. Q.; Yan, L. K.; Kan, Y. H.; Wang, R. S. *Synth. Met.* **2003**, *137*, 1351-1352.

(35) Zhang, G.; Li, S.; Jiang, Y. *Tetrahedron* **2003**, *59*, 3499-3504.

(36) Yoshioka, N.; Lahti, P. M.; Kaneko, T.; Kuzumaki, Y.; Tsuchida, E.; Nishide, H. *J. Org. Chem.* **1994**, *59*, 4272-4280.

(37) Shultz, B., Lee, Kampf, Incarvito, Rheingold *JACS* **2002**, *124*, 10054-10061.

(38) Inoue, K.; Iwamura, H. *Adv. Mater.* **1996**, *8*, 73-76.

(39) Inoue, K.; Iwamura, H. *Angew. Chem. Int. Ed. Engl.* **1995**, *34*, 927-928.

(40) Iwamura, H.; Inoue, K.; Haymizu, T. *Pure & Appl. Chem.* **1996**, *68*, 243-252.

(41) Lahti, P. M.; Esat, B.; Wagner, R. *J. Am. Chem. Soc.* **1998**, *120*, 5122-5123.

(42) Kumai, R.; Matsushita, M. M.; Izuoka, A.; Sugawara, T. *J. Am. Chem. Soc.* **1994**, *116*, 4523.

(43) Shultz, D. A.; Boal, A. K.; Lee, H.; Farmer, G. T. *J. Org. Chem.* **1998**, *63*, 9462-9469.

(44) Shultz, D. A.; Boal, A. K. *Mol. Cryst. Liq. Cryst.* **1995**, *272*, 75-79.

(45) Shultz, D. A.; Boal, A. K.; Driscoll, D. J.; Kitchin, J. R.; Tew, G. N. *J. Org. Chem.* **1995**, *60*, 3578.

(46) Dougherty, D. A. S., D. A.; Novak, J.; Jain, R.; Jacobs, S. J. *J. Am. Chem. Soc.* **1993**, *115*, 1744.

Chapter 3

Electron Paramagnetic Resonance and Super Conducting Quantum Interference Device (SQUID Magnetometry).

III. Electron Paramagnetic Resonance and Super Conducting Quantum Interference Device (SQUID Magnetometry).

III.A. EPR: The Basics.

Electron paramagnetic resonance (EPR) is a branch of spectroscopy in which molecules, ions, or atoms that have electrons with unpaired spins absorb radiation of microwave frequency. In the presence of a magnetic field there are two spin states, m_s: **a** (+1/2) and **b** (-1/2) with energy:

$$E = g_e \beta m_s H \tag{3.1}$$

where g_e is the electronic g-factor of an electron (Lande's constant), **b** is the Bohr magneton, m_S is the spin quantum number, and H is the applied magnetic field.
In the absence of a magnetic field these spin states are degenerate, but when a magnetic field is applied they split and their energies are different. There are some similarities between EPR and NMR spectroscopy that aid in the understanding of EPR. In NMR, two different energy states (when I = ½) arise from the alignment of the nuclear magnetic moments relative to the applied field, and a transition between them occurs upon the application of radio-frequency radiation. In EPR, different energy states arise from the interaction of the unpaired electron spin moment with the magnetic field, the electronic Zeeman effect.

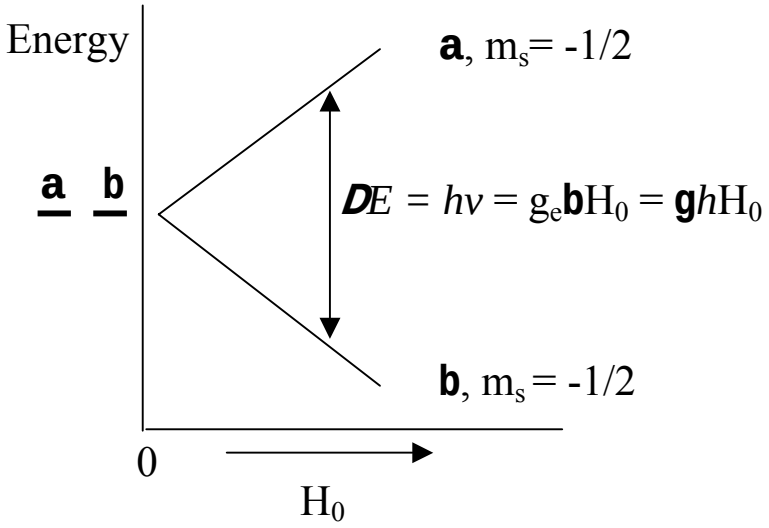

Figure III.1 The removal of the degeneracy of the **a** and **b** electron spin states by a magnetic field.

A magnetic dipole, such as an electron, will precess in a magnetic field. The processional (Larmor) frequency, **w**, is directly proportional to the gyromagnetic ratio of the electron, $\mathbf{g}_e$, and the strength of the applied magnetic field,

$$\omega = \gamma_e H \tag{3.2}$$

For X-band EPR the field strength is around 0.34 Tesla. This provides a resonance condition for the absorption of a quantum of electromagnetic radiation. Electromagnetic radiation of the Larmor frequency will cause the spins to flip,

$$\Delta E = h\nu = h\gamma_e H = E_+ - E_- = g_e \beta H \tag{3.3}$$

This follows the selection rule for multiplicity 2S + 1. An S=½ system will give rise to a doublet, an S=1 system will be a triplet. The allowed transitions obey the selection rule $\Delta m_S = \pm 1$, $\Delta m_I = 0$, where m_I is the nuclear spin quantum number.

Parameter g for a free electron, g_e, has the value close to two: $g_e = 2.0023193$. If the electron has a nonzero orbital angular moment, L, the g-value is anisotropic and becomes:

$$g = 1 + \frac{S(S+1) - L(L+1) + J(J+1)}{2J(J+1)} \tag{3.4}$$

The overall magnetic momentun, μ_{eff} , can be expessed via overall angular momentum, J, and the g-value:

$$\mu_{eff} = g\beta[J(J+1)]^{1/2} \tag{3.5}$$

For most of organic radicals and radical ions, unpaired electrons have L close to zero and the total electron angular momentum quantum number, J, is approximately the spin quantum number, S. As result, their isotropic g-values are close to 2. The situation becomes much more complicated with transition metals. Not only do they have large L's and S's, but these values depend on the surrounding electric fields of the ligands, making things more complicated. If $L = 0$ then $J = S$, and Eq. 3.1 will define the energies of all the possible projections of m_s from $-S, S - 1, S$ ($2S + 1$).

If the molecule contains nuclei with magnetic moments, such as protons, their interaction with the external field and the electronic magnetic moment will change stationary energies of Eq.3.1. The nuclear angular momentum quantum number I determines the nuclear magnetic moment the same way as for the electron:

$$\mu = g_N \beta_N [I(I+1)]^{1/2} \tag{3.6}$$

with β_N now being the nuclear Bohr magneton:

$$\beta_N = eh/4\pi m_p = 5.051\text{x}10^{-27}\ J/T \tag{3.7}$$

which is a much smaller value because of the ~2000 times more heavier proton m_p. The nuclear g factor, g_N, is obtained from a knowledge of the structure of the nucleus. Interaction with the external field splits the nuclear sublevels due to Zeeman interaction the same way as for the electron spin:

$$E_{m_I} = g_N \beta_N H_0 m_I \tag{3.8}$$

where m_I is one of the 2I + 1 projections of the nuclear spin. Electron-nuclear interaction will depend on the projections of both, electron and nuclear spins:

$$E_{electron-nuclear} = a m_I m_S \tag{3.9}$$

where coefficient a, hyperfine coupling constant(hfcc), depends not only on the g-values for the electron and the nucleus but also on the distance between them and their orientation with respect to the external field, dipole-dipole interaction which will be discussed in section III.A.2. In solutions, the anisotropic part of this interaction averages out because of the fast molecular rotation. The remaining isotropic part is given by the Fermi contact interaction in the form:

$$a = (8\pi/3) g_N \beta_N g_e \beta \rho(0) \tag{3.10}$$

where $\rho(0) = |\psi(0)|^2$ is the unpaired electron density at the nucleus. Summing up all of the energies, we arrive at modified Eq. 3.1:

$$E = g_e \beta m_S (H_0 + \Sigma a_i m_{Ii}) - g_N \beta_N H_0 m_I \tag{3.11}$$

III.A.1. The hyperfine interaction and solution phase EPR.

Solution phase EPR is useful in studying radicals. The spectra can give information on the radicals spin distribution and it's environment. If a radical containing one hydrogen atom is considered, a simple example EPR spectrum can be predicted and understood.

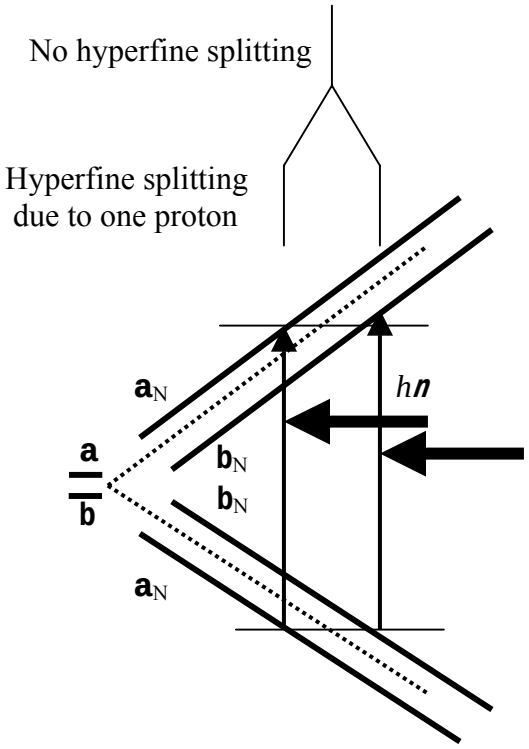

Figure III.2. Hydrogen atom.

As stated above, in EPR, allowed transitions correspond to the change of only m_s: $\Delta m_S = \pm 1$, $\Delta m_I = 0$. Thus, for the hydrogen atom in Figure III.2, only two transitions can be observed for a single resonant frequency hν. The separation of the transitions is equal to

the hyperfine coupling constant, *a*. If there is more than one hydrogen atom, each atom will contribute to the change in magnetic field on the electron. All combinations of the nuclear spin projections should be included but only EPR allowed transitions between sublevels with the same configurations of nuclear spins can be seen. When there are four equivalent protons, a ladder scheme is helpful in constructing an EPR spectrum.

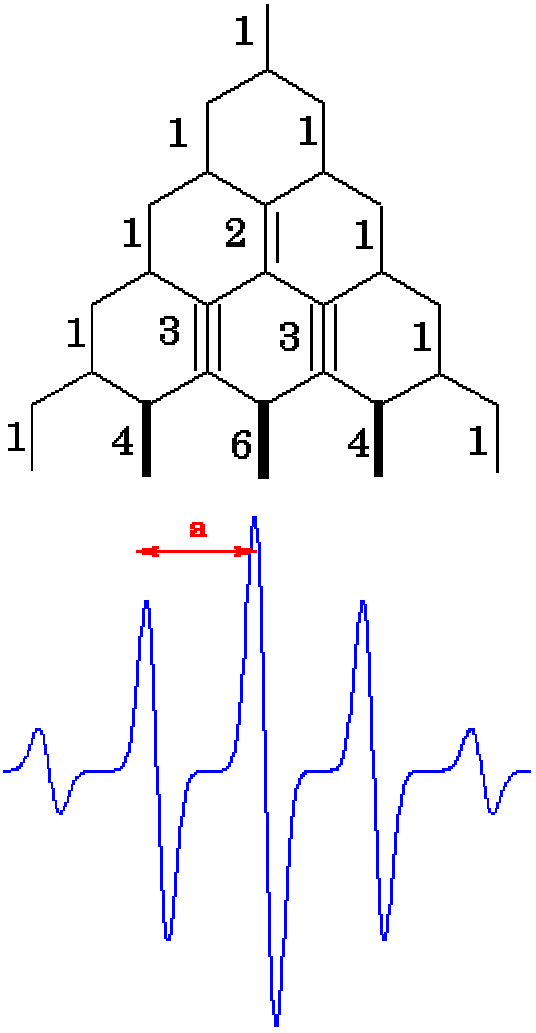

Figure III.3 EPR spectrum of radical distributed over 4 equivalent protons.

Each new level in the ladder corresponds to coupling to one more proton. In the first level, two lines appear that correspond to the two different orientations of m_I = -1/2 and

m_I = + 1/2. In the second level, each line splits into two, corresponding to the two different orientations of m_I = -1/2 and m_I = + 1/2, of the second proton. Since the two protons are equivalent, the splitting is the same on each level, resulting in three lines of 1:2:1 intesity ratio. For the four protons, there will be 5 lines with the 1:4:6:4:1 intensity ratio. A stick diagram for the radical can be constructed in order to predict what may be expected. Lines with the lengths of the intensity ratios separated by the appropriate constants represent a stick diagram for the radical.

If the spin of the nucleus is greater than 1/2, as in the case of ^{14}N (I = 1), it splits each of the electronic levels, **a** and **b**, into the 2nI + 1 sublevels resulting in 2nI + 1 obeserved lines of equal intensity. Where n = number of equivalent nuclei. In most cases, radicals contain a combination of different nuclei with different hyperfine coupling constants. Example of a radical with two different groups of hfcc constants and different nuclei is shown in Figure III.4 for a radical with one nitrogen atom and two equivalent hydrogen atoms.

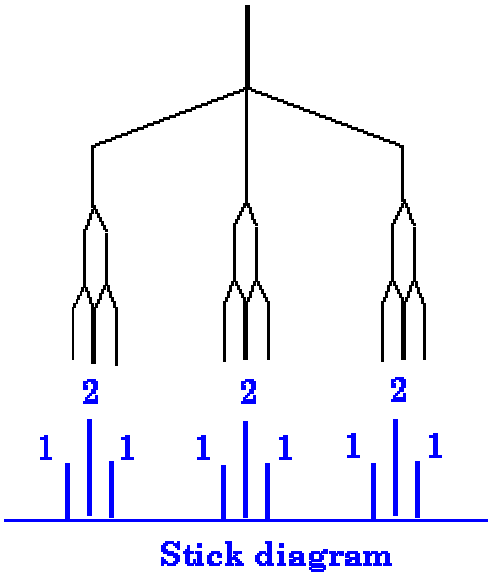

Figure III.4 Stick diagram of a radical containing one nitrogen atom and two equivalent hydrogen atoms.

The magnitude of the hyperfine coupling constants in a radical or radical ion reflects the extent of *s* character (only s-orbitals have nonzero density at the nucleus). In the previous section the mathematical description of the hyperfine coupling constant was given. Many radicals studied are mostly p character, but exhibit large hfcc's. For example, generally aromatic ion radicals are thought of as being purely p-systems, but there are substantial hfcc's on the hydrogen atoms within the aromatic radical. McConnell[6] showed that a portion of the unpaired p-electron density is transferred through the C-H sigma bonding electrons to the H nucleus via exchange interactions. These exchange interactions are commonly referred to as spin polarization.

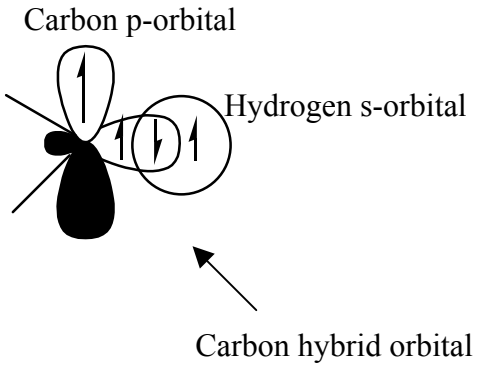

Figure III.5 Electron Spin Polarization through the **s**-framework.

He provided a simple formula which links the a_H on a hydrogen atom with the unpaired electron spin density on the nearest carbon atom $\boldsymbol{r}_{\mathbf{p}}$:

$$a_H(G) = Q\rho_\pi \tag{3.12}$$

The signal intensity in EPR depends on the amount of absorption of the microwave radiation. Intensity will increase with increasing difference of population between the α and β electron spin states. Following Boltzmann statistics, the latter can be estimated:

$$(n_\alpha - n_\beta)/n_\beta = e^{-\Delta E/kT} - 1 \approx g\beta H_0/k_B T \quad (3.13)$$

This is a small value for the X-band EPR spectrometer (9.5 GHz), which can be substanially increased by lowering the temperature.

III.A.2. Zero field splitting and frozen EPR spectra of triplet molecules.

The solution phase EPR spectrum can be used to observe the spin distribution of the radical molecule. For radicals with more than one unpaired electron, the solid or frozen EPR spectrum can be used to determine the zero field splitting parameters and give information about the geometry of the molecule.

As described in chapter 1 and 2, in a biradical system the two electrons can be aligned either parallel or antiparallel. If the two electrons are aligned antiparallel then the spin multiplicity is a singlet [2(0) + 1 = 1]. If the two electrons are aligned parallel then the spin multiplicity is a triplet [2(1) + 1 = 3]. These two spin states are exchange coupled. The singlet is EPR silent, no unpaired electrons. But the triplet can be observed by EPR. Because of the selection rule, for the EPR active triplet there are two allowed transitions since $m_s = \pm 1, 0$. A $\Delta m_s = 2$ transition will be further discussed later. Figure III.6 shows the $\Delta m_s = 1$ transitions.[1]

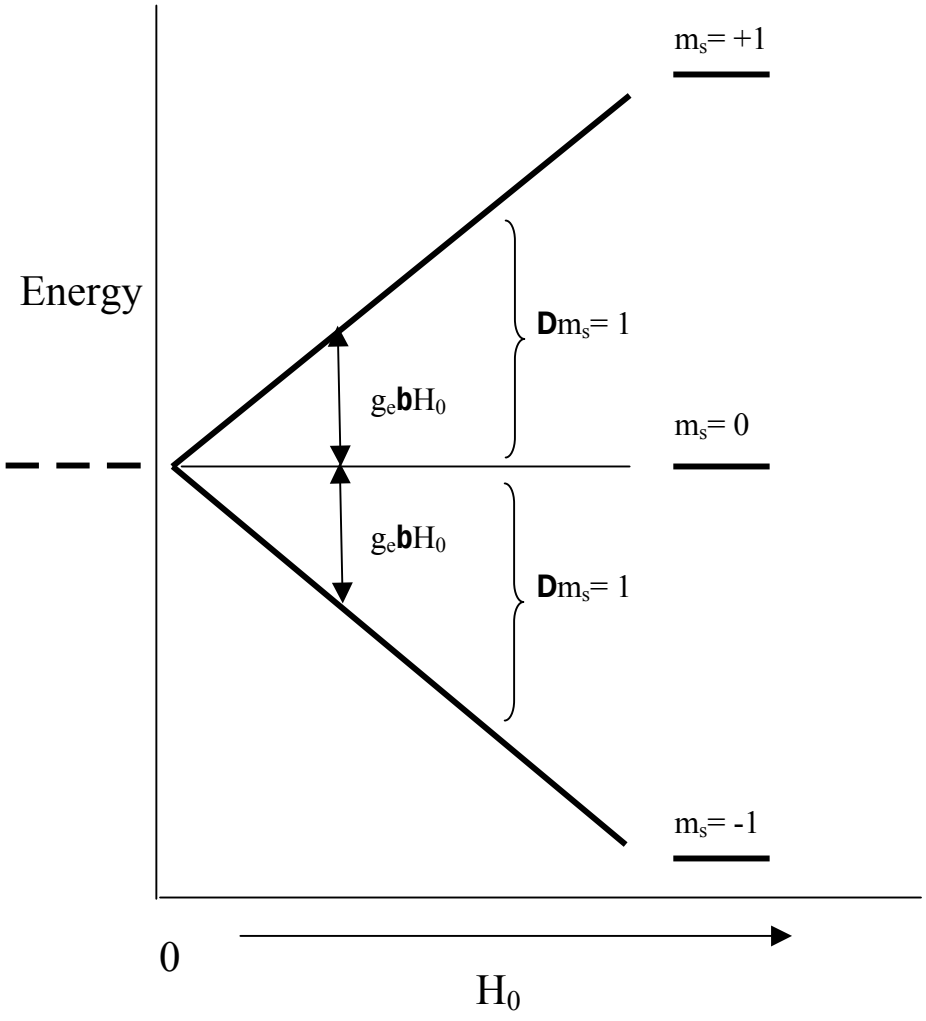

Figure III.6 EPR detectable two-electron system where $m_s = \pm 1, 0$, and $\Delta m_s = \pm 1$ transition.

The energy diagram depicted in Figure III.6 shows the degeneracy of the triplet microstates when no field is applied and the lifting of the degeneracy once a field is applied.

In the absence of any other coupling the three microstates of the triplet are degenerate and can be described by the isotropic Heisenberg Hamiltonian, $\hat{H} = -2J\hat{S}_1\hat{S}_2$. The degeneracy of the three microstates of the triplet can be lifted through spin-spin dipolar interactions in the absence of an applied field. The energy separation is described by the spin-spin Hamiltonian, $\hat{H} = \hat{S}_1 \bullet D \bullet \hat{S}_2$, and the eigenvalues are the Zero Field Splitting (ZFS) parameters D and E.[1] When two electrons interact, the exchange interaction lifts the degeneracy of the singlet and triplet states and the dipolar (ZFS) interactions lift the degeneracy of the three triplet microstates, Figure III.7.

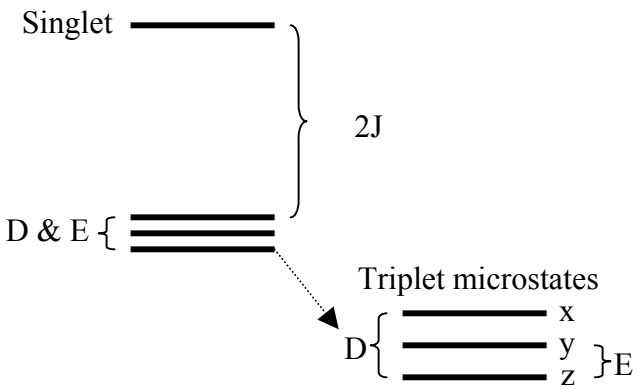

Figure III.7 Exchange parameter J in relation with the ZFS parameters D and E.

Figure III.7 is oversimplified and shows only the Zeeman interaction of spins and the magnetic field. As described in the first section, the effective magnetic field experienced by each electron is the sum of several magnetic fields: the magnetic field of the other electron, the magnetic fields of the nuclei and the magnetic field that arises from

each electron's own orbital angular momentum. The magnetic moment of the electron is much greater than that of the nulei and can be ignored. In organic systems, the contribution of spin-orbit coupling is almost zero and consequently can be ignored. The significant contribution, and the one we are concerned with, to the ZFS is the dipolar interaction between the electrons.

For organic systems, molecular geometries give rise to the anisotropic electron distributions, ZFS parameters discussed above. Figure III.8 depicts the ZFS parameters in relation to the molecular geometries of an atom, triplet excited benzene, and triplet excited naphthalene.

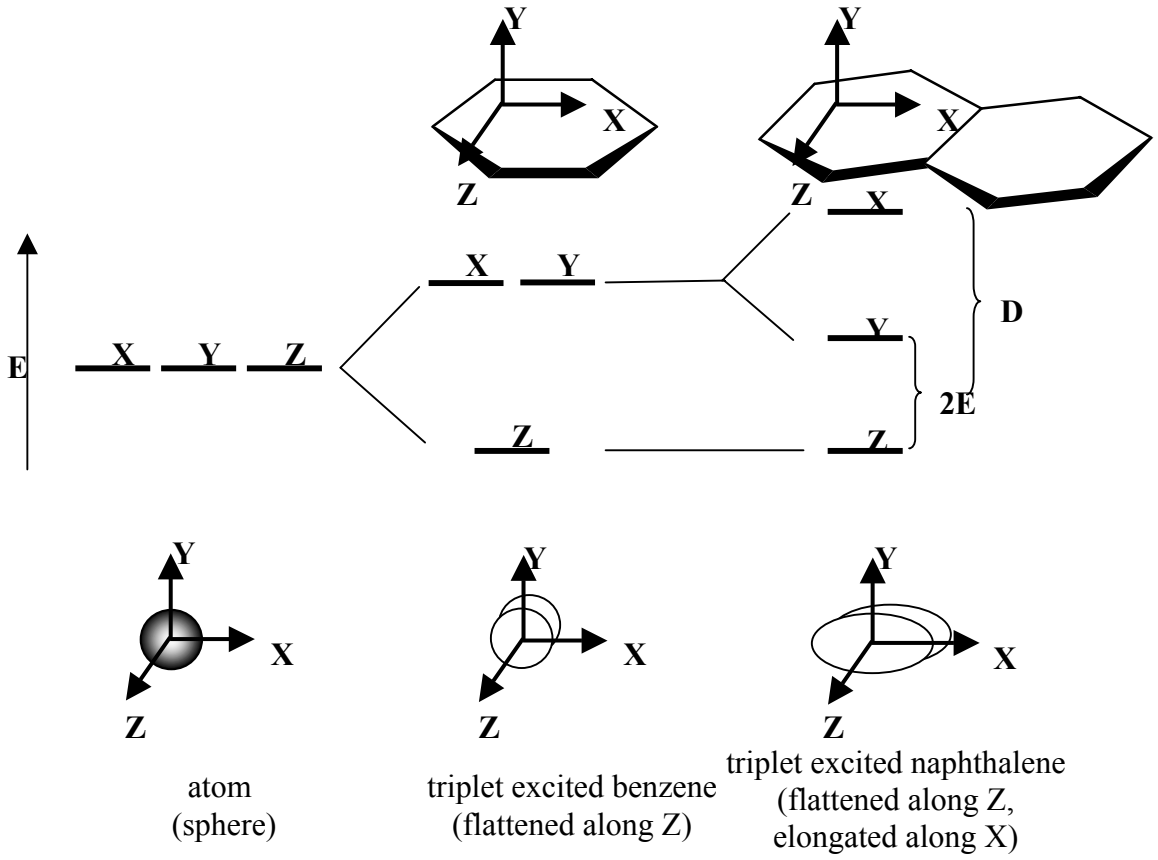

Figure III.8 Energy separation of microstates in relation with the molecular geometry of an atom, triplet excited benzene, and triplet excited naphthalene.

Figure III.8 depicts compression and elongation along certain axes in which the two electrons are confined to a certain plane, **XY**, **XZ**, or **YZ**. In an atom, the repulsive dipole-dipole interaction between the unpaired electrons cannot be minimized because there is no direction along which the electrons can move further apart. In benzene compression along the **Z**-axis maximizes the dipole-dipole interactions in the **XY** plane resulting in a lower energy Z state. In naphthalene compression along the **Z**-axis and elongation along the **X**-axis maximizes dipole-dipole interaction along the **YZ** plane resulting in a splitting of the two highest energy states. The sign of the ZFS parameter **D** is dictated by the compression along the **Z**-axis, or elongation along the **Z**-axis, to yield a positive value. Therefore, the geometrical shape of the spin distribution can be estimated from both the sign and magnitude of **D** and **E**.[1]

The three triplet species in Figure III.8 can be characterized to have three different types of symmetry; cubic, axial, and rhombic. An atom possesses cubic symmetry ($x = y = z$) but ZFS is nullified by virtue of the high symmetry. For a triplet species to have axial ($x = y \neq z$) symmetry the species must possess three-fold or higher rotational symmetry, and a magnetically isotropic plane perpendicular to the symmetry axis, as with benzene (D6h).[1]

When a triplet species with axial symmetry is placed in an external applied field this field is aligned, for example, with the **Z**-axis of the species, and only the electrons in the **XZ**- or **YZ** planes will be split by the field. The electrons in the **XY**-plane will not be affected since they are perpendicular with the applied field. With axial symmetry there are two allowed transitions but only one will be seen since they are at the same field strength. The ZFS would be dictated by the **D** parameter only ($E = 0$).

For a triplet species to have rhombic symmetry ($x \neq y \neq z$) the species must possess lower symmetry elements than a species of axial symmetry, for example naphthalene (D2h). The ZFS would be dictated by both parameters **D** and **E**. Each symmetry type will result in three distinctly different EPR spectra, where the number of signals increases as the symmetry is lowered, as shown in Figure II.9. Each signal represents where the magnetic field is oriented along one of the axes of the system.[1]

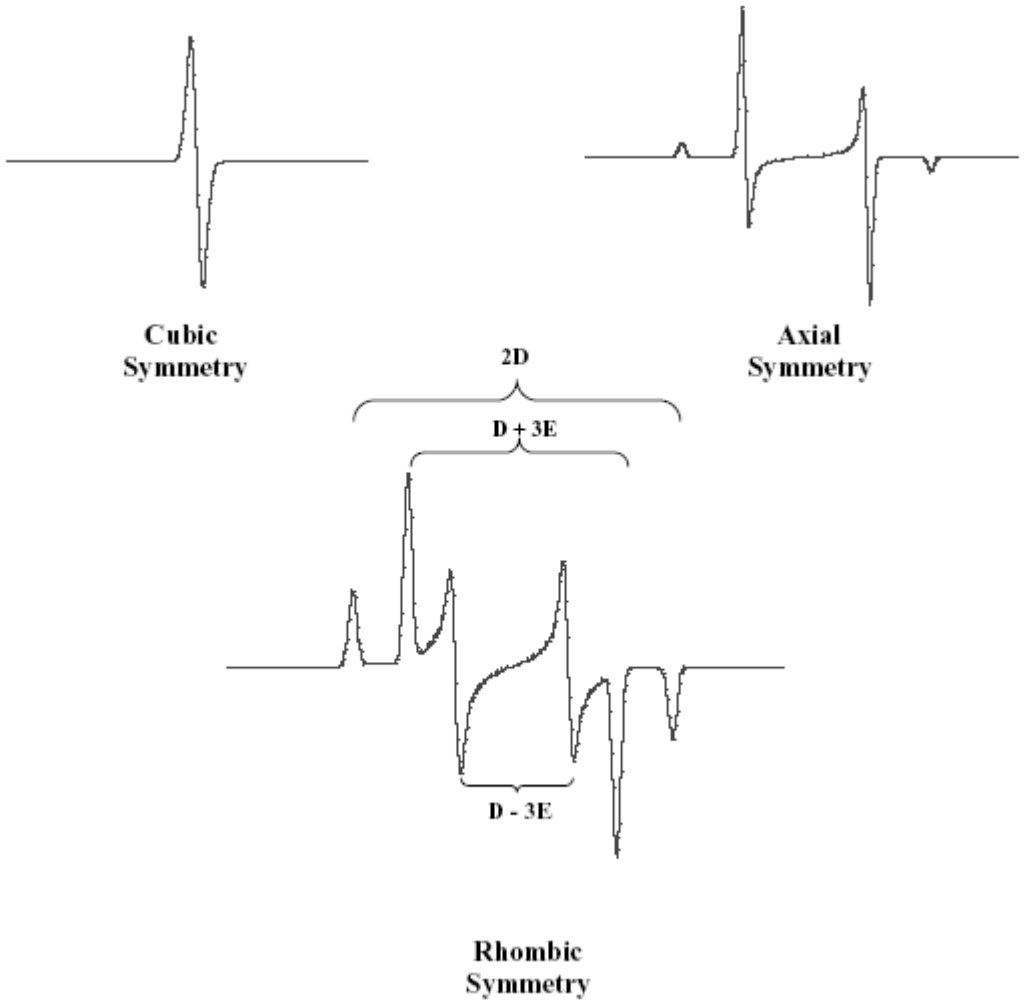

Figure III.9 Simulated spectra for a triplet excited species with cubic symmetry (D = 0), axial symmetry ($D \neq 0$; E = 0), and rhombic symmetry ($D \neq 0$; $E \neq 0$).

A species with axial symmetry has six allowed transition, but as shown in Figure III.9, there are only four. This is due to the degeneracy of two of the axes. A species with

rhombic symmetry has six allowed transition and as shown in Figure II.9, there are six displayed due to all the axes being different.[1]

All the previously mentioned transitions occur at high fields and correspond to the allowed $\Delta m_s = 1$ transitions.[1,2] Depiction of the allowed $\Delta m_s = 1$ transitions are shown in Figure III.10 denoted as the solid line double headed arrow. At lower fields the "forbidden" $\Delta m_s = 2$ transitions are sometimes observed.[1] Observation of this forbidden transition is indication that a triplet species is present.

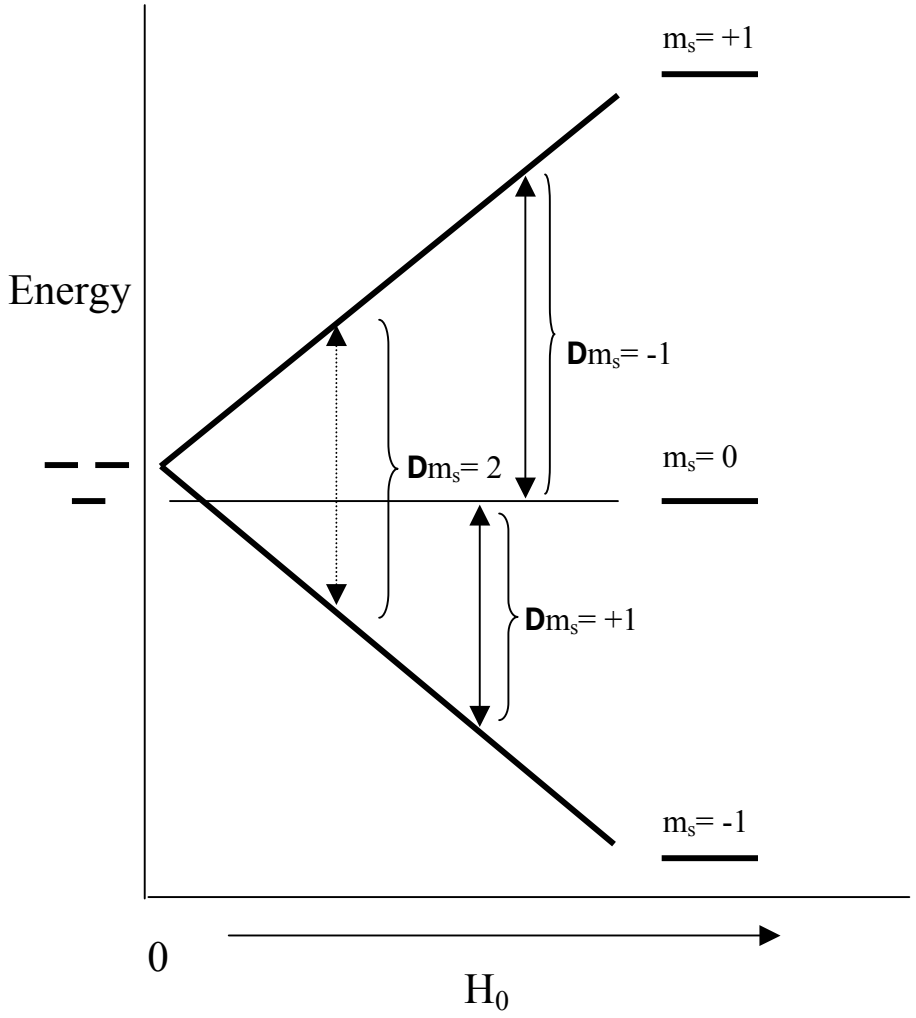

Figure III.10 The "forbidden" ΔMs = 2 transition in relation to the ΔMs = 1 transition of a triplet species.

III.B. Super Conducting Quantum Interference Device (SQUID).

In Chapter 1 it was presented that the magnetization of a material was directly proportional to the magnetic susceptibility of that material and the applied magnetic field,[2-9]

$$M = \chi_{\exp} H \tag{3.14}$$

The magnetic susceptibility is a constant; it is the sum of the diamagnetic and paramagnetic susceptibilities,[2-9]

$$\chi_{\exp} = \chi_{dia} + \chi_{para} \tag{3.15}$$

The diamagnetic susceptibility of a material can be tabulated from Pascal's constants.[9] The paramagnetic susceptibility of a material is temperature dependent and follows the Curie Law.[10]

$$\chi_{para} = \frac{C}{T} \tag{3.16}$$

We are primarily concerned with exchange-coupled spins. As described in Chapter 2, using the Heisenberg-Dirac-Van Vleck (HDVV) Hamiltonian the energy levels of the system can be predicted:

$$\hat{H}_{ab} = -2J_{ab}\hat{S}_a \bullet \hat{S}_b \tag{3.17}$$

By this definition, $\boldsymbol{J} > 0$ is ferromagnetic coupling and $\boldsymbol{J} < 0$ is antiferromagnetic coupling. Note, one must always know the definition of the Hamiltonian. If $\hat{H}_{ab} = -2J_{ab}\hat{S}_a \bullet \hat{S}_b$, then $\boldsymbol{J} < 0$ would be antiferromagnetic coupling and **D**E would equal $2\boldsymbol{J}$.

Van Vleck derived a field-independent expression relating magnetic susceptibility and the exchange coupling parameter, $\boldsymbol{J}$,[2,11]

$$\chi = \frac{Ng^2\beta^2}{3k_BT}\frac{\Sigma\left\{S(S+1)(2S+1)e^{-E_S/k_BT}\right\}}{\Sigma\left\{(2S+1)e^{-E_S/k_BT}\right\}} \tag{3.18}$$

where g is the electron g-value, **b** is the Bohr magneton, E_S is the energy of the exchange coupled spins determined using the HDVV Hamiltonian and the other constants have their usual meaning. Substituting the energy of the singlet (S=0) and triplet (T=2***J***) states:[2,11]

$$\chi = \frac{Ng^2\beta^2}{3k_BT}\frac{\left\{(0)(1)e^{-0_S/k_BT}\right\}+\left\{(2)(3)e^{-2J/k_BT}\right\}}{\left\{1e^{-0/k_BT}+3e^{-2J/k_BT}\right\}} \tag{3.19}$$

$$\chi = \frac{2Ng^2\beta^2}{k_BT}\frac{e^{-2J/k_BT}}{1+3e^{-2J/k_BT}} = \frac{2Ng^2\beta^2}{k_BT\left(3+e^{-2J/k_BT}\right)} \tag{3.20}$$

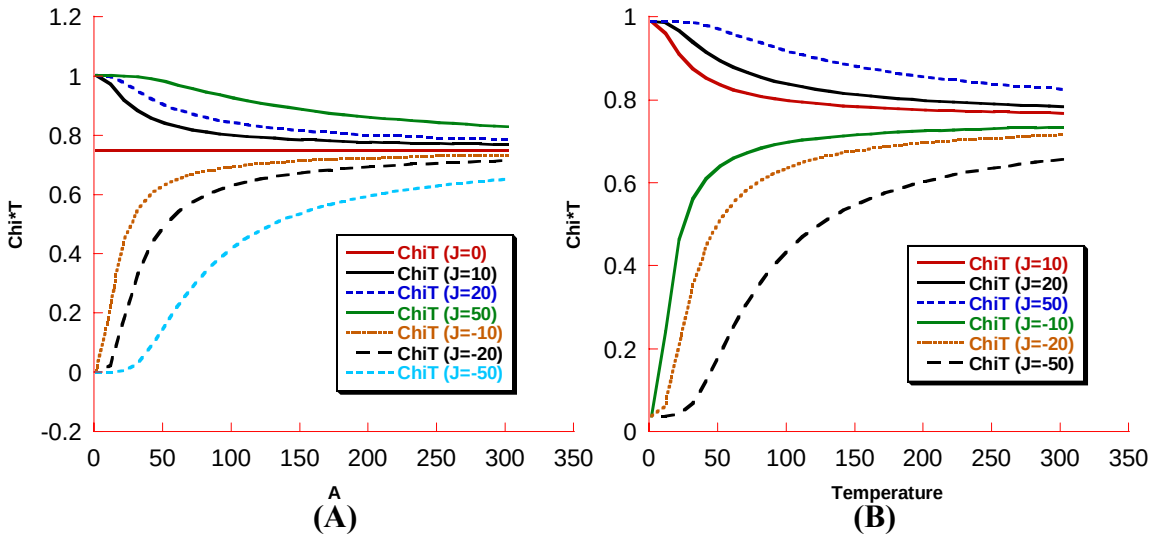

Figure III.11 Plot of **c**T vs. T for various ***J***-values. A. using Eq. 3.20. B. Using Eq. 3.21, with 5% monoradical impurity.

Note that for a ferromagnetically coupled biradical **c**T approaches unity at low temperatures and for an antiferromagnetically coupled biradical **c**T approaches zero. Both tend towards **c**T = 0.75 emu/mol at high temperatures, which is the expected value for uncoupled spins.

Monoradical impurities can be observed within the SQUID magnetometry data. These impurities can be modeled by adding the susceptibility of a monoradical to the field-independent Van Vleck expression, Eq. 3.21, assuming that the monoradical also displays Curie like behavior.[2]

$$\chi = (1-\rho)\frac{2Ng^2\beta^2}{k_BT\left(3+e^{-2J/k_BT}\right)} + \rho\frac{Ng^2\beta^2}{2k_BT} \qquad (3.21)$$

The plot of **c**T vs T for a monoradical is a straight line. Figure III.11B is a plot of **c**T vs T for a biradical with a 5% monoradical impurity. The effect on the **c**T plot is simple, ferromagnetically coupled spins approach a value below one, and antiferromangetically coupled spins approach a value greater than zero at low temperatures.

Figure III.12A is a plot of **c** vs T for a biradical. Note the difference between ferromagnetic coupling and antiferromangetic coupling. Antiferromagnetically coupled spins are typically plotted **c** vs. T, Figure III.12, which exhibits a maximum at T_{max} = 1.285 J/k.[2] Thus, a maximum in the plot of **c** vs. T is a signature of antiferromagnetic coupling.

Figure III.12B is a plot of **c** vs T for a biradical with a 5% monoradical impurity. There is very little difference in the plots of the ferromagnetically coupled spins. A **c** vs T for a biradical with a 5% monoradical impurity shows a sharp upturn at low temperatures.

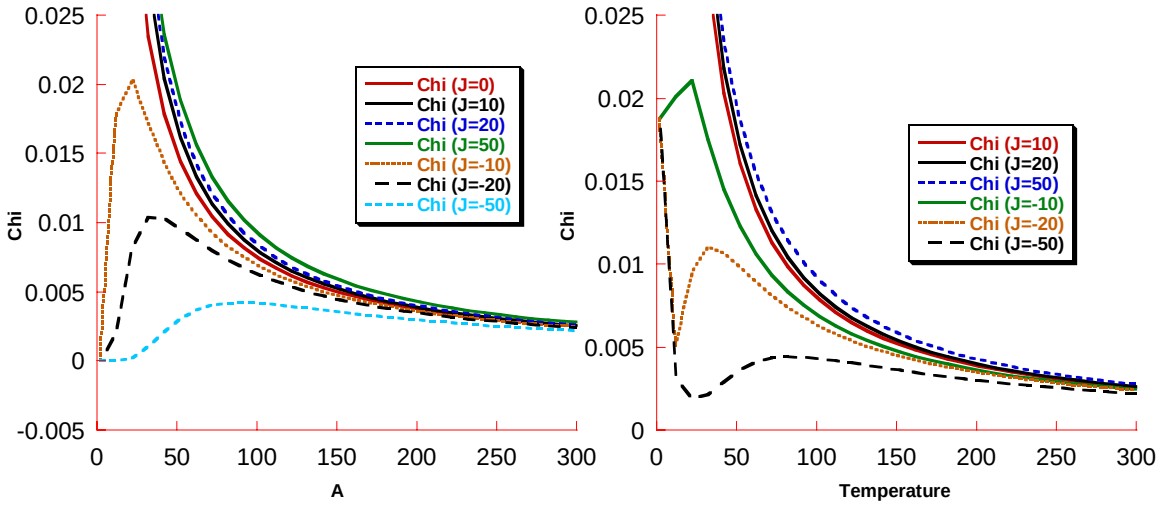

Figure III.12 Plot of **c** vs. T for various ***J***-values. A. Using Eq. 3.20. B. Using Eq. 3.21, with 5% monoradical impurity.

Our primary concern is intra*m*olecular exchange coupling, but in crystalline form there can also be intermolecular exchange coupling. Intermolecular exchange coupling can be accounted for with a Weiss mean-field correction, using the expression

$$\chi_{eff} = \frac{\chi}{1-\theta} \tag{3.22}$$

where $\theta = 2zJ'/(Ng^2\beta^2)$. [7] The origin of zJ' may be zero-field splitting, intermolecular interaction, saturation effects, or some combination of all three.[12]

III.C. References

(1) Wertz, J. E.; Bolton, J. R. *Electron Spin Resonance*; Chapman and Hall: New York, 1986.

(2) Kahn, O. *Molecular Magnetism*; VCH: New York, 1993.

(3) Drago, R. R. *Physical Methods for Chemists*; 2nd ed. ed.; HBJ Saunders: Orlando, 1992.

(4) Gatteschi, D. *Molecular Magnetic Materials*; Kluwer Academic Publishers: Amsterdam, 1991.

(5) Gatteschi, D.; Sessoli, R. *J. Magn. Magn. Mat.* **1992**, *104*, 2092.

(6) Lahti, P. M. *Magnetic Properties of Organic Materials*; Marcel Dekker, Inc.: New York, 1999.

(7) O'Connor, C. J. *Prog. Inorg. Chem.* **1982**, *29*, 203-283.

(8) Turnbull, M. M., Sugimoto, Toyonari, and Thompson, Laurence K. *Molecule-Based Magnetic Materials: Theory, Techniques, and Applications*; American Chemical Society: Washinton D.C., 1996.

(9) Carlin, R. L. *Magnetochemistry*; Springer-Verlag: New York, 1986.

(10) Curie, P. *Ann. Chim. Phys.* **1895**, 289.

(11) Van Vleck, J. H. *The Theory of Electric and Magnetic Susceptibilities*; Oxford University Press: Oxford, 1932.

(12) Caneschi, A.; Dei, A.; Mussari, C. P.; Shultz, D. A.; Sorace, L.; Vostrikova, K. E. *Inorg. Chem.* **2002**, *41*, 1086-1092.

Chapter 4

Molecular Orbital Model for Examining D-A Heterospin Biradicals.

IV. Molecular Orbital Model for Examining D-A Heterospin Biradicals.

IV.1. Using Molecular Orbital Considerations to Evaluate the Contributions to Exchange Coupling of Biradicals.

The theoretical foundations for the design principles of ferromagnetically coupled biradicals are not only well-known, but have been experimentally tested and confirmed.[1] The design motif consists of two paramagnetic functional groups attached via a "ferromagnetic coupling unit" (FCU) giving rise to SOMOs that are nondisjoint.[1-3] The qualitative approach to estimating the strength of the exchange coupling through using FCU's will be examined using a molecular orbital approach.

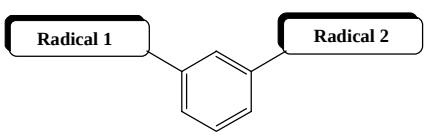

Radical 1 = Radical 1
Homospin biradical

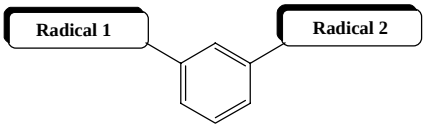

Radical 1 ∫ Radical 1
Heterospin biradical

Figure IV.1. Two paramagnetic groups attached via a ferromagnetic coupling unit with non-disjoint SOMOs, MPH type bis-SQ.

If the paramagnetic functional groups of the biradical are the same, radical 1 = radical 2, then the biradical is called homospin. If the paramagnetic functional groups are different, radical 1 ∫ radical 2, then the biradical is called heterospin.

A comprehensive table of biradicals with their exchange coupling values is presented in chapter 2. We have proposed that there is a third group of biradicals. We call this third group Donor-Acceptor (D-A) heterospin biradicals which are a special type of non-disjoint biradicals. These are like the heterospin biradicals of above in that the two

paramagnetic functional groups are different, radical 1 ∫ radical 2, but these biradicals differ in that there is no obvious coupling fragment. The design principles of D-A biradicals are quite different. In this chapter a molecular orbital description and a valence bond description will be used to explain the electronic origin of strong ferromagnetic exchange coupling in this new type of biradical. The molecular orbital description will be used to attempt to evaluate the *contributions* that D-A interactions have on the ferromagnetic coupling of D-A heterospin biradicals. The valence bond description will be used to evaluate the electronic coupling matrix element, $H_{ab,}$ which describes the efficiency of electron transfer within the biradical and promotes ferromagnetic coupling.

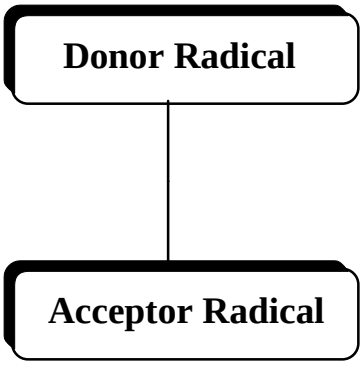

Donor ∫ Acceptor

Figure IV.2. Pictorial representation of D-A heterospin biradical, *without* coupler.

IV.1.A. The Donor-Acceptor Contributions to Ferromagnetic Exchange Coupling in HeteroSpin Biradicals.

In chapter 2 the exchange coupling in biradicals is explored. It is found that the magnetic exchange is manifest in the singlet-triplet gap.[1,3] The contributions to the exchange coupling parameter, ***J,*** and the energies of the triplet and singlet states have been derived.

$$J_{TOT} = J_F + J_{AF} = 2k - \frac{4\beta^2}{j^0 - j} \qquad (4.1)$$

If only electron-electron repulsions are considered, the first order correction to the energy is found to be 2*k*, twice the exchange integral. This is the ferromagnetic contribution to the exchange. However, if a second order perturbation is applied, where configuration interaction is considered, the new correction term is found to be $-\frac{4\beta^2}{j^0 - j}$, where **b** is the transfer integral, *j* is the two-center coulomb integral, and j^0 is the one-center coulomb integral. This is the antiferromagnetic contribution to the exchange because it mixes an excited singlet and the ground singlet with the consequence of lowering the ground singlet.

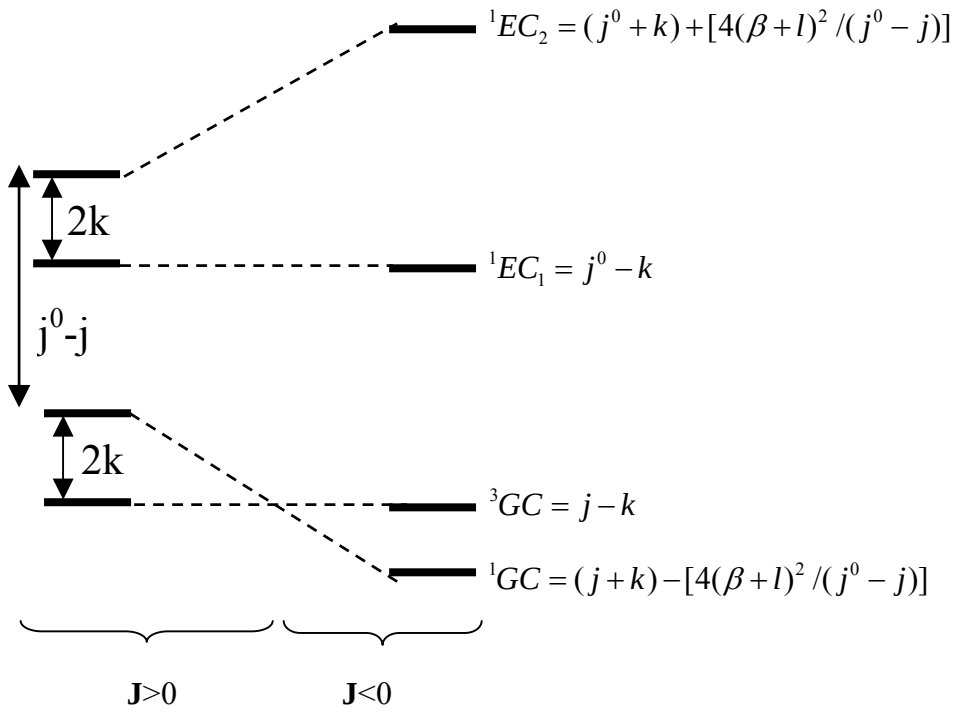

Figure IV.3. Energy states of the two electron two orbital system. Ground configuration (left) and Ground configuration with configuration interaction (right).

Molecular design principles for making ferromagnetically coupled biradicals have been developed. These design principles are represented in **p**-type biradicals that are

cross-conjugated.[1] Cross-conjugation prohibits annihilation of spins by **p**-bond formation, and provide nondisjoint SOMOs with sizeable exchange integrals.[2]

Heterospin biradicals are the simplest example of a spin diverse organic species, and are those in which the paramagnetic moieties are different.[4-8] A few representative examples are shown in Figure IV.4.

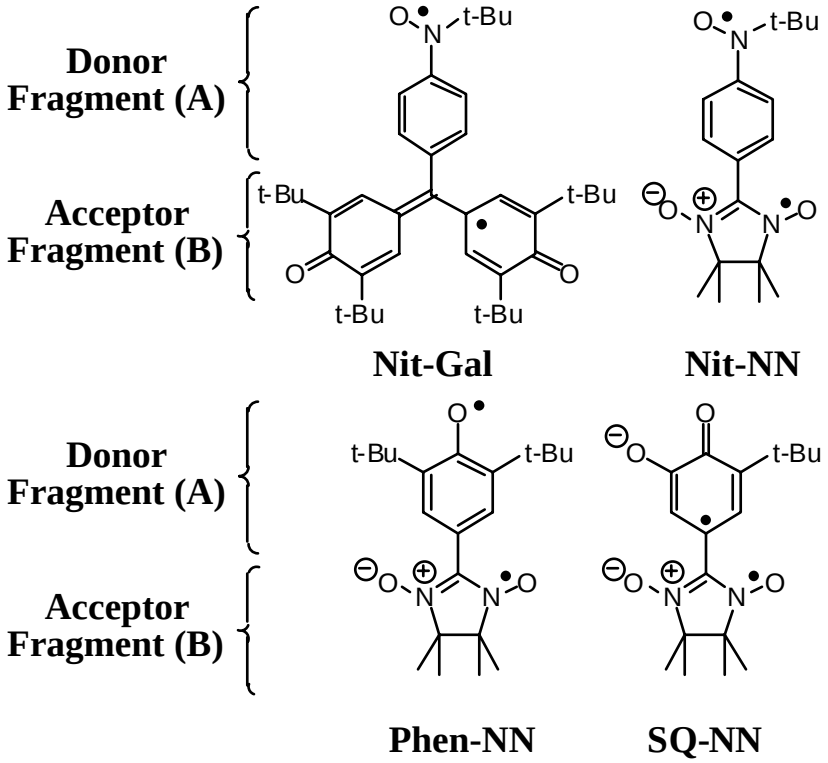

Figure IV.4. Examples of heterospin biradicals.

Donor-Acceptor interaction concepts can be used to evaluate the exchange coupling. It is important to point out that in order to construct nondisjoint SOMOs,[1-3,9] an atom of positive spin density in one radical group (fragment A) is attached to an atom with negative spin density in the second radical group (fragment B).[10,11] But in heterospin biradicals, it is the interaction of the SOMO of fragment A (the donor) with the LUMO of fragment B (the acceptor) that provides nondisjoint SOMOs. An example of frontier

orbital interactions is shown in Figure IV.5. We are going to show through this analysis that simple Hückel calculations can be used to estimate the D-A contributions to the exchange coupling.

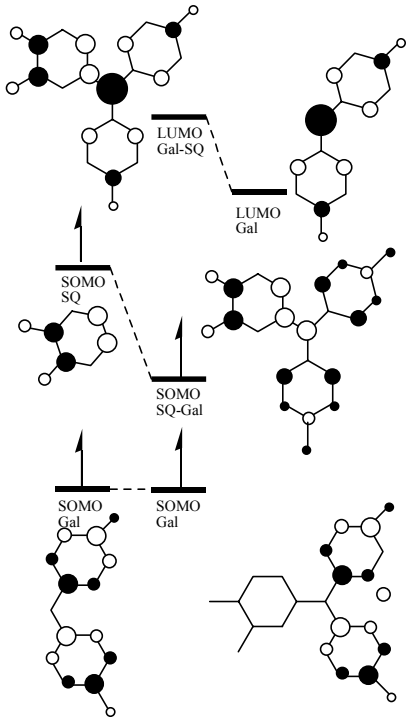

Figure IV.5. Example of a $SOMO_{donor}$ -$LUMO_{acceptor}$ interaction that creates nondisjoint heterospin biradical SOMOs.

Whangbo *et. al.* have previously used extended Hückel molecular orbital calculations for spin dimer analysis of antiferromagnetic exchange in metal dimers.[12-15]

Remember that the total exchange parameter is comprised of two components: $\boldsymbol{J_{TOT}} = \boldsymbol{J_{FM}} + \boldsymbol{J_{AFM}}$. Consider that each spin carrier in an exchange-coupled dimer contains one unpaired electron and the two spin sites are represented by magnetic orbitals $\boldsymbol{f}_a$ and $\boldsymbol{f}_b$ (i.e., singly occupied molecular orbitals representing the spin sites a and b, respectively). If t_{ab} is the hopping integral (i.e., the resonance integral) between *a* and *b*, then the J_{AF} term is related to t_{ab} as $J_{AF} = -2t_{ab}^2 / U_{eff}$, where U_{eff} is the effective on-site

repulsion, which should be nearly constant for closely related systems. In a magnetic dimer where superexchange interactions are operative, the two spin sites share at least one common atom so that their magnetic orbitals are not well defined for quantitative calculations of t_{ab}. In this case, the value of t is determined indirectly by performing molecular orbital calculations for a spin dimer.[12-15] For example, when the two spin sites in an exhange-coupled dimer are equivalent, the t_{ab} integral is related to the spin-orbital interaction energy, **D***e* (*i.e.*, the energy separation between the highest two singly occupied energy levels of a spin dimer) by t_{ab} = **D***e* /2 (Figure IV.6.).

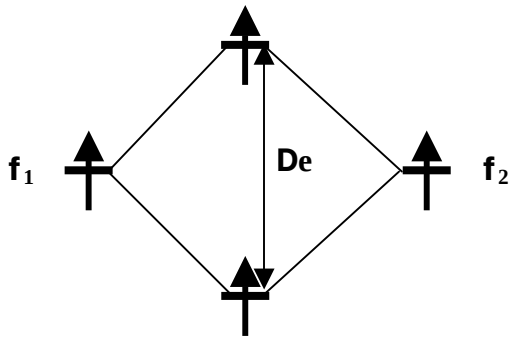

Figure IV.6. Spin-orbital interaction energy of a spin dimer made up of two equivalent spin sites.

The $\boldsymbol{J_{AF}}$ term becomes $-2\langle t_{ab}^2\rangle/U_{eff}$.[16] It has been shown that the trends in the $\boldsymbol{J_{AF}}$ parameters of extended AFM solids are explained in terms of the spin-orbital interaction energies calculated for their spin dimers using the extended Hückel method.[12-15]

The magnitude of frontier orbital interaction for a donor-acceptor dyad was first derived by Klopman and Salem for orbitally controlled chemical reactions, and is given by:[17-19]

$$\sum_{A}^{SOMO}\sum_{B}^{LUMO}\frac{2(c_{iA}c_{jB}\beta_{AB})^2}{E_A - E_B} \qquad (4.2)$$

This relationship shows that the interaction is inversely proportional to the difference in energy, E_A - E_B, between the highest occupied orbital of the donor, A, and the lowest

empty orbital of the acceptor, B, *i.e,* the frontier orbitals are proportional to the coefficients on the donor and acceptor. It should be noticed that Equation 4.2 has a similar second order form as the AF term of $\boldsymbol{J_{TOT}}$ in Equation 4.1, but Equation 4.2 contributes to the *ferro*magnetic coupling. The ferromagnetic term is now proportional to the interaction of frontier orbitals:[10]

$$J_F \propto \frac{2(c_{iA}c_{jB}\beta_{AB})^2}{E_A - E_B} \tag{4.3}$$

Because there is a node at the carbon atom of the Donor fragment, the common overlap density that creates non-disjoint SOMOs in ferromagnetic birdicals is absent in D-A biradicals. The interaction between the $SOMO_{Donor}$ and the $LUMO_{Acceptor}$ provides overlap density between the $SOMO_{Acceptor}$ and $SOMO_{Donor}$ in order to create non-disjoint SOMOs.

The exchange parameter now includes D-A interactions and can be evaluated using simple Hückel molecular orbital calculations. From Equation 4.3 it can be seen that the ferromagnetic contribution to $\boldsymbol{J_{TOT}}$ increases as the coefficients on the connecting atoms of the donor and the acceptor are maximized and the energy difference between the SOMO of the donor and the LUMO of the acceptor is minimized. Figure IV.7 contains the calculated Hückel coefficients on the fragments as well as the energies of the $SOMO_{Donor}$ and $LUMO_{Acceptor}$.[10]

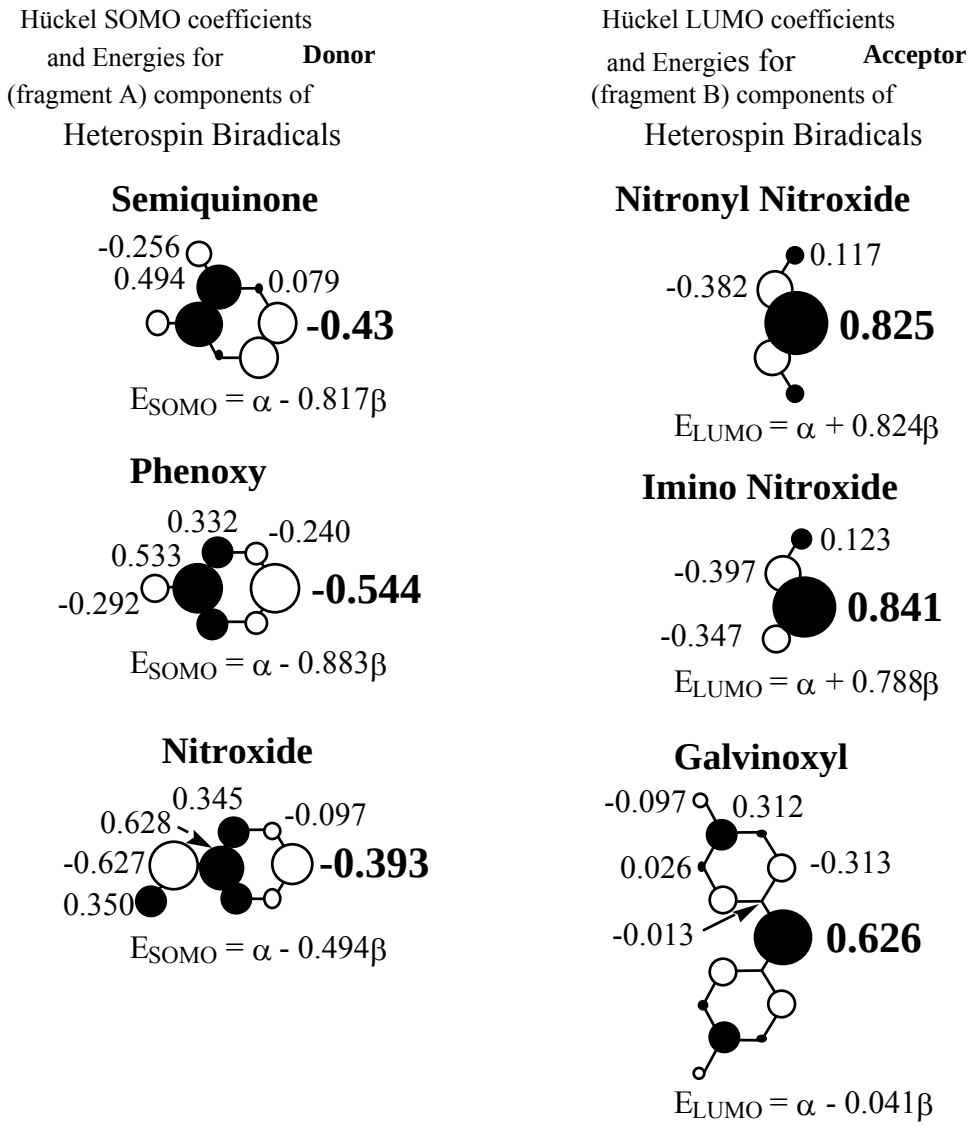

Figure IV.7. Hückel parameters used to calculate the Donor-Acceptor contribution to ferromagnetic exchange in heterospin biradicals. The bold-faced coefficients are used in the calculations.

Using the Hückel parameters the D-A contributions of heterospin biradicals to the ferromagnetic portion, $\boldsymbol{J_{FM}}$, of the total exchange parameter, $\boldsymbol{J_{TOT}}$, can be calculated. Table IV.1 contains the results of these calculations.[10]

Table IV.1. Contributions to the ferromagnetic exchange coupling due to donor-acceptor interactions.

Biradical: D/A Combination	$c_{iA} \bullet c_{jB}$ [a]	$\lvert\Delta E\rvert$ (**b**)	Ferromagnetic Contribution (**b**)[b]
SQ-NN	-0.3548	-1.641	0.1534
SQ-IN	-0.3616	-1.605	0.1630
SQ-Gal	-0.2692	-0.776	0.1868
Phen-NN	-0.4488	-1.707	0.2360
Phen-IN	-0.4575	-1.671	0.2506
Phen-Gal	*-0.3405*	*-0.842*	*0.2754*
Nit-NN	-0.3242	-1.318	0.1594
Nit-IN	-0.3305	-1.282	0.1704
Nit-Gal	-0.2460	-0.453	0.2672

[a]Product of the Hückel **b**-coefficients for the atoms providing the bonding between the Donor and Acceptor fragments of the heterospin biradical. [b]Ferromagnetic contribution to the exchange coupling calculated using the ferromagnetic term given by Eqn. 4.3.

From the Hückel calculated coefficients and energies in Figure IV.7 it is clear which fragments should allow the most interaction and therefore the highest contribution to the ferromagnetic exchange coupling parameter. Phenyl-nitroxide is the best donor and galvinoxyl should be the best acceptor. But when Equation IV.4 is used to calculate the contributions within each D-A biradical, the phenoxy-galvinoxyl D-A heterospin biradical has the largest contribution, *0.2754*(**b**). If this biradical is represented pictorially:

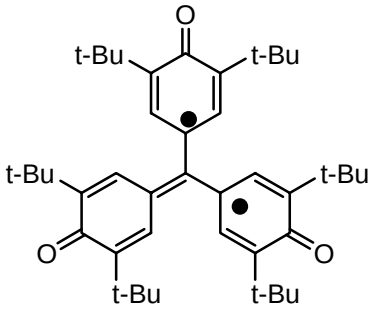

Figure IV.8. Phenoxy-galvinoxyl D-A heterospin biradical. But this is actually Yang's biradical.[20]

it is apparent that this is not a heterospin biradical, it is a homospin biradical (radical 1 = radical 2). In fact this is Yang's biradical whose exchange coupling parameter was found to be $\boldsymbol{J} \approx +240$ cm^{-1}.[20] This is strong ferromagnetic exchange coupling. Yang's biradical

is not the only known biradical from Table IV.1. We have synthesized the SQ-NN D-A heterospin biradical and found the exchange coupling parameter to be +310 cm^{-1} < ***J*** < +550 cm^{-1}.[11,21] Iwamura prepared the biradical Nit-NN, and found ***J*** ≥+ 300 cm^{-1}.[5] Paul Lahti's group prepared the biradical Phen-NN, and we reported Nit-Gal, but the ***J***- values were not measured.[22,23] By comparing Yang's biradical with our SQ-NN and Lahti's Phen-NN it can be concluded that our new D-A type heterospin biradicals can have larger exchange coupling parameters than many of the homospin biradicals. We believe that the enhanced ferromagnetic exchange coupling arises from excited state contributions to the ground state, which will be addressed further in following sections. Considering that D-A contributions to the exchange falls in line with the goal of molecular magnetism to design molecular magnets using a systematic approach coming from structure-property relationships.

We have now recast the ferromagnetic portion of exchange coupling in terms of D-A interactions and shown that these interactions are important to the total exchange. These D-A interactions give rise to non-disjoint SOMOs, which are a requirement in designing ferromagnetically coupled biradicals. In Whangbo's analysis of AFM coupled dimers, he used the interaction of the SOMOs to show trends in the AFM coupling of the dimers.[12-15] In our analysis, we use the interaction of the $SOMO_{Donor}$ and the $LUMO_{Acceptor}$ to show the contributions to the *ferro*magnetic term of the total exchange coupling parameter. The stronger the interaction between the SOMO of the Donor fragment and the LUMO of the Acceptor fragment, the stronger the ferromagnetic contribution. The frontier orbital interaction is easily calculated using Equation 4.3.

IV.1.B. Molecular orbital and spin densities are used to predict exchange coupling parameter, *J*.

Spin-coupling units have been used to rationalize qualitatively the type and strength of spin coupling in biradicals. We attempt here a semi-empirical approach to strong ferromagnetic coupling in biradicals based upon MPH and TMM as the ferromagnetic coupling units. It has been found that within some of the MPH coupled series, the existing experimental and computational data on the exchange coupling parameter, ***J***, for such biradicals may be related to spin densities on the corresponding monoradicals, which contain the spin coupling unit of interest: $J \propto \rho$ (spin density in ferromagnetic coupling unit).[11] As discussed in chapter 2, McConnell pointed out that the observed proton hyperfine splitting results from **s**-**p** electron exchange interaction called spin polarization.

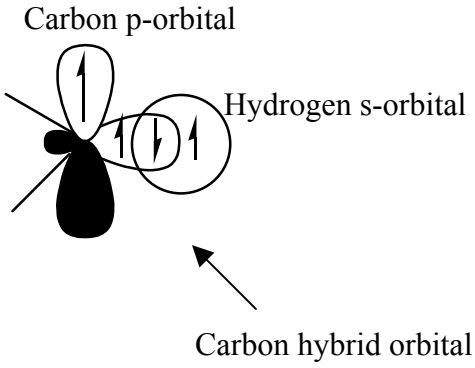

Figure IV.9. Spin polarization of CH bond.

He later suggested that the proton hyperfine splittings can be used to measure unpaired electron distributions on the carbon atoms. He developed an expression that shows that if a_i is the hyperfine splitting due to proton *i*, then a_i is related to the "spin density" at the attached carbon atom *i* by:

$$a_i = Q\rho_i \qquad (4.4)$$

Here Q is a constant, Q = -22.5 Gauss, and Q is assumed to be approximately the same for all aromatic CH bonds.[24,25]

We adapt this expression to evaluate the exchange coupling within some MPH and TMM coupled biradicals and polyradicals. Because the exchange coupling of a bi/polyradical should scale with the spin density within the coupling unit, we use the hyperfine coupling constants found experimentally via EPR or the spin densities found theoretically via Huckel MO calculations. For comparison, we use the existing exchange coupling data for the parent biradical, which contains the coupling unit in question. The expression becomes:

$$J_{NB} = \rho_A \rho_B J_{PB} \qquad (4.5)$$

Where $\boldsymbol{J_{NB}}$ is the exchange coupling parameter for the "new biradical" in question, $\mathbf{r}_A$ and $\mathbf{r}_B$ is the spin density at the point of attachment of the monoradical containing the FCU, and $\boldsymbol{J_{PB}}$ is the exchange coupling parameter of the "parent biradical" containing the FCU in question. We used this expression to evaluate some MPH coupled biradicals with reported nitroxides as the spin containing fragment.

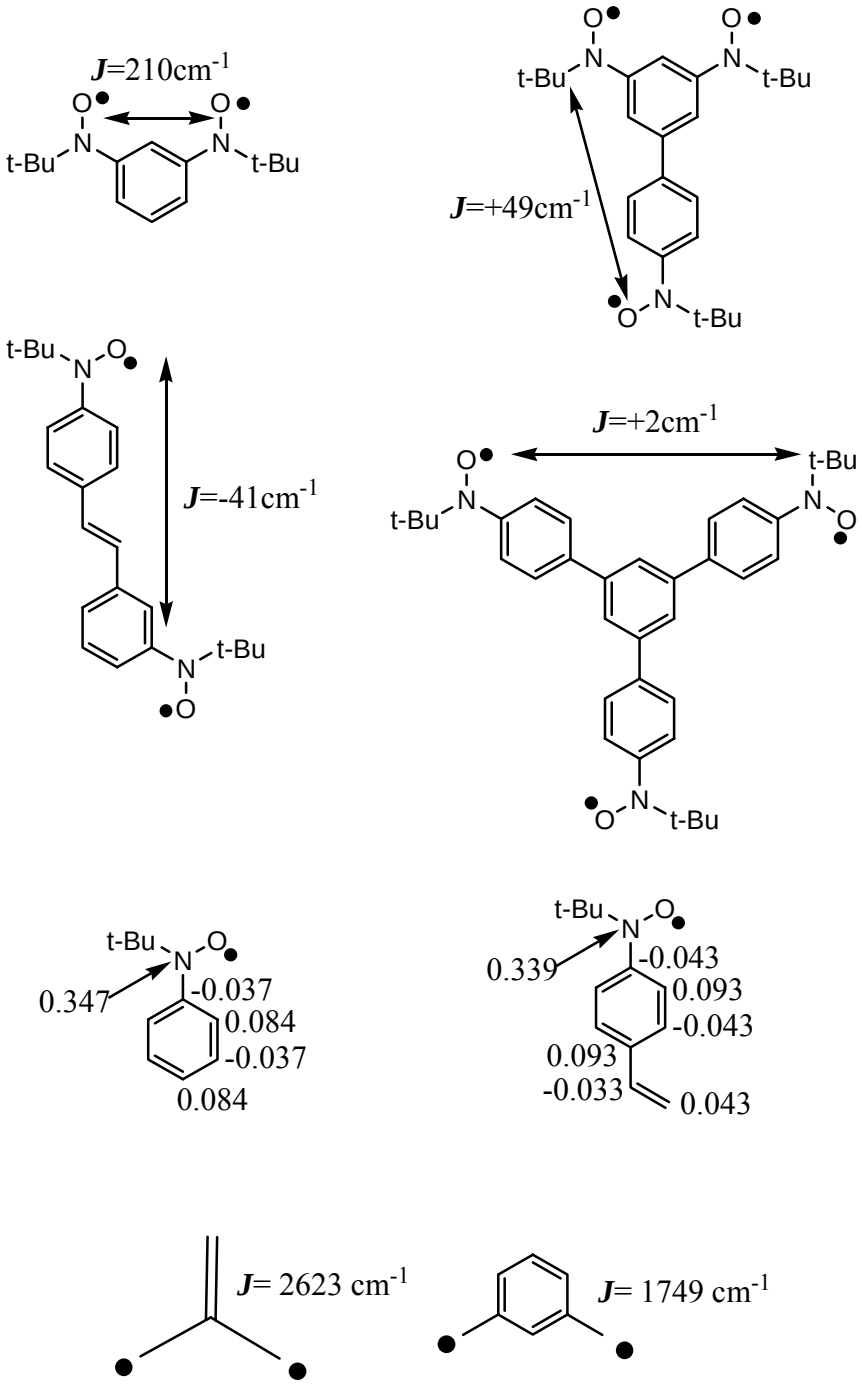

Figure IV.10. MPH coupled nitroxide biradicals with experimentally found *J*. And the spin densities found experimentally via EPR measurements. *J* values for the parent biradical.[4,26]

The calculations are as follows:

Calculated ***J*** for I: $(0.347)^2 * 1749 = 211\ cm^{-1}$

Calculated ***J*** for II: $(0.347 * 0.084) * 1749 = 51\ cm^{-1}$

Calculated ***J*** for III: $(0.084)^2 * 1749 = 12\ cm^{-1}$

Calculated ***J*** for IV: $(0.347 * 0.043) * 1749 = 26\ cm^{-1}$

If the calculated ***J*** values are compared to the experimental ***J*** values, it is evident that there is good agreement between experiment and theory.

If we do the same for our biradicals it is found that there is good agreement between experiment and theory.

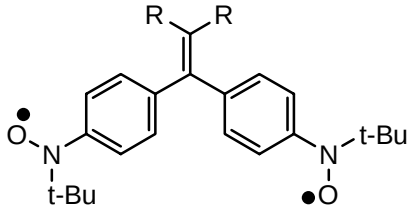

exp ***J***-values range from -14 to +26cm^{-1}

Figure IV.11. TMM coupled bis-nitroxide (Nit) with experimental *J* values.[27]

Calculated ***J*** for TMM bis-Nit: $(0.084)^2 = 18.5\ cm^{-1}$

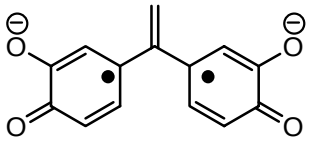

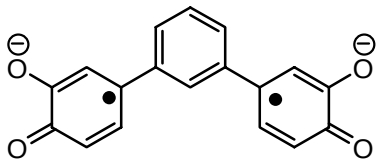

exp ***J***-values range from -26 to +160cm^{-1} exp ***J***-values range from +30 to +60cm^{-1}

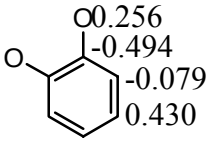

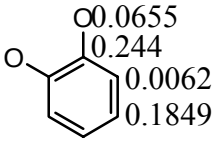

Figure IV.12. Huckel predicted SQ coefficients(bottom left), and spin densities (bottom right). (Top) TMM coupled bis-SQ (I) and MPH coupled bis-SQ (I) with experimental *J* values.[28,29]

Calculated ***J*** for TMM bisSQ: $(0.1849)^2 * 2623 = 89\ cm^{-1}$

Calculated ***J*** for MPH bisSQ: $(0.1849)^2 * 1749 = 60\ cm^{-1}$

We can use the experimentally found hyperfine coupling constant to develop an expression to predict the ***J*** values for our biradicals.

$$J_{NB} = \left(\frac{a_H(MX)}{a_H(SQ)}\right) J_{PB} \qquad (4.6)$$

Calculated ***J*** for I: $(0.094/3.34) * 2623 = 74\ cm^{-1}$

Calculated ***J*** for II: $(0.094/3.34) * 1749 = 49\ cm^{-1}$

The difference between the calculated values and the experimental values found for the TMM bis(SQ), TMM bis-nitroxides, and the MPH bis(SQ) arises from the geometrical differences. The monoradicals do not have the same geometry or twisting as the biradicals. Therefore, we see a difference in the values, but the values do fall within the range of experimental values. If we were to make monoradicals with the same geometries as the biradicals the values would be in better agreement. It is clear that a close prediction can be made as to the expected exchange coupling parameter using simple Hückel MO calculations. Using the MO design principles we will attempt to make new D-A heterospin biradicals. We will then evaluate them according to the spin density analysis given above.

IV.2. The design, synthesis and evaluation of the exchange coupling of new D-A heterospin biradicals.

Within the D-A heterospin biradicals we found that Yang's birdical would have the strongest contributions to ferromagnetic exchange, phenoxy Donor and galvinoxyl Acceptor. And as we pointed out this was actually a homospin biradical. Yang's biradical

has been found to have an exchange coupling parameter of $J = +240\ cm^{-1}$.[30] Previously we synthesized a D-A heterospin biradical with Galvinoxyl (Gal) as the Acceptor and nitroxide as the Donor. The biradical was found to be unstable in solution for long periods of time. But we were able to perform variable temperature EPR in order to find that the exchange coupling within this biradical was $J \neq 0$, either the singlet and triplet are degenerate or the triplet is the ground state.[23]

We routinely make semiquinone biradicals; therefore, it was an obvious choice to use our SQ as the Donor and the galvinoxyl (Gal) as the Acceptor. We also wanted to probe the effects of bridges within this biradical, as we did with the MSQNN birdical series. We attempt the synthesis of SQ-Ph-Gal D-A biradical. In this section the attempted synthesis of SQ-Gal and SQ-Ph-Gal D-A heterospin biradicals is described. We compare this biradical with structurally similar biradicals.

IV.2.A. Synthesis and Characterization of $Tp^{Cum,Me}$ZnSemiquinone-Galvinoxyl (SQ-Gal).

We begin the synthesis by making a methyl ester, **4.2**, of the dimethoxy protected arylbromide, **4.1**. This was reacted with two equivalents of TMS protected 2,6-ditertbutyl-4-bromo phenol, **4.3** and following workup with sodium hydroxide we obtain dimethoxy aryl galvinol, **4.4**. This is deprotected using boron tribromide to give the catechol galvinol (Cat-Gal) **4.5**. This is complexed with our $Tp^{Cum,Me}$Zn(OH) in an attempt to obtain the $Tp^{Cum,Me}$Zn(SQGal), **4.6**.

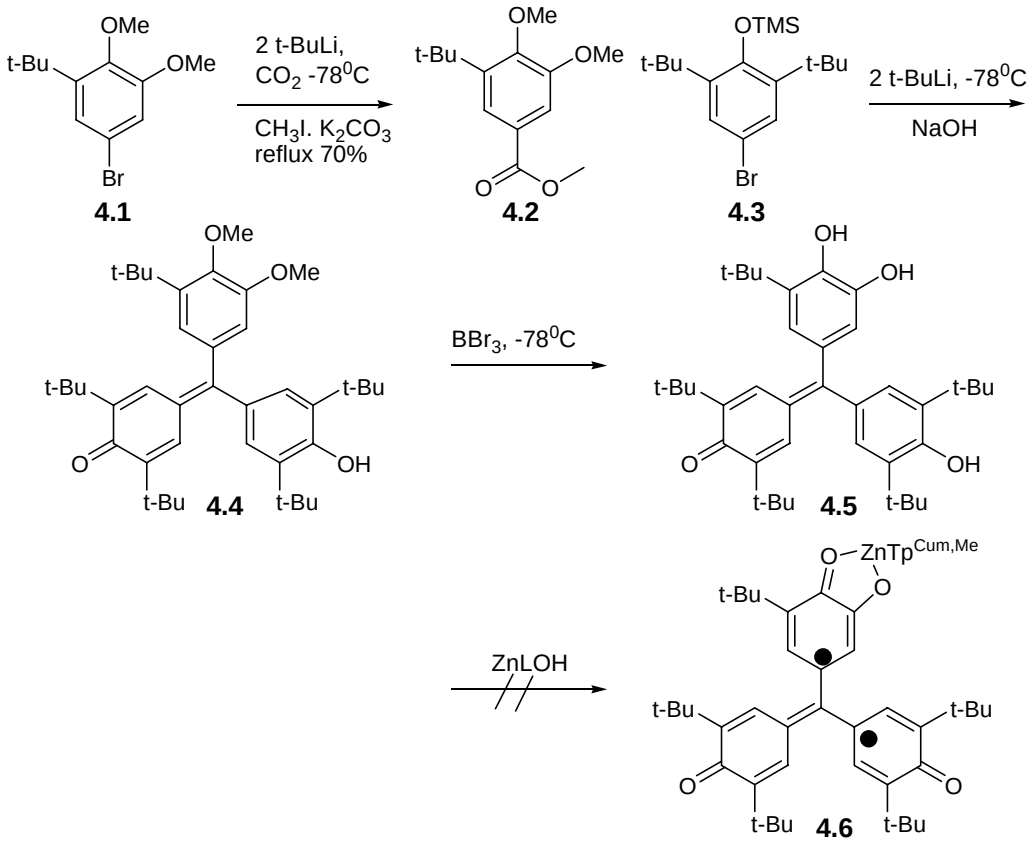

Scheme IV.1. Attempted synthesis of SQ-Gal.

After complexation we obtain a purple solid, and record an EPR spectrum in order to determine if we have the biradical. The fluid solution EPR spectrum should appear similar to the monoradical galvinoxyl with half the value of the a_H of the monoradical, but it actually had larger a_H values. Galvinoxyl monoradical is a five line pattern, resulting from 4 equivalent protons with $a_H = 1.33$ G. The fluid solution EPR spectrum is inconsistent with a biradical. We can compare the 77K EPR spectrum with known galvinoxyl-like biradicals. Figure IV.13 is the room temperature EPR spectrum (left) of Aryl-Gal for comparison and the 77K EPR spectrum (right) of "SQGal". Figure IV.14 is the 77K EPR spectra of similar galvinoxyl type biradicals.[4,20,23]

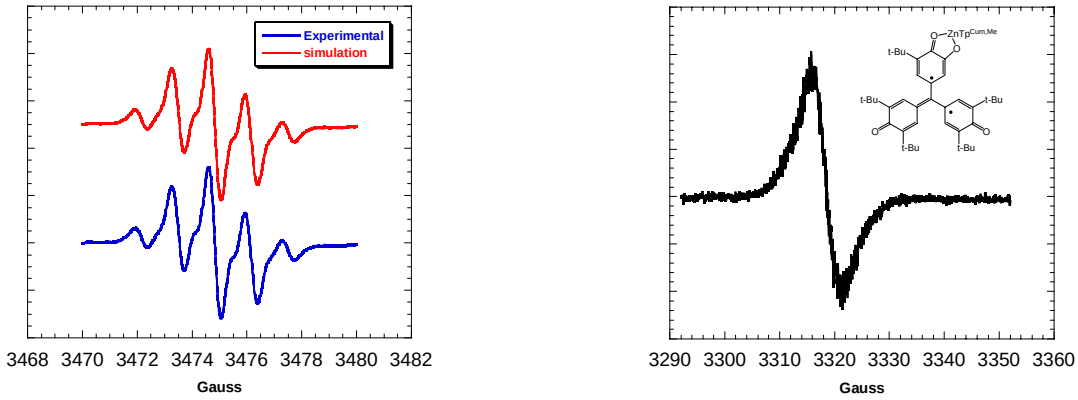

Figure IV.13. EPR spectra of: (left) fluid solution room temperature of Aryl-Gal with blue experimental and red simulation and (right) 77 K EPR spectrum of SQGal in 2-methyl THF.

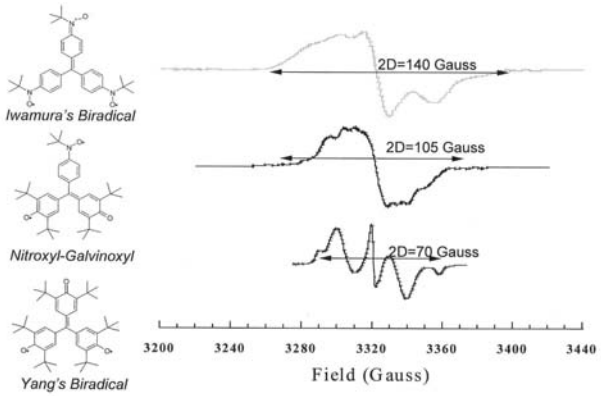

Figure IV.14. 77K spectra: from top to bottom Iwamura's bis-nitroxide, our nitroxide-Gal and Yang's biradical.[4,20,23]

It is clear that the molecule that we have made does not show the expected hyperfine couplings at room temperature or the expected zero-field splitting at 77K. Another indication that a biradical is present via EPR spectrometry is a half field transition, the **D**m_S = 2 transition. A half field signal for our sample was not observed at 77K in the EPR.

We can look at the other spectroscopic data for more information. The IR shows a strong stretch at 1560 cm^{-1}. The phenoxy radical has been found to have this

corresponding stretch.[31,32] There is another stretch in the carbonyl reagion at 1652 cm^{-1} which is consistent with the quinone stretch. There are no apparent OH stretches in the IR, indicating the absence of the catechol. The BH stretch of the $Tp^{Cum,Me}$ ligand is also present at 2500 cm^{-1}.[33] The purple color is similar to the color of Yang's biradical. Our SQGal has absorptions at 24,000, 25,000, and a broad band at 16,000 cm^{-1}. Yang's biradical has a maxium absorption at 23,000.[20] Galvinoxyl monoradical is found to have 25,000, 23000 and weak absorption max at 12,950cm^{-1}.[34] It has been found that Aryl-SQ has a SQ n**Øp** broad absorption at 10,000 cm^{-1}.[11] Our "SQGal" has the absorptions that are consistant with Yang's and galvinoxyl, but it does not have the SQ signature absorption. With the absorption data, IR data, and the EPR data it can be inferred that if we are making a biradical at all it is such small amounts that it cannot be detected spectroscopically: no half-field in the EPR and no fine structure in the 77K EPR spectrum; and no SQ n**Øp** band in the electronic absorption spectrum.

If we leave the complex in solution for longer than a few minutes the compound turns yellow and the EPR signal disappears. This result is similar to what we found for the nitroxide galvinoxyl biradical.[23] If Nit-Gal is left in solution it begins to decompose over time. This decomposition could be attribituable to the delocatization of the nitroxide radical into the ring of the galvinoxyl with which it is conjugated followed by hydrolysis. A similar situation could be happening in "SQGal". The unpaired electron could be delocalized into the galvinoxyl portion of the molecule. Which then undergoes decomposition.

We next tried to form SQGal by intramolecular electron transfer (ET). To determine if an intramolecular ET is thermodynamically favorable we use the following relationship

$$\Delta G = E_{ox}(D) - E_{red}(A) \tag{4.7}$$

We proposed the synthesis of the conjugate base of Q-GalH, Figure IV.15 (top left). We use this relationship to calculate the thermodynamically favored products of the Quinone-Galvinoxide interaction.

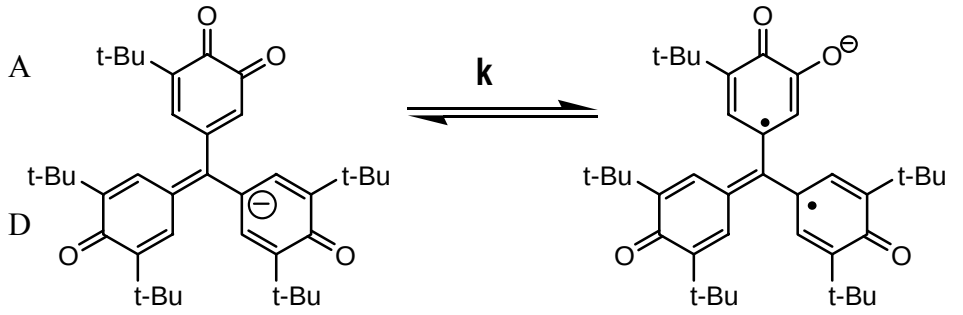

$$\mathbf{D}G = E_{ox}(D) - E_{red}(A) = -0.2V - (-0.6V) = 0.4$$

$$\mathbf{D}G = E_{ox}(D) - E_{red}(A) = -0.2V - (0.4V) = -0.6V$$

Figure IV.15. Use of oxidation potential of Donor (D) and reduction potential of Acceptor (A) to determine **D**G values to determine if the reaction is thermodynamically favored.

As can be seen, the Q-galvinoxide form is favored in the asence of a metal ion, whereas, the interaction of the (metal)quinone-galvinol, the thermodynamically favored product is the M(SQGal). Therefore, to make the M(SQGal) we need to oxidize the catechol to the quinone and the galvinol to its corresponding anion and complex with our $Tp^{Cum,Me}Zn(OH)$. When this is tried it is found that like our catechol-nitronyl nitroxide,

we cannot oxidize it to the quinone. This has been attributed to the strong electron withdrawing character of the galvinol.

In conclusion using our typical methods, complexation of a catechol to the $Tp^{Cum,Me}Zn(OH)$, does not form the $Tp^{Cum,Me}ZnSQGal$. This is evident from the lack of a half field signal in the EPR and new quinone stretch in the IR. The decomposition of the product follows what we have previously found for the nitroxide galvinoxyl biradical. If we try the complexation of our $Tp^{Cum,Me}Zn(OH)$ with the quinone-galvinoxide the thermodynamic calculations predict that the $Tp^{Cum,Me}ZnSQGal$ product is favored. But making the quinone is difficult.

IV.2.B Synthesis and Characterization of $Tp^{Cum,Me}$ZnSemiquinone-Phenyl-Galvinoxyl (SQ-Ph-Gal).

We thought that if we placed a phenyl bridge between the SQ and the Gal that would be more likely to make the biradical for two reasons: in order to "pull" the unpaired electron into the galvinoxyl, the aromaticity of the phenyl would have to be broken; we found in the MSQNN series that when a phenyl is placed between the SQ and the NN the oxidation of the catechol to the quinone is possible. We proceeded with the synthesis of the SQ-Ph-Gal.

Synthesis of the SQ-Ph-Gal is similar to our attempted synthesis of the SQGal. In the synthesis of SQPhGal, 4-bromo-phenyl-galvinol **4.9** is coupled in a Suzuki reaction with the dimethoxy protected catechol **4.1**. Deprotection of the aryl phenyl galvinol is carried out to obtain the catechol-phenyl-galvinol (Cat-Ph-Gal) **4.10**. This is complexed with $Tp^{Cum,Me}Zn(OH)$ in an attempt to form the $Tp^{Cum,Me}ZnSQPhGal$ **4.11**.

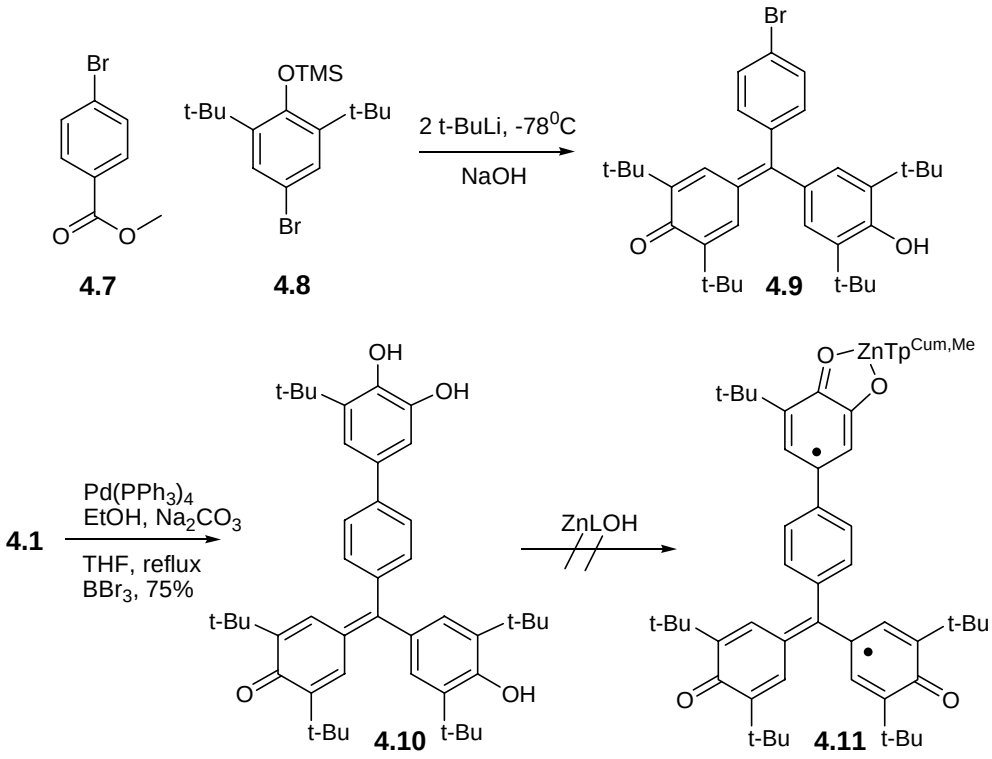

Scheme IV.2. Attempted synthesis of $Tp^{Cum,Me}$ZnSQ-Ph-Gal.

Upon complexation with the $Tp^{Cum,Me}$Zn(OH) we find a similar situation as before. The frozen solution EPR spectrum shows no structure and there is no signal at half field, suggesting the absence of a biradical in any appreciable quantity.

We attempt the method that we laid out for the SQGal, complexing the metal ligand to the quinone-galvinoxide. We make the Q-Ph-Galvioxide, and the IR has stretches at 1660 and 1600 cm^{-1}, indicative of the quinone and the phenoxy radical. But the IR does not have a stretch in the OH region, indicating the removal of the OH groups from the catechol. After complexation, the solution and frozen EPR looks like what we found for the SQGal. Again, there was no half-field signal.

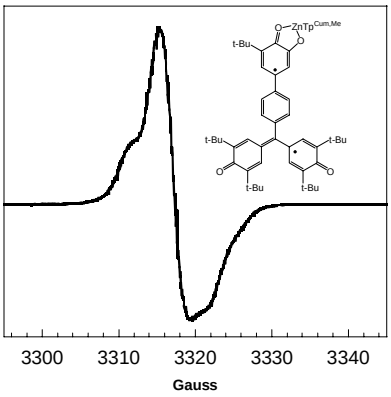

Figure IV.16. 77K EPR spectrum of SQ-Ph-Gal in 2-methyl THF.

The IR showed a strong stretch at 1654 cm^{-1}, indicative of a carbonyl compound probably the phenoxy radical. This result is much like that of the "SQGal" and the nitroxide-Gal.[23]

In conclusion, the phenyl-spaced biradical behaves like the "SQGal". Similar spectral features as the "SQGal" indicate that this biradical could be forming a biradical localized on the galvinoxyl portion of the molecule. These biradicals have similar behavior to what we have found before for a structurally similar biradical, nitroxide-galvinoxyl. This series of SQ-B-Gal cannot be made using our conventional methods.

IV.3. The Bridge (phenyl, thiophene, ethylene) Effects on the Exchange Coupling of $Tp^{Cum,Me}Zn$(Semiquinone-Bridge-Nitronyl Nitroxide).

In our analysis above we discuss the design of D-A heterospin biradicals and explain how to evaluate the extent of the strong exchange coupling in these biradicals using MO calculations and spin densities. These design principles have previously been tested and found to be in accordance with theory. We found the exchange coupling in one of these types of biradicals ($Tp^{Cum,Me}$ZnSQNN) to be quite large, $+300 < \boldsymbol{J} < +500$ cm^{-1}.[11] When we added a bridge, phenyl, between the donor and acceptor ($Tp^{Cum,Me}$SQ-Ph-NN) the exchange coupling was attenuated, $\boldsymbol{J} = +100$ cm^{-1}, but still large.[11] This is due to fact that $\boldsymbol{J}$ is expected to scale with spin density of the radical moieties.[3,35,36]

The electronic absorption spectra of the MSQ-NN complexes and the $Tp^{Cum,Me}$ZnSQ-Ph-NN complex have similar features that we expect these new D-A biradicals to possess.[11] For $Tp^{Cum,Me}$Zn(SQNN), a broad low-energy absorption feature is found in the 10,000 –15,000 cm^{-1} region, assignable as an SQ n**Øp*** transition by analogy with other SQ based chromophores. Similarly, the ~18,000 cm^{-1} band is assigned as an NN based n**Øp*** transition based on the spectroscopic similarity with the aryl nitronylnitroxide, ArNN. Additional, higher energy transitions are observed at 24,500 cm^{-1}, and 29,000 cm^{-1}. The 29,000 cm^{-1} band is assigned as the electronic origin of a NN based **pØp*** transition. The ~24,500cm^{-1} band is not present in the absorption spectra of either $Tp^{Cum,Me}$Zn(SQ) or the ArNN, which possess the SQ and NN constituent chromophores of the SQNN ligand, indicating that this transition is intrinsic to the SQNN chromophore. This is the CT band that we look for in the SQ-B-NN.[11] In Figure IV.17, the electronic absorption spectra of the $Tp^{Cum,Me}$ZnSQNN and $Tp^{Cum,Me}$ZnSQPhNN, as well as that of the constituent chromophores, ArNN and $Tp^{Cum,Me}$ZnSQ, are shown.

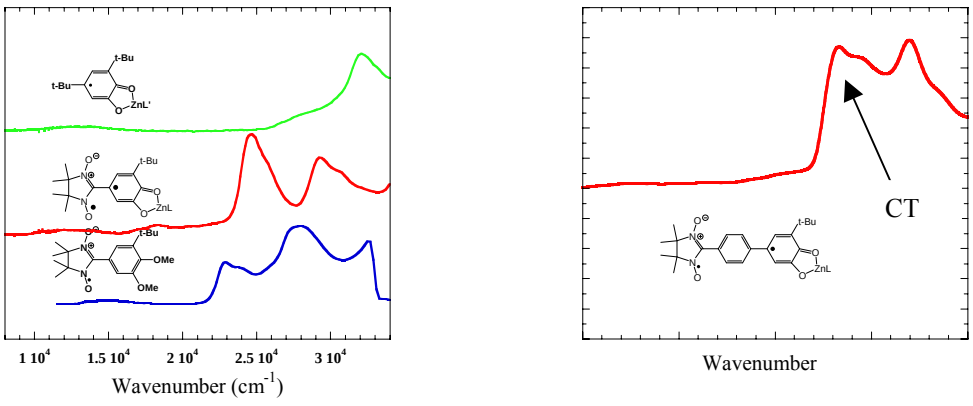

Figure IV.17. Electronic absorption spectra of ZnSQ-NN and SQ-Ph-NN with comparisons to the constituent chromaphores, MSQ and ArNN.

We wanted to investigate this further with the development of new D-Bridge-A biradicals of the form SQ-B-NN. We wished to design new D-A biradicals not only to

investigate the attenuation of exchange coupling and compare to the phenyl analogue, but also to relate the exchange coupling mechanism to electron transfer. The bridges that we proposed were thiophene and ethylene. We chose these bridges because of the anticipated ease of synthesis and these bridges have previously been used in electron transfer studies.[37]

The initial hypothesis supported by Hückel calculations was that putting a bridge between the SQ and the NN would attenuate the exchange coupling in the order: ethylene < thiophene < phenyl, this is similar to trends in conducting polymers.[37] As the number of atoms of the bridge decreases the ferromagnetic exchange coupling would be expected to increase because there would be fewer p-orbitals over which the spin density would be delocalized; therefore, greater spin density resides on the atom of attachment to the radical moieties. These results could not be substantiated because the final biradicals could not be synthesized in great enough yields. However, the preliminary optical results suggest that thiophene affects stronger coupling than phenyl, and the EPR results suggest the same.

IV.3.A Synthesis of $Tp^{Cum,Me}Zn$(Semiquinone-Bridge-Nitronyl Nitroxide): Bridge = Ethylene.

The attempted synthesis of the $Tp^{Cum,Me}$(SQ-E-NN) begins with the dimethoxymethylether protected arylbromide, **4.1**, being refluxed with tetrabutyl ammonium acetate, potassium carbonate, potassium chloride, palldium(II)acetate and acrolein diethyl acetal to yield the protected catechol-ethylene-aldehyde **4.12**. Without purification, **4.12** is deprotected to give the catechol-ethylene-aldehyde (Cat-E-CHO) **4.13**. The catechol **4.13** was then condensed with bishydroxyamine **4.17** to yield the adduct **4.14** in low yield. This adduct **4.14** was then oxidized with sodium periodate to

yield the nitronyl nitroxide catechol **4.15**. Radical **4.15** was reacted with ZnL(OH), and exposed to air oxidation.

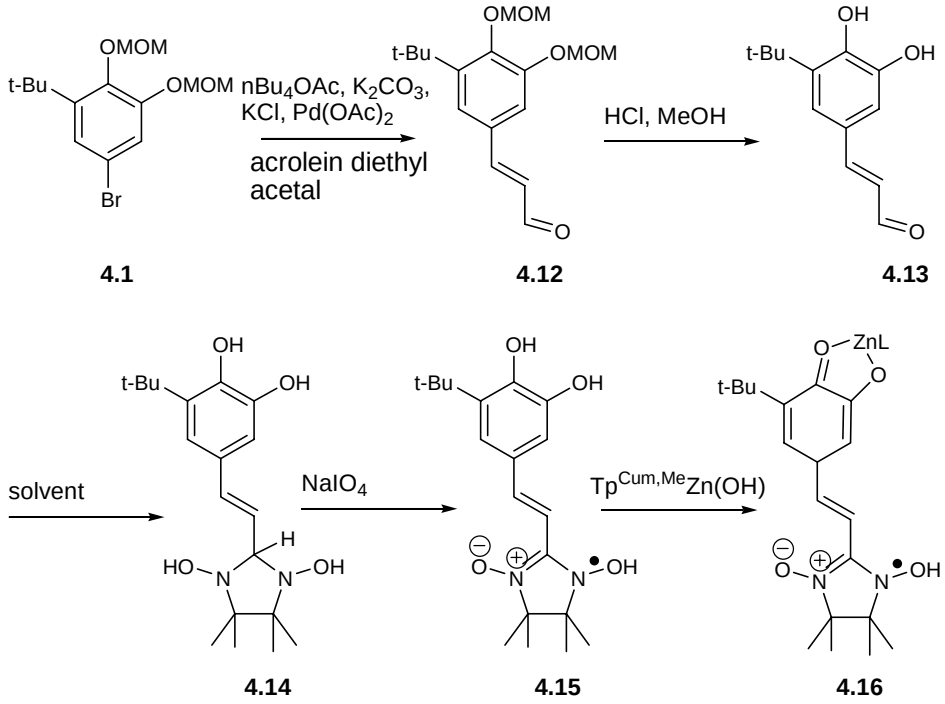

Scheme IV.3. Attempted synthesis of $Tp^{Cum,Me}$Zn(Semiquinone-Ethylene-Nitronyl Nitroxide) (SQ-E-NN).

IV.3.B. Synthetic problems.

The synthesis of Cat-T-CHO was accomplished, it seemed, in good yield, 80%. The NMR showed no impurities, the elemental analysis is consistent with the empirical formula, and the mass spectrum gave a good match to the molecular weight of the compound (all data on each compound is at end of this section). But something was peculiar about the color of the molecule. It was maroon. Because there are no obvious chromophores that absorb in the visible within this molecule, it was expected to be white. The NMR spectrum and elemental analysis suggested that whatever the impurity was, there was not a significant amount to show up in the analysis. So we decided to proceed in the usual manner.

In the typical synthesis of NN compounds an aldehyde is condensed with bis-hyroxylamine in chloroform or benzene at reflux and the result is a bis-hydroxylamine adduct.[38] During the reaction the product usually crashes out of solution and is filtered without further purification. The desired product, **4.14**, did not crash out when the aldehyde **4.13** was condensed with the bis-hydroxylamine in benzene. After examination of the NMR it was clear that there was a breakdown of the product.

We thought that the heat may be causing the breakdown. Therefore, the reaction was then conducted without any heat in order to determine if this was the problem. The reaction was monitored by NMR. After several days there was no precipitate within the reaction mixture and no appreciable amount of product seen in the NMR spectrum. We then decided to conduct the reaction in different solvents, because Dr. Scot Bodnar and Jessica Queen, former members of our group, found that this reaction is solvent dependent. We conducted the reaction in several solvents, tetrahydrofuran (THF), methanol, chloroform, and dichloromethane, following the reaction with NMR. The solvent that showed promise was THF.

The condensation was set-up in THF and the reaction conditions were modified in order to try to maximize the yield of the desired compound. After allowing for the reaction to go for several days, the NMR spectrum showed that new peaks were growing in. These peaks were consistent with the imine adduct being formed, the amine complex looses water to form the imine.

During this reaction solid did crash out. The solid was collected by filtration and washed with cold THF to yield a light pink solid, 10% yield. Inspection of the precipitate by NMR shows that it is the bis-hydroxylamine adduct **4.14** and excess bis-hydroxylamine starting material. Comparing the ratios of the adduct peaks with the ratios

of the bis-hydroxylamine peaks it was determined that the solid was about 50% pure product, making the yield of this reaction 5%. Trying to purify this compound with typical purification techniques of chromatography and crystallization did not prove effective. The compound broke down when left to crystallize in solution and on the column. With no way of purifying this compound, it was decided that this impure product would be taken on to the oxidation step.

The oxidation is carried out in dichloromethane, water and sodium periodate. The oxidation was follwed by TLC and monitored closely for color change, for the indication of the completion. In the SQ-NN parent the oxidation takes about 3 hours and is obtained in good yield, 84%, the color changes from clear colorless solution to a blue solution. Oxidation of the phenyl analogue is complete within 15 minutes. This reaction has to be monitored closely as it can overoxidize the catechol to the quinone and the nitronyl nitroxide to the iminonitroxide.

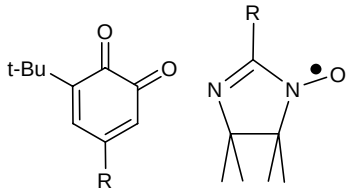

Figure IV.18. The over-oxidation products: (left) quinone and (right) imino nitroxide.

The color change of this oxidation is from clear colorless to green, nitronyl nitroxide formation, to olive, partial imino nitroxide and quinone formation, to brown, complete quinone and partial imino nitroxide formation, and if allowed to go for longer periods it goes completely to quinone imino nitroxide. Oxidation of the adduct yielded the desired compound in 10% yield. In the EPR there were 5 lines with a_N = 7.73 Gauss, indicative of a compound with 2 equivalent nitrogen atoms. There was no indication of the

corresponding imino nitroxide which would have had a 7 line pattern with a_{N1} = 4 Gauss and a_{N2} = 5 Gauss, 2 inequivalent nitrogen atoms.[1,39]

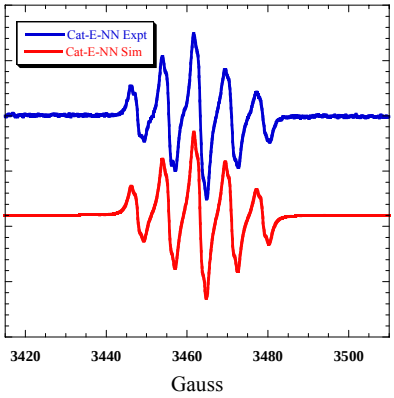

Figure IV.19. EPR spectrum of: left Cat-E-NN experimental (red) and simulated (blue).

The IR did not show any appreciable amount of quinone as indiacted by the lack of a 1660 cm^{-1} carbonyl stretch. There was a stretch at 3600 cm^{-1} indicating that the OH groups were intact. Therefore, we proceeded with the complexation.

The Cat-E-NN was complexed with $Tp^{Cum,Me}Zn(OH)$. The fluid solution room temperature spectrum does not indicate that the biradical is formed. When the exchange coupling is much greater than the hfcc the a_N of the biradical should be half the value of a_N of the monoradical. This means that the a_N of the biradical should be a_N ° 3.75 Gauss. It is unclear from the solution EPR what is present, but no 5-line pattern with a_N ° 3.75 G is discernable.

We can simulate the expected spectrum of the SQ-E-NN and overlay it with the experimental spectrum to see the difference

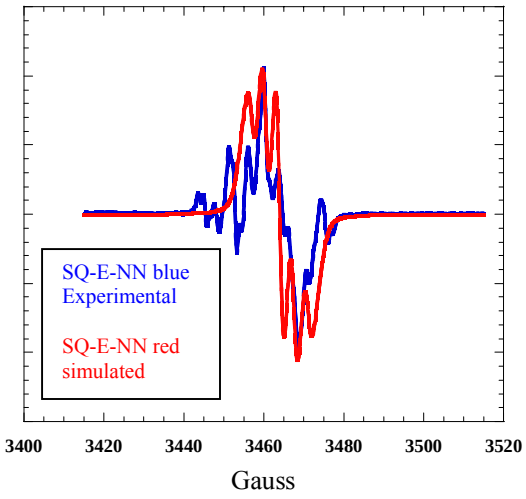

Figure IV.20. Overlay of (blue) SQ-E-NN experimental and expected simulated spectrum of (red) SQ-E-NN to show impurity of biradical.

As explained in chapter 3, biradicals exhibit a formerly forbidden transition, $\mathbf{D}m_s = 2$, at half field. If we take an EPR at half field at 77K, there seems to be some biradical present, but the signal is very weak.

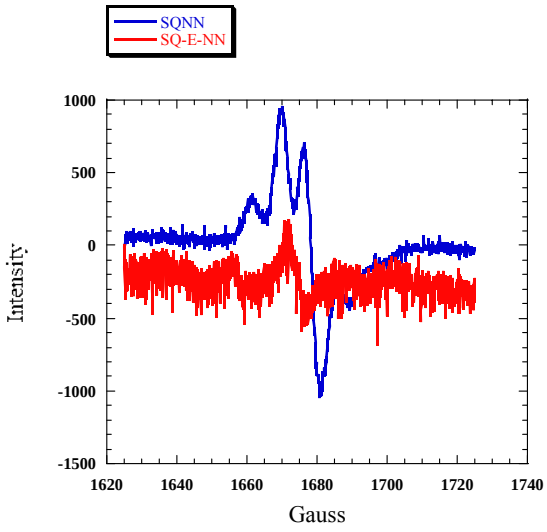

Figure IV.21. Overlay of 77K EPR spectrum of SQ-E-NN (red) and SQ-NN (parent biradical) (blue) in 2-methyl THF at half field, looking for the signature biradical transition, $\mathbf{D}m_s = 2$.

If we look at an overlay of the spectrum of the parent biradical, SQ-NN, we can see that they have similar structure.

If we inspect the electronic absorption spectrum of the assumed biradical SQENN, there is no apparent CT band that we expect to see in these D-A heterospin biradicals.

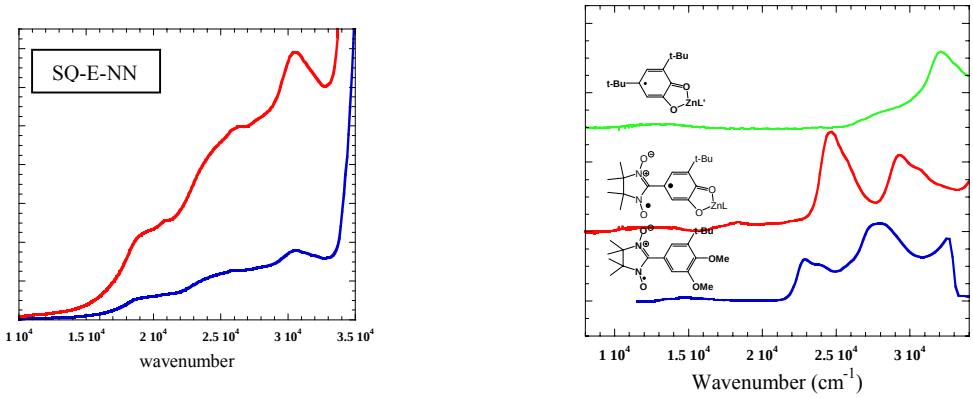

Figure IV.22. Electronic absorption spectrum of left SQ-E-NN and right ZnSQ-NN parent biradical.[11]

From the **D**m_s = 2 EPR spectrum being very weak and no apparent structure in the electronic absorption, we can infer that very little of the biradical is being formed.

During the synthesis of the biradical it was noticed that when the Cat-E-CHO was placed in $CDCl_3$ for NMR the solution turned from a maroon color to green. When the NMR was taken it was a mess. It did not look like the NMR that was taken in d_6-DMSO, which was a maroon solution with all the correct peaks and splittings expected for the compound. Because one of the breakdown products of $CDCl_3$ is hydrochloric acid, it is suspected that the molecule may be undergoing acid catalyzed keto-enol tautomerization within the tube.

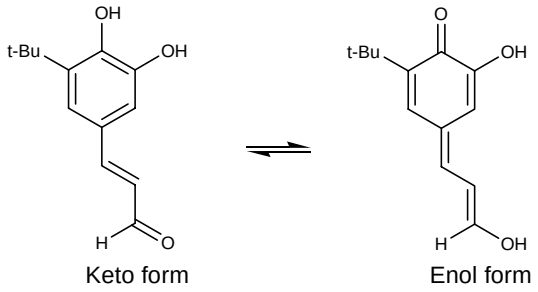

Figure IV.23. The keto-enol tautomers of Cat-E-CHO.

IV.3.C. Conclusions on the synthetic problems and proposed solutions of $Tp^{Cum,Me}$Zn(Semiquinone-Ethylene-Nitronyl Nitroxide).

The problem with this synthetic procedure seems to begin with the deprotection of the dimethoxymethylether catechol-ethylene-aldehyde **4.13**. The solid product formed should be white and it is maroon. Therefore, an obvious solution to this problem is to find a protecting group that can be carried through to the oxidation of the bis-hydroxylamine and be removed after the formation of the nitronyl nitroxide. This could be helpful for two reasons, it would prevent keto-enol tautomerization from occurring (if that in fact is occurring), and it could allow for the clean oxidation of the catechol-bridge-nitronyl nitroxide. Currently there is a student in our group pursuing this effort.

IV.3.D. Synthesis of $Tp^{Cum,Me}$Zn(Semiquinone-Bridge-Nitronyl Nitroxide): Bridge = Thiophene.

The attempted synthesis of the $Tp^{Cum,Me}$(SQ-E-NN) starts with the dimethoxymethylether protected arylbromide, **4.1**, two equivalents of t-BuLi was added to undergo a lithium-halogen exchange. The aryl lithium was quenched with trimethyl borate to give the boronic ester **4.17** of the starting material. The boronic ester **4.17** is coupled with 2-bromo-5-thiophene carboxyaldehyde in a Suzuki coupling to give the dimethoxymethylether catechol thiophene carboxaldehyde **4.18**, which upon deprotection yielded the catechol thiophene carboxaldehyde (Cat-T-CHO) **4.18**. The catechol **4.18** was

then condensed with bishydroxyamine **4.8** to yield the adduct **4.19** not in good yield and impure. This adduct **4.19** was then oxidized with sodium periodate to yield the nitronyl nitroxide catechol **4.20**. The Zn^{II} complex was attempted **4.21** to be made using $Tp^{Cum,Me}Zn(OH)$, and air oxidation as seen below in Scheme IV.4.

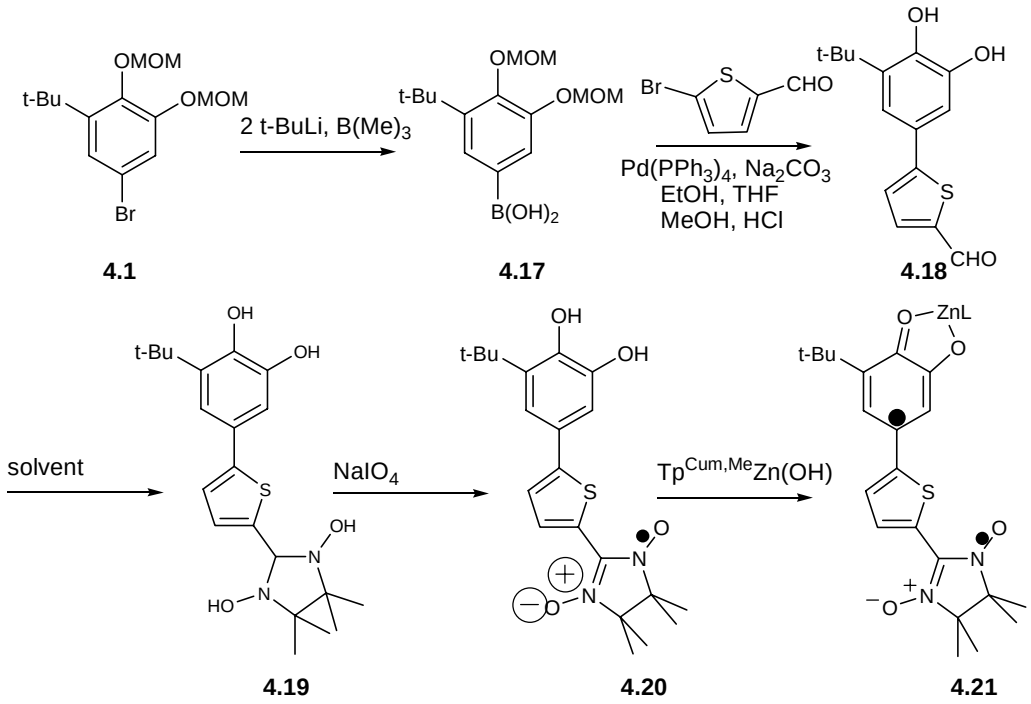

Scheme IV.4. Attempted synthesis of $Tp^{Cum,Me}Zn$(Semiquinone-Thiophene-Nitronyl Nitroxide) (SQ-T-NN).

IV.3.E Synthetic problems.

The synthetic issues with this molecule also seem to have their origins in the deprotection of the dimethoxylmethylether protected catechol. When the deprotection is performed we get a green solid. The green solid gives a the expected NMR spectrum in d_6-DMSO, shows good agreement with elemental analysis and the mass spectrum is in good agreement with the calculated molecular mass. Unlike the ethylene analogue, most of the green can be rinsed away with dichloromethane. But this is at a cost of product. After rinsing with dichloromethane, only 20% of the expected product is recovered.

When the condensation of the bis-hydroxylamine and the aldehyde of the thiophene is carried out we have similar problems as with the ethylene analogue. When the reaction is refluxed in any of the solvents the bis-hydroxylamine product looses water to form the corresponding imine product like the ethylene. Because of this issue we tried to do this reaction in the absence of heat and for longer periods. There was product being formed, but very slowly. As the reaction went for longer periods it appeared as though the product began to breakdown into the imine. The longer the reaction went the more imine product was formed. This was clearly not the answer.

We separarted the compound using MPLC, due to streaking on a conventional column. Although, it still streaked and left some of the imine product behind. The yield of the reaction to begin with was less than 20% of impure product, and after separation there was about 5% of the product expected.

Nevertheless, small amounts of product were isolated. It was taken on to oxidation with sodium periodate. In the course of the oxidation it was difficult to obtain the nitronyl nitroxide only was impossible. Mixtures of quinone, imino nitroxide and NN were obtained. It seemed to behave like the phenyl analogue. Separation of products needed to be performed. Upon separation, we obtained the Cat-T-NN with the signature five line pattern and a_N = 7.55 Gauss. The IR showed little to no quinone, by the absence of 1660 cm^{-1}, and the OH stretch at 3600 cm^{-1}.

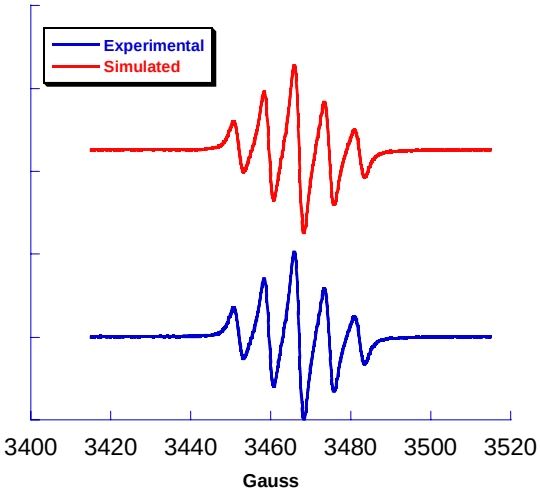

Figure IV.24. Fluid solution room temperature spectrum of Cat-T-NN in 2-methyl THF, blue experimental and red simulated.

This was reacted with the $Tp^{Cum,Me}Zn(OH)$ to form the SQ-T-NN. After complexation an EPR is taken. The spectrum is expected to have a_N values that are half that of the monoradical. The EPR spectrum looked similar to that found for the ethylene analogue. It is unclear what is present, but no 5 line pattern with a_N ° 3.75 G is discernable. If the spectrum is overlaid with the Cat-T-NN it seems as though some of the nitronyl nitroxide remains.

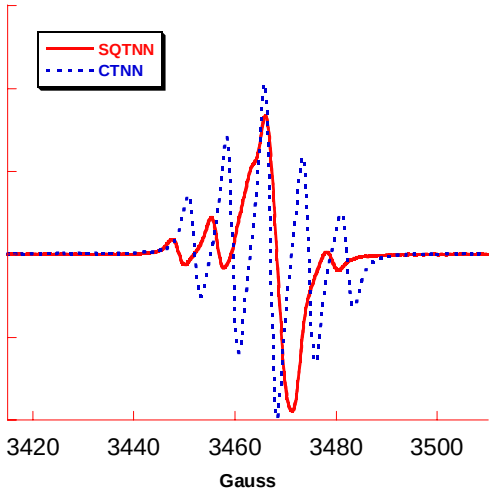

Figure IV.25. Overlay of fluid solution EPR spectrum of (blue) Cat-T-NN and (red)SQ-T-NN to show that the expected hfcc is not present.

We use the IR spectrum for clues as to what is happening. If a stretch in the OH region remains, then the molecule is either not fully oxidized or there is protonated catecholate present.

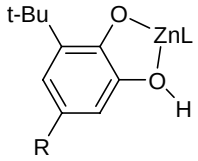

Figure IV.26. Protonated catecholate.

In either case further oxidation would be required. If there is a stretch in the 1660 cm^{-1} this is indicative of the quinone being formed. And finally if there is a stretch around 1720 cm^{-1} an anhydride is expected.[40] The IR spectrum shows that there are multiple stretches in the carbonyl region. There is a stretch present at 1660 and 1721 cm^{-1}. So the remaining nitronyl nitroxide that is present in the EPR spectrum could be a combination of quinone-T-NN and anhydride-T-NN.

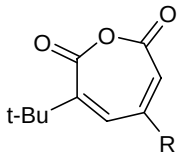

Figure IV.27. Anhydride T-NN.[40]

We look for the signature biradical **D**m_s = 2 signal at half field in the EPR spectrum. Indeed it is present and strong.

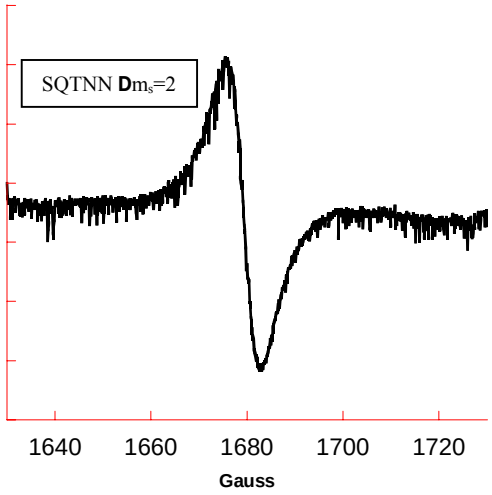

Figure IV.28. EPR spectrum of SQ-T-NN, **D**m_s = 2 signal at 77K at half field, in 2-methyl THF.

This is a good indication that we have a triplet biradical species present and in good amount.

We investigate the electronic absorption spectrum to see if it contains the CT band that we believe to be present in these D-A biradical, Figure IV.29. There appear to be a few bands in the region in which we expect to see the CT band. The bands that are present are lower in energy than the CT band of the phenyl analogue.

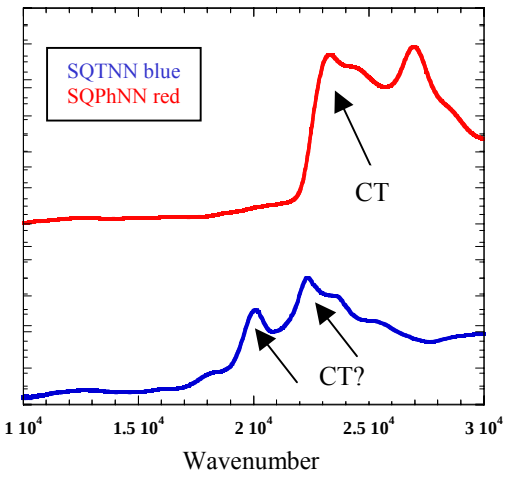

Figure IV.29. Electronic absorption spectrum of SQ-T-NN (blue) in comparison to the phenyl analogue (red). (Note: Arrows indicate CT band.)

These bands not only have the possibility of arising from the SQ**Ø**NN CT, but they could also be due to the CT's from the bridge, for example, if we consider a CT from the $HOMO_B$ to the $SOMO_{SQ}$ we would expect a ^{3}CTC which would mix with the ^{3}GC lowering the ^{3}GC, Figure IV.30. If we consider a CT from the $HOMO_B$ to the $LUMO_{NN}$ we would expect a ^{1}CTC, which would mix with the ^{1}GC lowering the ^{1}GC, Figure IV.30. If we consider a CT from the $HOMO_B$ to the $SOMO_{NN}$ we would expect a ^{1}CTC, which would mix with the ^{1}GC lowering the ^{1}GC, Figure IV.30.Without more spectroscopic data we cannot assign one of these bands to any of these CT processes.

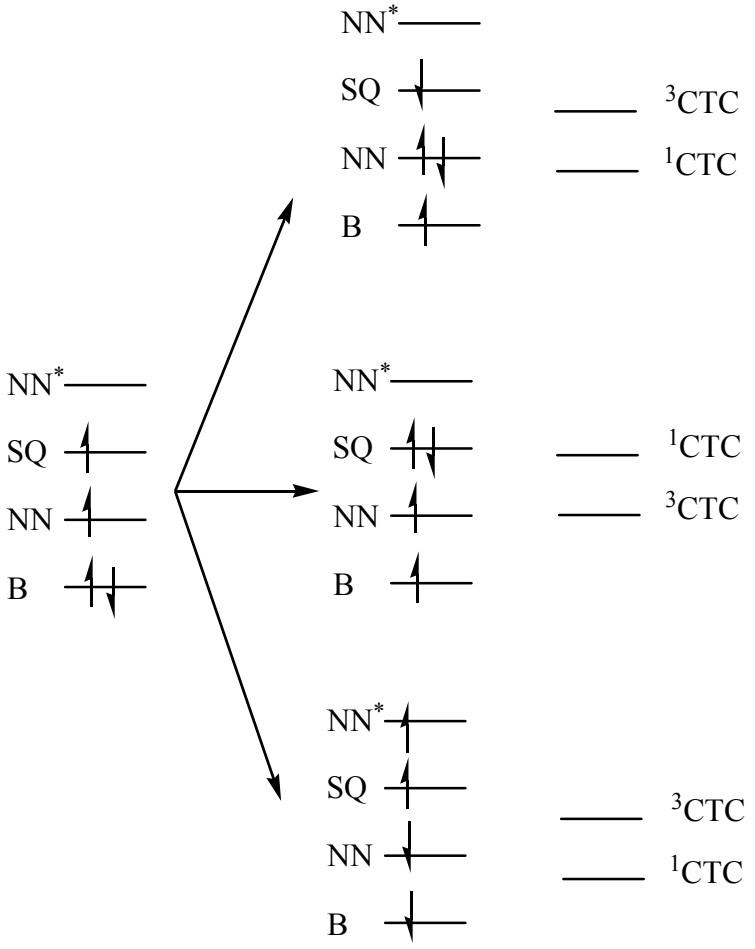

Figure IV.30. Possible CT from the $HOMO_{Bridge}$ (thiophene) to: (top) $SOMO_{NN}$, (middle) $SOMO_{SQ}$ and (bottom) $LUMO_{NN}$, and the possible CTC states that arise.

We performed variable temperature magnetic susceptibility measurement to obtain the exchange coupling parameter. Because the sample was impure it had to be fit using an impurity factor as discussed in chapter 3. The data was fit with the following equation from chapter 3:[41]

$$\chi = (\rho)\chi_{Blean-Bowers} + (1-\rho)\chi_{J=0} = (\rho)\frac{2Ng^2\beta^2}{kT\left[3+e^{-2J/kT}\right]} + (1-\rho)\frac{Ng^2\beta^2}{2kT}$$

$$\chi = (\rho)\frac{3.00375}{T\left[3+e^{-2J/kT}\right]} + (1-\rho)\frac{0.751}{T} \qquad (4.8)$$

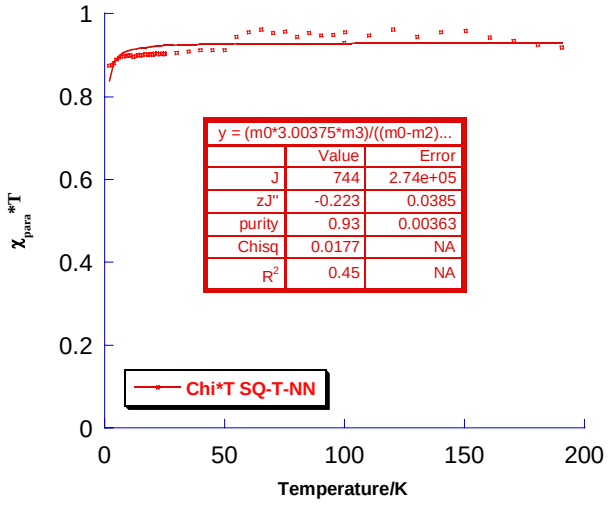

Figure IV.31. $\chi_{para}T$ vs T for the impure biradical SQ-T-NN.

Because the exchange coupling was found to be constant over the temperature range used, we can put a lower limit on the ***J*** value of +300 cm^{-1}.[11]

IV.3.F. Conclusions and possible solutions to synthetic problems.

There appears to be evidence of strong ferromagnetic coupling within the thiophene analogue. Irrespective of the possible shift of the CT band of the SQTNN in the electronic absorption spectrum to lower energy than the phenyl analogue, which suggests less mixing of the $SOMO_{Donor}$-$LUMO_{Acceptor}$, the magnetic data suggest otherwise.

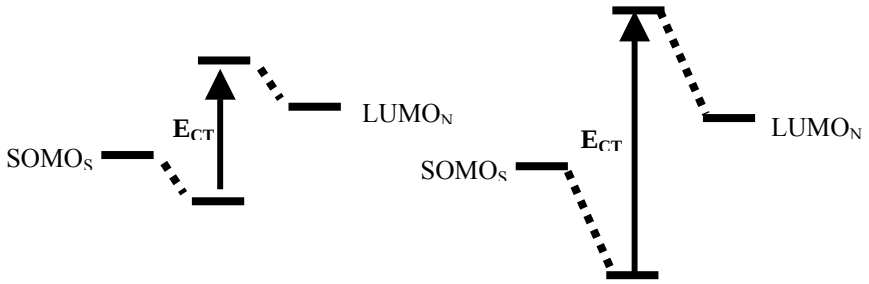

Figure IV.32. Relative energy levels of the $SOMO_{Donor}$-$LUMO_{Acceptor}$ of the (left) thiophene and (right) phenyl as suggested by the electronic absorption spectrum.

And finally, the magnetic data suggest that there is strong ferromagnetic coupling present. However a more pure sample and a crystal structure is needed to verify this information. In accordance with the ethylene analogue, in order for this project to be completed a protecting group for the catechol must be found. This could alleviate the significant loss of product in the deprotection step. It will also allow for the Cat-T-NN to be synthesized in greater yield. This would allow for larger amounts to be complexed with the $Tp^{Cum,Me}Zn(OH)$ and the greater possibility of growing X-Ray quality crystals. In the next section, we describe the synthesis and spin density ananlysis of the SQ-T-NN and SQ-E-NN model compounds.

IV.4. Spin Density Analysis of Exchange Coupling within SQ-T-NN and SQ-E-NN.

We wanted to use the same analysis as in the above section to determine the expected exchange coupling within the bridge analogues of SQ-NN. We use EPR to probe the delocalization of the SQ spin density into the bridge. The ***J*** is expected to scale with the spin density of the radical moieties.[3,35,36] Spin density in the spacer is obtained from hyperfine coupling constants (hfcc), using McConnell relation to estimate:[1,3,11,42]

$$\boldsymbol{J}_{\text{SQ-spacer-NN}} = \boldsymbol{J}_{\text{NN-SQ}} \left(\rho_{\text{spacerSQ}} / \rho_{\text{SQ}}\right) =$$

$$\boldsymbol{J}_{\text{NN-SQ}} \left(\mathbf{a}_{\text{spacerSQ}} / \mathbf{a}_{\text{SQ}}\right) \qquad (4.9)$$

If we use this analysis for the phenyl analogue. In Figure IV.33, the solution EPR spectrum of the the SQPh is shown along with the molecule used to for the investigation. The a_H found for the H_4 proton is 0.6 Gauss, and the a_H for the proton of the SQ is 3.33 Gauss.

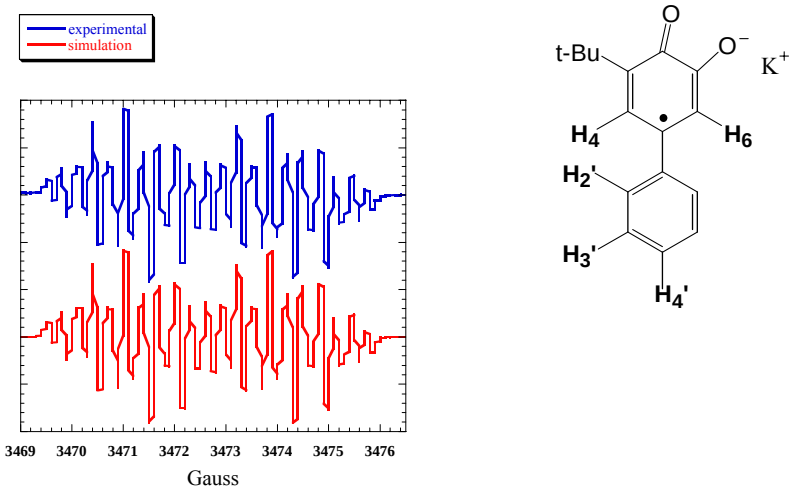

Figure IV.33. SQ-Ph (right) used to determine the hfcc's using EPR. EPR spectrum of SQ-Ph-NN blue is experimental spectrum and red is simulated spectrum.

If we use equation 4.9 for the phenyl analogue we get

$$J_{\text{SQ-Ph-NN}} = +550\ \text{cm}^{-1}\ (0.6\ \text{G}/3.33\ \text{G}) \cdot 100\ \text{cm}^{-1}$$

This is exactly what was found with variable temperature magnetic susceptibility measurements. [11] Therefore, it should be useful to use this method to predict or get a sense of the exchange coupling within the bridge analogues.

IV.4.A. Synthesis of SQ-E-Ph Model Compound for Spin Density Analysis.

The semiquinone-ethylene-phenyl analogue of the SQ-E-NN was synthesized for EPR studies. Starting with the dimethoxymethylether protected arylbromide, **4.1**, two equivalents of t-BuLi were added to undergo a lithium-halogen exchange, making the aryl compound nucleophilic. Excess dimethylformamide was then added to the reaction mixture and upon workup, the aldehyde **4.22** was formed. The aldehyde was reacted in a

Wittig type reaction with bromo-phenylehtylenetriphenylphosphorane and worked-up with sodium hydroxide to yield the protected catechol-ethylene-phenyl **4.23**. The protected catechol **4.23** was then deprotected using well precedented conditions to give catechol **4.24**.

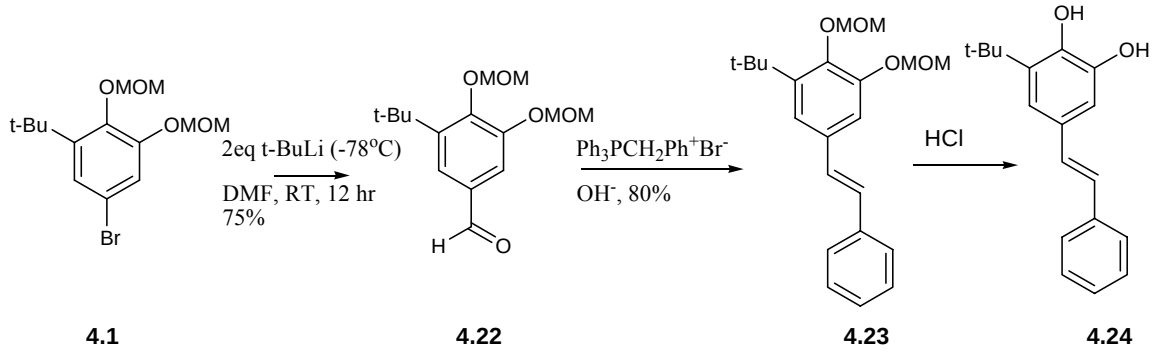

Scheme IV.5. Synthesis of SQ-E-Ph. Analogue for study of spin density.

IV.4.B. Spin Density Analysis of SQ-E-Ph.

We use the same method as for the phenyl analogue. We use the SQ-E-Ph for the EPR spin density studies. Figure IV.34 contains the solution EPR spectrum for the SQ-E-Ph analogue, and the structure with the protons that were being investigated. Table IV.2 contains the values for the a_H for each of the protons is found in Table IV.2.

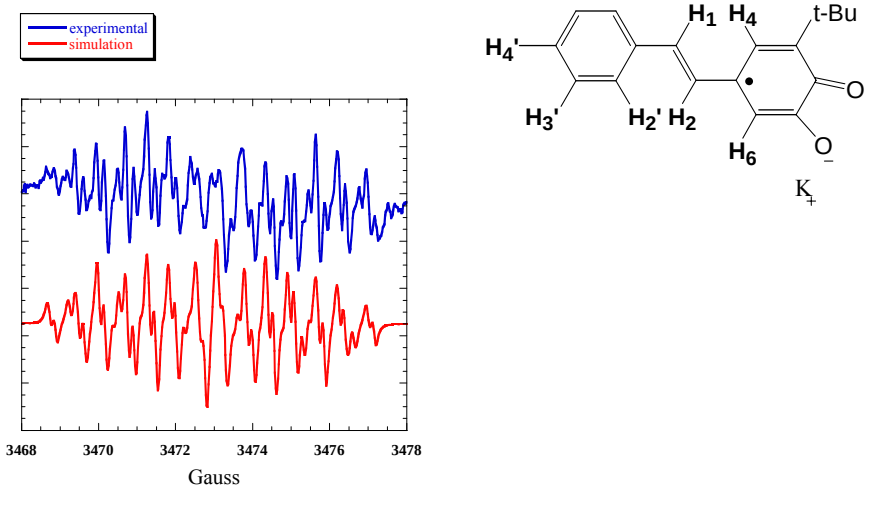

Figure IV.34. SQ-E-Ph used to determine the hfcc's using EPR. EPR spectrum of SQ-E-Ph: blue is experimental spectrum and red is simulated spectrum.

Table IV.2. Experimentally found hfcc's for SQ-E-Ph 4.4 using EPR.

Proton	Coupling Cnst (G)
H_4	1.29
H_6	3.08
H_1	**1.85**
H_2	0.53
$H_{2'}$	0.76
$H_{3'}$	0.0
$H_{4'}$	0.15

If we use the value obtained for the H_1 and the a_H for the SQ found previously we find

$$J_{\text{SQ-E-NN}} = +550\ \text{cm}^{-1}\ (1.85\text{G}/3.33\text{G}) \approx 305\ \text{cm}^{-1}$$

These values of the hfcc's of the SQ-E-Ph are similar to those found by Ullman in the original synthesis of nitronyl nitroxides.[38]

Table IV.3. The hfcc's of NN-E-Ph as synthesized by Ullman.

Nucleus	hfcc (G)
H_1	1.4
H_2	1.4
N (eq)	7.5

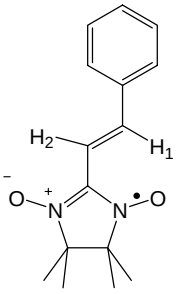

Figure IV.35. (Right) Phenyl-Ethylene-Nitronyl Nitroxide: molecule used to determine hfcc of ethylene.

The exchange coupling using a spin density analysis, which has been used previously with success, predicts that the SQ-E-NN will be approximately 3X the exchange coupling

as the phenyl analogue. So our hypothesis so far is substantiated with respect to the exchange coupling being greater in the ethylene analogue than in the phenyl analogue.

IV.4.C. Synthesis of SQ-T Model Compound for Spin Density Analysis.

The semiquinone-thiophene (SQ-T) analogue of the final product was synthesized for EPR studies. Starting with the dimethoxymethylether protected arylbromide, **4.1**, two equivalents of t-BuLi was added to affect a lithium-halogen exchange. The aryl lithium was quenched with trimethyl borate to give the boronic ester **4.25** of the starting material. The boronic ester **4.25** is coupled with 2-bromo thiophene in a Suzuki coupling to give the dimethoxymethylether thiophene catechol, which upon deprotection yielded the catechol thiophene (Cat-T) **4.27**. A similar procedure as that for the Cat-E-Ph was followed to give the SQ-T **4.28**.

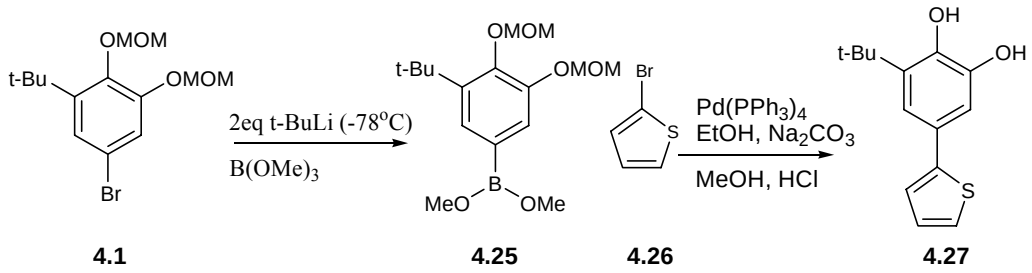

4.1 **4.25** **4.26** **4.27**

Scheme IV.6. Synthesis of SQ-T.

IV.4.D. Spin Density Results for SQ-T.

We investigate of the spin density distribution of SQ-T-NN using the model compound SQ-T. Figure IV.36 shows the fluid EPR spectrum of the SQ-T and the molecule used in the study is pictured. Table IV.4 gives the a_H values for the corresponding protons.

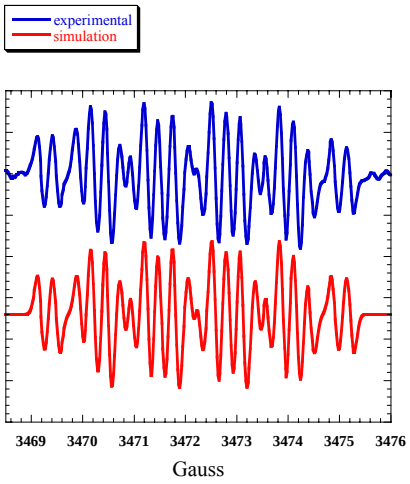

Figure IV.36. SQ-T used to determine the hfcc's using EPR. EPR spectrum of SQT: blue is experimental spectrum and red is simulated spectrum.

Table IV.4. Experimentally found hfcc's for SQ-T using EPR.

Proton	Coupling Cnst (G)
H_4	2.63
H_6	1.02
$H_{2'}$	0.77
$H_{3'}$	0.29
$H_{4'}$	**1.30**

If we use equation 4.9 we find that the predicted exchange coupling in the thiophene analogue is

$$J_{\text{SQ-T-NN}} = +550\ \text{cm}^{-1}\ (1.30\text{G}/3.33\text{G}) \approx 215\ \text{cm}^{-1}.$$

This is about twice as large as that found in the phenyl analogue. Therefore our hypothesis gains positive reinforcement that the order of the exchange coupling in the D-B-A systems is ethylene > thiophene > phenyl.

IV.4.E. General conclusions about the SQ-B-NN (B = ethylene and thiophene) heterospin biradicals.

The success of this project lies in finding a protecting group for the catechol. Fortunately, there is a student currently working on finding a protecting group. This group will allow for the alleviation of loss of product in the deprotection step, allow for the clean oxidation to the NN, and halt the keto-enol tautomerization.

The data thus far suggests that these are good candidates to test our new theories. The spin density analysis suggests that J_{FM} for E > T> Ph. Although the electronic absorption spectra suggests that there is less mixing of the $SOMO_{SQ}$ and $LUMO_{NN}$, the magnetic data inidicates that there is strong ferromagnetic coupling within this biradical. Further work is needed to make solid conclusions.

We have previously made a series of D-A heterospin biradicals $Tp^{Cum,Me}$MetalSQNN and $Tp^{Cum,Me}$ZnSQ-Ph-NN which exhibit strong ferromagnetic coupling, $\boldsymbol{J} > +100\ cm^{-1}$. Therefore, we will use these biradicals to inviestigate the D-A interactions and their influence on exchange coupling. In the subsequent chapter, we will develop a new model to describe the coupling within these biradicals and relate exchange coupling with electron transfer.

IV.5. Experimental Section.

2,6-Di-tert-butyl-4-bromo-TMS-phenol. 2,6-Di-tert-butyl-4-bromo-phenol was silylated in 99% yield with n-BuLi followed by Me_3SiC1 in THF according to the method of Kurreck et al.[43]

3-*tert*-Butyl-4,5-bis-methoxy-phenyl-methyl ester. To a 100 mL round bottom containing distilled THF was added the starting material (.5510 g, 2.017 mmol). The solution was purged with nitrogen and cooled to –78°C. tert-butyl lithium (3 mL, 4.44 mmol) was added dropwise and left to stir at –78°C for one hour. The solution was cannulated onto dry ice in a round bottom under nitrogen atmosphere. This was left to stir

under nitrogen until all of the carbon dioxide gas had evolved. The solution was washed three times with 100 ml of saturated ammonium chloride solution and extracted with diethyl ether. The extract was dried over sodium sulfate, filtered, and the solvent was removed with rotary evaporation. The acid was dissolved in 50 mL of distilled acetone and placed into a 100 mL round bottom flask. Methyl iodide (4.018 mL, 64.54 mmol) and potassium carbonate (.4182 g, 3.026 mmol) was added. The flask was fitted with a condensor and set-up to reflux under nitrogen for 12 hours. The acetone was removed with rotary evaporation. The remaining oil was resolvated with diethyl ether and filtered thru a pad of celite. The diethyl ether was removed with rotary evaporation. The crude product was purified by column chromatography (100% petroleum ether) to give the methyl ester (.4062 g, 80%). ^{1}H NMR ($CDCl_3$) δ (ppm): 7.671 (d, 1H, J=1.6Hz), 7.523 (d, 1H, J = 2 Hz), 3.966 (s, 3H), 3.931 (s, 3H), 3.781 (s, 3H), 1.423 (s, 9H). ^{13}C ($CDCl_3$) δ (ppm): 30.7, 31.14, 51.23, 56.9, 57.1, 115.4, 119.4, 122.2, 137.8, 150.2, 153.6, 166.1. IR (film from CH_2Cl_2) ν(cm^{-1}): 2954, 1721, 1582, 1433, 1399, 1319, 1230, 1165, 1081, 1013, 937. Anal. Calcd. for $C_{16}H_{24}O_6$: C 61.52, H, 7.74. Found: C, 61.37; H, 7.95.

3-*tert*-Butyl-4,5-bis-methoxy-phenyl-galvinol. Place 2,6-Di-tert-butyl-4-bromo-TMS-phenol (2.14 g, 5.99 mmol) was added to a 100 ml round bottom with 40 ml of distilled THF and purged with nitrogen. The solution was cooled to –78°C and tert-butyllithium (7 ml, 11.97 mmol) was added dropwise. The 3-*tert*-Butyl-4,5-bis-methoxy-phenyl-methyl ester (.624 g, 1.996 mmol) was added as a solution in 10 ml of distilled THF under nitrogen and let to stir for one hour at –78°C. The yellow solution was warmed to room temperature and allowed to stir for 4 hours. The solution was quenched with 10 ml of 20% sodium hydroxide solution and allowed to stir for 30 min. The blue solution was

acidified with hydrochloric acid and turned orange. The solvent was removed with rotary evaporation and the orange solid was washed three times with 100 ml saturated sodium chloride solution, extracted with diethyl ether, dried over sodium sulfate, filtered, and solvent removed with rotary evaporation. The orange solid was purified by column chromatography (1:1, diethyl ether:petroleum ether) (74% yield). ^{1}H NMR ($CDCl_3$) δ (ppm): 7.225 (d, 2H, J=1.6), 7.051 (s, 2H), 6.838 (d, 1H, J=2.4), 6.68 (d, 1H, J=1.6), 5.529 (s, OH), 3.963 (s, 3H), 3.781 (s, 3H), 1.556 (s, 9H), 1.414 (s, 18H), 1.362 (s, 9H), 1.289 (s, 9H, 1.273 (s, 9H). ^{13}C ($CDCl_3$) δ (ppm): 29.9, 29.9, 30.55, 30.77, 34.63, 35.46, 56.12, 60.82, 115.4, 125.2, 128.6, 130.9, 131.9, 133.3, 133.4, 135.3, 135.7, 142.4, 146.3, 146.4, 150, 153, 155.9, 159.3, 186.3. IR (film from CH_2Cl_2) ν(cm^{-1}): 3625, 2956, 1595, 1490, 1434, 1360, 1334, 1294, 1253, 1174, 1032, 962, 842. Anal. Calcd. for $C_{41}H_{58}O_4$: C 80.09, H, 9.51. Found: C, 80.17; H, 8.92.

3-*tert*-Butyl-4,5-bis-hydoxy-phenyl-galvinol. Place 3-*tert*-Butyl-4,5-bis-methoxy-phenyl-galvinol (.250 g, .362 mmol) in round bottom flask and purge with nitrogen. Add 20 ml of distilled dichloromethane via syringe. Cool to -78±C with acetone dry ice bath. Add boron tribromide (.171 ml, 1.809 mmol) slowly. Let stir for 1 hour and warm to room temperature. Quench with ice and deionized water. Extract with dichloromethane and saturated sodium chloride. Dry over sodium sulfate, filter off solid, and remove solvent with rotary evaporation (100% yield).^{1}H NMR ($CDCl_3$) δ (ppm): 7.217 (s, 2H), 7.146 (s, 2H), 7.062 (s, 1H), 7.043 (s, 1H), 6.858 (s, 2H), 5.562 (s, 1H), 1.333 (s, 936H), 1.364 (9H). ^{13}C ($CDCl_3$) δ (ppm): 29.9, 29.9, 30.55, 30.77, 34.63, 35.46, 56.12, 60.82, 115.4, 125.2, 128.6, 130.9, 131.9, 133.3, 133.4, 135.3, 135.7, 142.4, 146.3, 146.4, 150, 153, 155.9, 159.3, 186.3. IR (film from CH_2Cl_2) ν(cm^{-1}): 3625, 2955, 1704, 1586, 1433,

1359, 1304, 1250, 1068. Anal. Calcd. for $C_{39}H_{53}O_4$: C 79.96, H, 9.12. Found: C, 80.01; H, 9.10.

4-bromo-phenyl-galvinol. 2,6-Di-tert-butyl-4-bromo-trimethylsilylphenol (.3919 g, 1.097 mmol) was added to a 100 ml round bottom with 40 ml of distilled THF and purged with nitrogen. The solution was cooled to –78°C and tert-butyllithium (.1033 ml, 2.194 mmol) was added dropwise. The p-bromo-methyl ester phenyl was added as a solution in 10 ml of distilled THF under nitrogen and let to stir for one hour at –78°C. The yellow solution was warmed to room temperature and allowed to stir for 4 hours. The orange solution was quenched with 10 ml of 20% sodium hydroxide solution and allowed to stir for 30 min. The blue solution was acidified with hydrochloric acid and turned orange. The solvent was removed with rotary evaporation and the orange solid was washed three times with 100 ml saturated sodium chloride solution, extracted with diethyl ether, dried over sodium sulfate, filtered, and solvent removed with rotary evaporation. The orange solid was purified by column chromatography (3:7, diethyl ether:petroleum ether). Dome product used was from Kay Sandberg and Greg Tew. The synthesis of this molecule is from group member Greg Tew's thesis and DAS I p.94, concult for spectral data.

3-*tert*-Butyl-4,5-bis-methoxy-phenyl-4-phenyl-galvinol. Starting material (.9320 g, 3.412 mmol) was added to a 250 ml schlenck flask with 100 ml distilled THF and purged with nitrogen. The solution was cooled to –78°C. tert-butyllithium (4.014 ml, 6.824 mmol) was added dropwise and allowed to stir at –78°C for one hour. Trimethyl borate (1.163 ml, 10.24 mmol) was added to the solution and allowed to warm to room temperature. The solvent was removed on the schlenck line. While on the schlenck line, ethanol (twice the mmol of ester), 2M sodium carbonate (3/2 ml of ethanol), p-

bromophenyl galvinol (1.877 g, 3.249 mmol), tetrakis (triphenyl phosphine) palladium (.3760 g, .3250 mmol), and 20 ml of distilled THF was added to the schenlck flask under nitrogen and a condensor was added. The solution was pump/purged three times and setup to reflux for three days. The solvent was removed with rotary evaporation. The resulting oil was run thru a celite/silica plug with methylene chloride. The solution was washed three times with 100 ml saturated sodium chloride and extracted with methylene chloride, dried over sodium sulfate, filtered and the solvent removed. The crude material was purified by column chromatography (2:8, diethyl ether: petroleum ether) to give the starting material phenyl galvinol (g, 74%). ^{1}H NMR ($CDCl_3$) δ (ppm): 7.640 (s, 1H), 7.619 (s, 1H), 7.336 (s, 1H), 7.316 (s, 1H), 7.219 (d, 1H, J=1.6), 7.250 (s, 2H), 7.219 (d, 1H, 2.0), 7.138 (d, 1H, J=1.6), 7.060 (s, 2H), 5.519 (s, OH), 3.966 (s, 3H), 3.931 (s, 3H), 1.562 (s, 9H), 1.451 (s, 9H), 1.413 (s, 9H), 1.289 (s, 9H), 1.252 (s, 9H). ^{13}C ($CDCl_3$) δ (ppm): 29.9, 29.9, 30.55, 30.77, 34.63, 35.46, 56.12, 60.82, 115.4, 125.2, 127.17, 125.15, 128.6, 130.9, 131.9, 133.3, 133.4, 135.3, 135.7, 140.32, 142.4, 146.3, 146.4, 150, 153, 155.9, 159.3, 186.3. IR (film from CH_2Cl_2) ν(cm^{-1}): 3625, 2956, 1595, 1494, 1434, 1359, 1334, 1294, 1253, 1174, 1032, 962, 844, 822. Anal. Calcd. for $C_{47}H_{61}O_4$: C 81.81, H, 8.91. Found: C, 81.79; H, 8.90.

3-*tert*-Butyl-4,5-bis-hydroxy-phenyl-4-phenyl-galvinol. Place 3-*tert*-Butyl-4,5-bis-methoxy-phenyl-4-phenyl-galvinol (.144 g, .208 mmol) in round bottom flask and purge with nitrogen. Add 20 ml of distilled dichloromethane via syringe. Cool to -78**±**C with acetone dry ice bath. Add boron tribromide (.098 ml, 1.042 mmol) slowly. Let stir for 1 hour and warm to room temperature. Quench with ice and deionized water. Extract with dichloromethane and saturated sodium chloride. Dry over sodium sulfate, filter off solid, and remove solvent with rotary evaporation (98% yield).^{1}H NMR ($CDCl_3$) δ (ppm):

7.217 (s, 2H), 7.146 (s, 2H), 7.062 (s, 1H), 7.043 (s, 1H), 6.858 (s, 2H), 5.562 (s, 1H), 1.333 (s, 936H), 1.364 (9H). ^{13}C ($CDCl_3$) δ (ppm): 29.9, 29.9, 30.55, 30.77, 34.63, 35.46, 56.12, 60.82, 115.4, 125.2, 128.6, 130.9, 131.9, 133.3, 133.4, 135.3, 135.7, 142.4, 146.3, 146.4, 150, 153, 155.9, 159.3, 186.3. IR (film from CH_2Cl_2) ν(cm^{-1}): 3625, 2955, 1704, 1586, 1433, 1359, 1304, 1250, 1068. Anal. Calcd. for $C_{45}H_{58}O_4$: C 81.53, H, 8.82. Found: C, 81.42; H, 8.59.

General procedure for complexation of Cat-Gal or Cat-Ph-Gal. Add Cat-Gal (Ph) to round bottom flask with minimal amount of distilled dichloromethane. Add $Tp^{Cum,Me}Zn(OH)$ as a solution in minimal distilled methanol. Let stir 2 hours and open to air over night.

3-*tert*-Butyl-4,5-bis-methoxymethylether-cinnamaldehyde. A 100 mL Schlenk flask containing bromide **4.1**[44] (2.18 g, 2.54 mmol), acrolein diethyl acetal ((3ml, 19.61 mmol), tetrabutylammonium acetate (3.941 g, 13.07 mmol), potassium carbonate (1.36 g, 9.80 mmol), potassium chloride (.4873 g, 6.54 mmol), and palladium (II) acetate (.044 g, .1961 mmol) in DMF (8 mL) was pumped/purged 3 times on the schlenk line and heated to 80°C under nitrogen for 5 hours. 2N hydrochloric acid (5 ml) was added and stirred at room temperature for 10 minutes. Saturated brine was added and the mixture was extracted three times with ether. The organic layer was separated, dried over Na2SO4, filtered, and evaporated to dryness. The crude product was taken onto the next because in the work-up process the molecule is partially deprotected.

3-*tert*-Butyl-4,5-dihydroxy-cinnamaldehyde. To a 100 mL round bottom flask containing 30 mL of distilled MeOH were added crude 3-*tert*-Butyl-4,5-bis-methoxymethylether-cinnamaldehyde and 3 drops of concentrated aq. HCl. The reaction was stirred at room temperature for 12 hrs. The solution washed with brine, and dried

over Na_2SO_4. (g, 80%) as a maroon solid. ^{1}H NMR (DMSO-d_6) δ(ppm): 9.56 (d, 1H, J=7.8), 7.596 (d, 1H, *J* = 16 Hz), 7.02 (s, 2H), 6.47 (dd, 1H, *J* = 16 Hz), 1.35 (s, 9H,). 13C NMR (DMSO-d_6) δ(ppm): 194.4, 155.6, 148.8, 146.1, 136.7, 125.5, 124.8, 120.9, 112.672, 35.0, 29.9. IR (film from CH2Cl2) (cm-1): 3271, 2948, 2867, 1647, 1609, 1589, 1510, 1484, 1435, 1410, 1357, 1370, 1300, Anal. Calcd. for $C_{13}H_{16}O_3$; C, 70.89; H, 7.32; found: C, 69.94; H, 7.37.

2-(3-*tert*-Butyl-4,5-dihydroxy-phenyl-4-ethylenyl)-4,4,5,5-tetramethyl-imidazolidine-1,3-diol. To a 100 mL round bottom flask were added **4.X** (110 mg, 0.5 mmol), **4.X** (150 mg, 1 mmol), and a minimal amount of distilled THF to dissolve both reactants. Nitrogen was bubbled through the reaction mixture for 20 min, the solution was stirred at room temperature for 2 days under N2. The reaction was concentrated to obtain a maroon solid (mg, 10%). ^{1}H NMR (DMSO-d_6) δ(ppm): 7.66 (s, 2H), 6.78 (s, 1H), 6.68 (s, 1H), 6.35 (d, 2H, *J* = 16 Hz), 5.923 (dd, 1H, *J* = 16 Hz), 4.109 (d, 1H, *J* = 0.046 Hz), 1.33 (s, 9H), .992 (s, 12H), 1.38. ^{13}C NMR (DMSO-d_6) δ(ppm): 145.4, 143.7, 140.4, 140.0, 135.8, 130.4, 128.9, 125.4, 115.5, 111.2, 87.4, 67.1, 34.4, 29.4, 24.4, 15.2. IR (film from CH_2Cl_2) (cm^{-1}): 3231, 2984, 2932, 1607, 1577, 1536, 1405, 1385, 1266, 1154, 1090, 972. HRMS for $C_{19}H_{30}N_2O_4$ (M^+) Calc. 350.2206; Obs. 350.2249.

NN-E-CatH_2. 2-(3-*tert*-Butyl-4,5-dihydroxy-phenyl-4-ethylenyl)-4,4,5,5-tetramethyl-imidazolidine-1,3-diol is stirred with 1 equivalent of $NaIO_4$ in 10 ml of DI H_2O and 10 ml of distilled CH_2Cl_2 for 1 hour, until observe complete color change to bright green. Extract with CH_2Cl_2 and remove solvent. (5% not pure) EPR a_N = 7.73 Gauss. IR (film from CH_2Cl_2) (cm^{-1}): 2960, 1591, 1431, 1366, 1303, 1176, 1037,801.HRMS (M^+) $C_{19}H_{27}N_2O_4$ Calc. 347.1971; Obs. 358.0067.

3'-*tert*-Butyl-4',5'-bis-methoxymethyl-phenyl-4-thiophene-carbaldehyde. A 50 mL

Schlenk flask containing (4.08 g, 10.7 mmol) of starting boronic ester of starting bromide[44] , 2-bromo-5-thiophenecarbaldehyde (1.98 g, 10.7 mmol), $Pd(PPh_3)_4$ (2.47 g, 2.1 mmol), Na_2CO_3 (2M, 10.7 mL) and EtOH (5 mL) in distilled THF (100 mL) was pump/purged under N_2 three times. The reaction mixture was refluxed for 36 hrs. Once cool, the solvent was removed under reduced pressure. The crude material was diluted with ether and filtered through a pad of Celite to remove the inorganic salts. The filtrate was then diluted with CH_2Cl_2 and washed with brine (2 x 20 mL), deionized H2O (1 x 15 mL), dried over Na_2SO_4, filtered, and evaporated to dryness. The orange oil was difficult to purify therefore took onto deprotection to purify.

3-*tert*-Butyl-4,5-dihydroxy-thiophene-5-carbaldehyde. To a 100 mL round bottom flask containing 30 mL of distilled MeOH were added crude 3'-*tert*-Butyl-4',5'-bis-methoxymethyl-phenyl-4-thiophene-carbaldehyde and 3 drops of concentrated aq. HCl. The reaction was stirred at room temperature for 12 hrs. The solution washed with brine, and dried over Na_2SO_4. as a green solid. The green solid is run down a column with 1:1 pet ether: ether) to obtain a green solid. This is rinsed with cold CH_2Cl_2 to obtain a yellow solid (20%). ^{1}H NMR (DMSO-d_6) δ (ppm): 9.85 (s, 1H), 9.82 (s, 1H), 8.71 (s, 1H), 7.89 (d, 2H, *J* = 3.9 Hz), 7.43 (d, 2H, *J* = 4.2 Hz), 7.21 (d, 1H, *J* = 1.5 Hz), 7.18 (d, 1H, *J* = 2.1 Hz), 1.45 (s, 9H). ^{13}C NMR (DMSO-d_6) δ (ppm): 196.8, 147.2, 146.7, 143.9, 137.1, 134.5, 130.6, 129.4, 127.8, 120.6, 112.1, 35.1, 30.6. IR (film from CH2Cl2) ν (cm-1): 3481, 3238, 2954, 2865, 1656, 1637, 1588, 1428, 1375, 1323, 1074, 855. Anal. Calcd. for $C_{15}H_{16}O_3S$: C, 65.19; H, 5.84. Found: C, 65.87; H, 6.02.

2-(3-*tert*-Butyl-4,5-dihydroxy-phenyl-4-thiophene)-4,4,5,5-tetramethyl-imidazolidine-1,3-diol. To a 100 mL round bottom flask were added (110 mg, 0.5 mmol), bishydroxylamine (150 mg, 1 mmol), and a minimal amount of distilled THF to

dissolve both reactants. Nitrogen was bubbled through the reaction mixture for 20 min, the solution was stirred at reflux for 12 hours under N_2. The precipitate was collected and MPLC is performed with 100% THF. The reaction was concentrated to obtain a orange solid (mg, 5% impure). ^{1}H NMR (DMSO-d_6) δ(ppm): 7.96 (s, 2H), 6.99 (s, 1H), 6.97 (s, 1H), 6.90 (s, 1H), 6.87 (s, 1H), 4.70 (1, 1H), 1.36 (s, 9H), 1.023 (s, 12H). ^{13}C NMR (DMSO-d_6) δ(ppm): 147.4, 144.7, 140.4, 139.9, 139.0, 135.8, 127.3, 128.9, 120.4, 111.2, 87.4, 66.7, 34.4, 31.4, 24.4, 15.0. IR (film from CH_2Cl_2) (cm^{-1}): 3398, 3162, 2956, 2865, 1595, 1432, 1382, 1325, 1147, 1067. HRMS for $C_{21}H_{30}N_2O_4S$ (M^+) Calc. 406.1926; Obs. 405.1756.

NN-T-CatH_2. 2-(3-*tert*-Butyl-4,5-dihydroxy-phenyl-4-thiophene)-4,4,5,5-tetramethyl-imidazolidine-1,3-diol is stirred with .5 equivalent of $NaIO_4$ in 10 ml of DI H_2O and 10 ml of distilled CH_2Cl_2 for 15 minutes, until observe complete color change to bright green. Extract with CH_2Cl_2 and remove solvent. (10% not pure) EPR a_N = 7.75 Gauss. IR (film from CH_2Cl_2) (cm^{-1}): 3238, 2964, 1649, 1554, 1424, 1257, 1057, 855.HRMS (M^+) $C_{21}H_{27}N_2O_4S$ Calc. 403.1691; Obs. 405.1999.

General procedure for complexing Cat-B-NN to metal. Add Cat-B-NN to round bottom flask with distilled minimal dichloromethane. Purge flask with nitrogen. Add $Tp^{Cum,Me}Zn(OH)$ as a solution in minimal distilled methanol via syringe. After 2 hours of stirring, open to air overnight. Remove solvent by rotary evaporation.

IV.6. References

(1) Lahti, P. M., Ed. *Magnetic Properties of Organic Materials*; Marcel Dekker: New York, 1999.

(2) Borden, W. T.; Davidson, E. R. *J. Am. Chem. Soc.* **1977**, *99*, 4587-4594.

(3) Rajca, A. *Chem. Rev.* **1994**, *94*, 871-893.

(4) Iwamura, H.; Inoue, K.; Hayamizu, T. *Pure Appl. Chem.* **1996**, *68*, 243-252.

(5) Inoue, K.; Iwamura, H. *Angew. Chem. Int. Ed. Engl.* **1995**, *34*, 927-928.

(6) Shultz, D. A.; Boal, A. K.; Lee, H.; Farmer, G. T. *J. Org. Chem.* **1998**, *63*, 9462-9469.

(7) Shultz, D. A.; Boal, A. K.; Lee, H.; Farmer, G. T. *J. Org. Chem.* **1999**, *64*, 4386-4396.

(8) Nishizawa, M.; Shiomi, D.; Sato, K.; Takui, T.; Itoh, K.; Sawa, H.; Kato, R.; Sakurai, H.; Izuoka, A.; Sugawara, T. *Journal of Physical Chemistry B* **2000**, *104*, 503-509.

(9) Dougherty, D. A. *Acc. Chem. Res.* **1991**, *24*, 88-94.

(10) Shultz, D. A. *Polyhedron* **2003**, *22*, 2423-2426.

(11) Shultz, D. A.; Vostrikova, K. E.; Bodnar, S. H.; Koo, H.-J.; Whangbo, M.-H.; Kirk, M. L.; Depperman, E. C.; Kampf, J. W. *J. Am. Chem. Soc.* **2003**, *125*, 1607-1617.

(12) Koo, H. J., Whangbo, M.H. **2000**, 263.

(13) H.J. Koo, M. H. W. *J. Solid State Chem.* **2000**, 96.

(14) H.-J. Koo, M.-H. W., S. Coste, S. Jobic *Inorg. Chem* **2001**, 2161.

(15) H.-J. Koo, M.-H. W., S. Coste, S. Jobic *J. Solid State Chem.* **2001**, 464.

(16) Hay, P. J.; Thibeault, J. C.; Hoffmann, R. *J. Am. Chem. Soc.* **1975**, *97*, 4884-4899.

(17) Kloopman, G. *J. Am. Chem. Soc.* **1968**, *90*, 223.

(18) Salem, L. *J. Am. Chem. Soc.* **1968**, *90*, 543.

(19) Fukui, K.; Yonezawa, T.; Shingu, H. *J. Chem. Phys.* **1952**, *20*, 722-725.

(20) Yang, N. C.; Castro, A. J. *J. Am. Chem. Soc.* **1960**, *82*, 6208.

(21) Shultz, D. A.; Bodnar, S. H.; Vostrikova, K. E.; Kampf, J. W. *Inorg. Chem.* **2000**, *39*, 6091-6093.

(22) Liao, Y.; Xie, C. P.; Lahti, P. M.; Weber, R. T.; Jiang, J. J.; Barr, D. P. *J. Org. Chem.* **1999**, *64*, 5176-5182.

(23) Shultz, D. A.; Boal, A. K. *Mol. Cryst. Liq. Cryst.* **1995**, *272*, 75-79.

(24) McConnell, H. M.; Chestnut, D. B. *J. Chem. Phys.* **1958**, *28*, 107-117.

(25) McConnell, H. M.; McLachlan, A. D. *J. Chem. Phys.* **1961**, *34*, 1-12.

(26) Iwamura, H.; Murata, S. *Mol. Crys. Liq. Crys.* **1989**, *176*, 33.

(27) Shultz, D. A., Fico,Rosario M., Lee,Hyoyoung, Kampf,Jeff W., Kirschbaum,Jeff W., Pinkerton, A. Alan, and Boyle, Paul D. *J. Am. Chem. Soc.* **2003**, *125*, 15426-15432.

(28) Shultz, D. A.; Fico, R. M., Jr.; Bodnar, S. H.; Kumar, R. K.; Vostrikova, K. E.; Kampf, J. W.; Boyle, P. D. *J. Am. Chem. Soc.* **2003**, *125*, 11761-11771.

(29) Shultz, D. A.; Bodnar, S. H.; Lee, H.; Kampf, J. W.; Incarvito, C. D.; Rheingold, A. L. *J. Am. Chem. Soc.* **2002**, *124*, 10054-10061.
(30) Mukai, K.; Ishizu, K.; Deguchi, Y. *J. Phys. Soc. Japan* **1969**, *27*, 783.
(31) Norcross, C. D. C. a. B. E. *J. Am. Chem. Soc.* **1960**, *79*, 3797.
(32) Coppinger, G. M. *J. Am. Chem. Soc.* **1957**, *79*, 501.
(33) Ruf, M.; Vahrenkamp, H. *Inorg. Chem.* **1996**, *35*, 6571-6578.
(34) FUNAHASHI, P. D. B. A. T. *J. Am. Chem. Soc.* **1962**, *84*, 2596.
(35) Jacobs, S. J.; Shultz, D. A.; Jain, R.; Novak, J.; Dougherty, D. A. *J. Am. Chem. Soc.* **1993**, *115*, 1744-1753.
(36) Borden, W. T., Ed. *Diradicals*; Wiley: New York, 1982.
(37) Astruc, D. *Electron Transfer and Radical Processes in Transition-Metal Chemistry*; Wiley-VCH: New York, 1995.
(38) Ullman, E. F.; Boocock, D. G. B. *J. Chem. Soc. Chem. Commun.* **1969**, 1161-&.
(39) Wertz, J. E.; Bolton, J. R. *Electron Spin Resonance*; Chapman and Hall: New York, 1986.
(40) Pierpont, C. G.; Lange, C. W. *Prog. Inorg. Chem.* **1994**, *41*, 331-442.
(41) Kahn, O. *Molecular Magnetism*; VCH: New York, 1993.
(42) McConnell, H. M. *J. Chem. Phys.* **1963**, *39*, 1910.
(43) Gierke, W.; Harrer, W.; Kurreck, H.; Reusch, J. *Tetrahedron Lett.* **1973**, *38*, 3681.
(44) Shultz, D. A.; Boal, A. K.; Driscoll, D. J.; Kitchin, J. R.; Tew, G. N. *J. Org. Chem.* **1995**, *60*, 3578.

Chapter 5

Moving Beyond Molecular Orbital Considerations to Explain Exchange Coupling in D-A heterospin biradicals: Valence Bond Configuration Interaction (VBCI) model.

This work has been conducted in collaboration with

Dr. Martin Kirk, Dr. Ezra Depperman, The University of New Mexico

Synthesis of Metal Semiquinone-Nitronyl Nitroxide series

Performed by Dr. Scot Bodnar and Dr. Krishna Kumar

V. Moving beyond molecular orbital to explain exchange coupling in D-A heterospin biradicals: Valence Bond Configuration Interaction (VBCI) model.

Designing high-spin systems for use in molecular spintronic materials is the focus of many magnetic materials groups.[1] In transition metal systems high-spin ground states are not only difficult to design, but are difficult to achieve. This is due to the fact that there are low-lying excited states that can mix with the ground state. In metal systems the antiferromagnetic exchange pathways usually dominate and cause the total exchange to be antiferrmagnetic.[2] This is not necessarily true in organic biradicals. In such cases, an effective approximation that is commonly used consists of taking into account only the two unpaired electrons occupying the magnetic orbitals *a* and *b*; all other electrons are considered passive. This is called the active electron approximation and it was used in chapter 2 to evaluate exchange coupling.[1,3] The intramolecular exchange coupling in organic biradicals is usually described this way making the design of these molecules easier than their inorganic counterparts. In the previous section we used a frontier molecular orbital description to account for the strong ferromagnetic exchange in D-A biradicals. Here we present a new valence bond configuration interaction (VBCI) model to describe the strong exchange in D-A biradicals.

Within the active electron approximation, the total intramolecular exchange interaction of biradicals, $\boldsymbol{J_{TOT}}$, is a sum of antiferromagnetic and ferromagnetic contributions:[3]

$$J = J_F + J_{AF} = 2k_{ab} - \frac{4\beta^2}{j^0 - j} \qquad (5.1)$$

where k is the two-center exchange integral, β is the resonance integral j^0 *and* j have the same definitions as before. This equation is the result of a second order pertubation taking into account configuration interaction.

We can consider this from an ET perspective. Wolfsberg and Helmholtz used the relation that when ionic integrals of excited states are neglected, the electronic coupling matrix element between orbitals a and b, H_{ab}, is approximately equal to β.[3,4] Using this relation we can rewrite equation 5.1 as[5,6]

$$J = J_F + J_{AF} = 2k_{ab} - \frac{4H_{ab}^{\ 2}}{U} \qquad (5.2)$$

Since H_{ab} is proportional to the overlap integral, $\langle a|b\rangle$, ferromagnetic coupling is favored when the SOMOs are either strictly or accidentally orthogonal.[3] When this is true, $\langle a|b\rangle = 0$ and J reduces to $2k_{ab}$. When organic biradicals possess orthogonal SOMOs H_{ab} is zero. The presence of large overlap density, $\rho(i)$, results in an appreciable value for k_{ab}, and a ferromagnetic interaction results[1,3,7]

$$k = \int_{space} \rho(1)\rho(2) r_{12}^{-1} d\tau \,. \qquad (5.3)$$

This is the model commonly used for non-disjoint homo and heterospin biradicals.[8]

If we use this model on the D-A biradicals we immediately find a problem. Figure V.1 is a frontier orbital picture of the D-A biradical semiquinone-nitronyl nitroxide (SQNN).

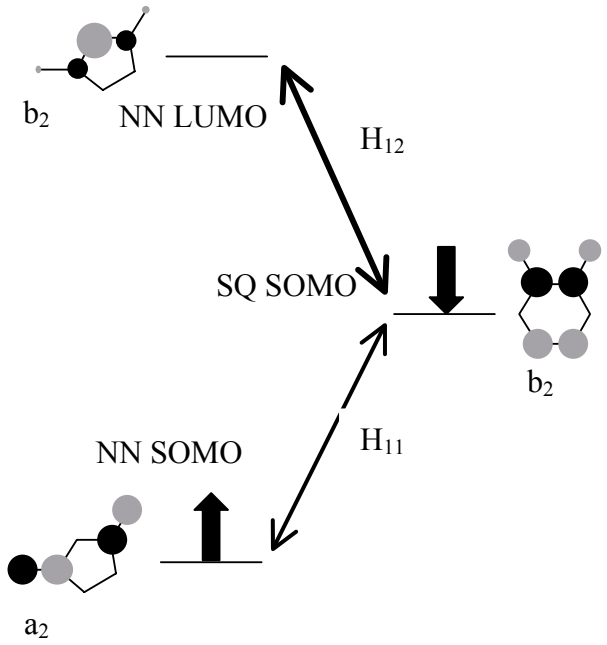

Figure V.1. Frontier orbitals for SQNN biradical. Symmetry labels are for idealized C_{2v} symmetry of the donor (SQ) and the acceptor (NN).

Because the NN and SQ SOMOs are orthogonal, H_{11} is zero and the singlet (^{1}GC) and triplet (^{3}GC) ground configurations are degenerate in first-order. Within the active electron approximation the total exchange coupling is expected to be equal to zero, $J_{SQ\text{-}NN}=0$, because both H_{11} and k_{11} are zero. This is in contradiction to what has been observed for this and other D-A biradicals.[9,10,11] High-spin metal complexes of the SQNN ligand have been found to have exchange coupling parameters between +300 $< J_{SQ\text{-}NN} >$ +550 cm^{-1}.[9] If we look again at Figure V.1 we see that a SQ → NN charge transfer is possible because $H_{12} \neq 0$. Electronic absorption spectroscopy should be an effective probe of this charge transfer. We must develop another model in order to understand the electronic origin of this strong coupling.

In order to evaluate the electronic origin of the FM coupling we need to use a model that includes a state description of the system, allowing for spectroscopic investigation. Presented here is a VBCI model that will be used to explain and evaluate the electronic

origin of the strong intramolecular ferromagnetic interactions in D-A heterospin biradicals. The VBCI method has been used to understand excited state contributions to the ground state intramolecular exchange interaction, ***J***, in multinuclear transition metal systems.[12-17,18] This will link exchange coupling studies of inorganic and organic systems and provide a connection that had not been presented previously.

We will consider a mechanism that is based on the interaction between the ground configuration and an excited configuration where an electron has been transferred from a SOMO centered on *a* and an empty orbital centered on *b*. This mechanism was first proposed by Goodenough.[3,19] First the qualitative arguments in favor of this mechanism must be presented. If we consider the a_1 and a_2 orbitals centered on A, and b_1 and b_2 orbitals centered on B, with one electron occupying the orbitals of lower energy.

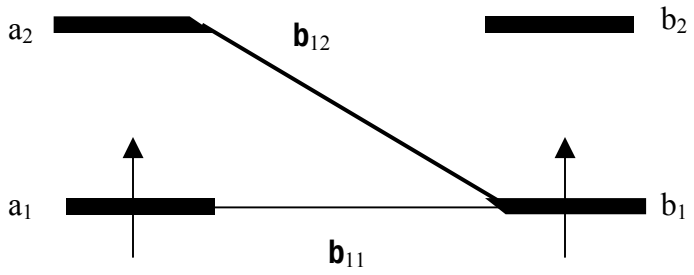

Figure V.2. The a_1 and a_2 orbitals centered on A, and b_1 and b_2 orbitals centered on B, with one electron occupying the orbitals of lower energy. $\mathbf{b}_{11}$ represents a transfer of an electron from b_1 to a_1, and $\mathbf{b}_{12}$ represents a transfer of an electron from b_1 to a_2.

The transfer of the unpaired electron from b_1 to a_2 (or from a_1 to b_2) leads to the charge transfer excited configuration a_1a_2 (or b_1b_2). The triplet state arising from this configuration is lower in energy than the singlet state, due to Hund's rule in the excited state. Consequently, the interaction between the two triplet states arising from the ground and excited configurations, respectively, may be expected to be more important than the

interaction between the two singlet states. Thus, the low-lying triplet state will be stabilized with respect to the low-lying singlet in the ground configuration.

It follows that the states arising from the ground configuration a_1b_1 are ^{1}GC and ^{3}GC. One singlet state, ^{1}CTC, and one triplet, ^{3}CTC, arise from the charge transfer configuration a_1a_2 (or b_1b_2). The orbital parts of the wavefunction, which we have derived previously, are:

$$\psi_{S(T)} = (1/2)[a_1(1)a_2(2) \pm a_1(2)a_2(1) \pm b_1(1)b_2(2) \pm b_1(2)b_2(1)] \tag{5.4}$$

where the positive sign holds form ^{1}CTC and the negative for ^{3}CTC. The coupling matrix elements may be calculated as:

$$\left\langle {}^1CTC \middle| H \middle| {}^1GC \right\rangle \approx \beta_{12} \tag{5.5}$$

$$\left\langle {}^3CTC \middle| H \middle| {}^3GC \right\rangle \approx \beta_{12} \tag{5.6}$$

with

$$\beta_{12} = \left\langle a_2(1) \middle| h(1) \middle| b_1(1) \right\rangle \tag{5.7}$$

b is the resonance integral. The energy gaps **D**$E_{S=0}$ between the two singlet states, and **D**$E_{S=1}$ between the two triplet states are obtained as:

$$\mathbf{D}E_{S=0} = U + K^0 \tag{5.8}$$

$$\mathbf{D}E_{S=0} = U - K^0 \tag{5.9}$$

with

$$\begin{aligned} U = {} & \alpha_1 - \alpha_2 + \left\langle a_1(1)a_2(2) \middle| r_{12}^{-1} \middle| a_1(1)a_2(2) \right\rangle - \left\langle a_1(1)b_1(2) \middle| r_{12}^{-1} \middle| a_1(1)b_1(2) \right\rangle \\ & + \left\langle a_1(1)b_1(2) \middle| r_{12}^{-1} \middle| a_2(2)b_2(1) \right\rangle \end{aligned} \tag{5.10}$$

$$K^0 = \left\langle a_1(1)a_2(2) \middle| r_{12}^{-1} \middle| a_1(2)a_2(1) \right\rangle + \left\langle a_1(1)b_2(2) \middle| r_{12}^{-1} \middle| a_2(2)b_1(1) \right\rangle - \left\langle a_1(1)b_1(2) \middle| r_{12}^{-1} \middle| a_1(2)b_1(1) \right\rangle \tag{5.11}$$

U is the cost in energy of transferring an electron from b_1 to a_2, and K^0, which is dominatied by a one-center exchange integral, accounts for Hund's rule in the excited

configuration. The low-lying singlet is stabilized by $-H_{12}^{\,2}/(U+K^0)$ and the low-lying triplet by $-H_{12}^{\,2}/(U-K^0)$. The S-T energy gap J becomes

$$
\begin{aligned}
E'(^1GC) &= E^0(^1GC) - \frac{H_{12}^{\,2}}{U+K^0} \\
E'(^3GC) &= E^0(^3GC) - \frac{H_{12}^{\,2}}{U-K^0} \\
2J &= E'(^1GC) - E'(^3GC) = -\frac{H_{12}^{\,2}}{U+K^0} - \frac{H_{12}^{\,2}}{U-K^0} \\
2J &= -\frac{(U-K^0)H_{12}^{\,2}}{(U+K^0)(U-K^0)} + \frac{(U+K^0)H_{12}^{\,2}}{(U+K^0)(U-K^0)} \\
2J &= \frac{2K^0 H_{12}^{\,2}}{U^2 + K^{0^2}}
\end{aligned}
\tag{5.12}
$$

This effect opposes the stabilization of the low-lying singlet, that was previously shown in chapter 2, due to interaction between the GC and the a_1a_1 (or b_1b_1) charger transfer configuration. This stabilization of the singlet is roughly:

$$J_{AF} = \frac{-4H_{11}^2}{U} \tag{5.13}$$

$$\beta_{11} = \langle a_1 | h(1) | b_1(1) \rangle \tag{5.14}$$

K^0 in equation 2J 5.12 is much smaller than U; it turns out that J due to this mechanism is smaller than the normal J_{AF} by approximately a factor of K^0/U. J in equation 5.12 becomes significant contribution with respect to J_{AF} only when $|\beta_{12}|$ is much larger than $|\beta_{11}|$. We can draw a new configuration interaction diagram.

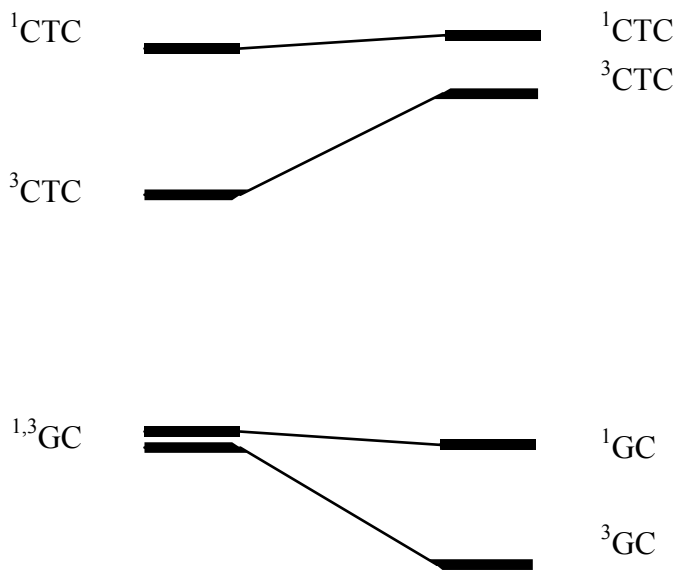

Figure V.3. GC and CTC state diagrams. On the left before configuration interaction between the GC and CTC. On the right the lowering of the ^{3}GC after charge transfer configuration interaction.

This model can now be adapted to our SQ-NN D-A biradicals.

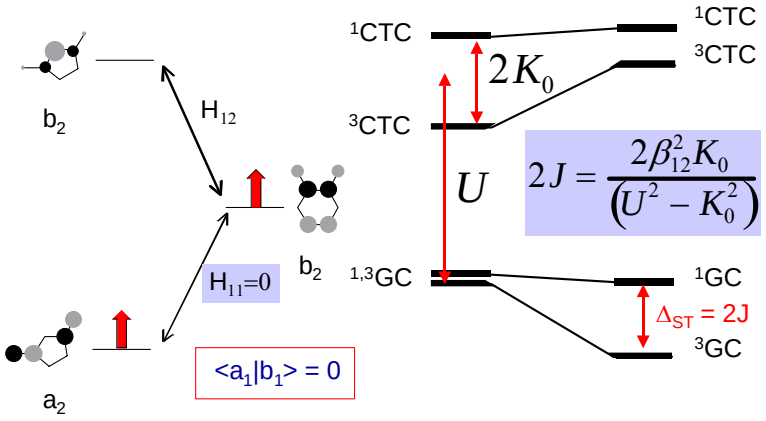

Figure V.4. Frontier orbitals and configurations for the SQNN biradical ligand. Symmetry labels are for idealized C_{2v} symmetry of the donor (SQ) and acceptor (NN) fragments.

V.1. Donor-Acceptor Biradicals as Ground State Analogues of Photoinduced Charge Separated States.

In chapter 4 we expressed the strong exchange coupling of our new class of heterospin biradicals in donor-acceptor terms. When one thinks of D-A interactions, generally electron transfer comes to mind. Electron transfer (ET) is the most fundamental of chemical reactions. In a donor-acceptor system, it is a transfer of an electron from one

orbital centered on a donor site to another orbital centered on an acceptor site. Just like any chemical reaction, the time-scale, mechanism and driving force for the reaction depends on the structural and energetic features of reactants, products and surrounding medium. Since Marcus' semi-classical theory on ET, much effort has been devoted to mapping out the precise role and proper theoretical treatment of the intervening medium between the donor and acceptor.

ET is ubiquitous in nature and can occur readily despite very large D-A distances between ET sites as well as poor orbital overlap. Organic chemists have tried to emulate nature's ET processes in an effort to gain insight into general ET properties. The knowledge gained here can be used in molecular electronics where charge transport is essential to the design of nanoscale devices that require ET at determined distances, directions and/or timescales. A significant part of this effort has been devoted to the study of photoinduced charge separation reactions. Synthetic models have been prepared in which the dependencies of electron-transfer rate constants on donor-acceptor distance and orientation, free energy of reaction, and electronic coupling have been studied.[20,21] The degree of success with which these models have been able to address solely these factors varies widely.

Experimentally, photoinduced electron transfer (PET) can be studied using flash photolysis.[22] Absorption of a laser pulse generates a transient species that can be detected spectroscopically. In D-B-A systems, photoexcitation of the D fragment results in an excited D*-B-A state that can undergo electron transfer to form a D^{+}-B-A^{-} charge separated (CS) state. This CS state can be detected by absorbance, fluorescence, resonance Raman. Irradiation in the cavity of an EPR spectrometer at low temperature allows the recording of EPR. And NMR can be used to follow the reaction kinetics.

These methods include evalutaing H_{ab} via *rate constant*.There are three fundamental mechanisms that have been determined to be responsible for non-resonant charge transfer processes in molecular systems.[14,23] In the superexchange mechanism, the bridge solely serves to mediate donor and acceptor wavefunctions, but in the hopping mechanism the electron is located at the bridge for a short time during its journey from one redox center to the other. The other mechanism is incoherent e^-/h^+ tunneling.

An observed ET rate within a complex system is usually a mixture of rates through several different orbital pathways. The electronic coupling and vibronic overlap, which are very sensitive to molecular conformation, may vary widely from pathway to pathway.[22] The process of identifying the contributions of several pathways to the overall ET process is experimentally challenging.[12]

Molecules for which the donor-acceptor distances and orientations are accurately known provide a useful vehicle for understanding mechanisms of ET. Because the typical method used for evaluating these molecules is PET the molecules are in their excited states, the structural details of the molecule cannot be probed with a great amount of accuracy. Furthermore, key excited state contributions to the nature of the D^+-B-A^- CS configuration have not been and prove difficult to be explored in detail. **Stable D-B-A biradicals are effectively *ground state analogues* of the charge separated state.**

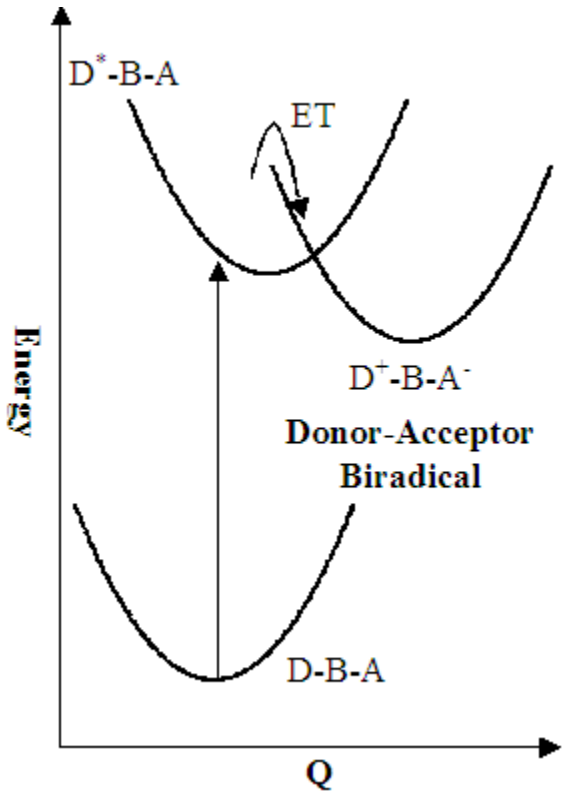

Figure V.5. Top: potential energy diagram for PET showing the charge separated state as a D-B-A biradical.

It is important to note that no ET actually occurs within these molecules, they are ground state analogues. The structural details of these molecules are provided via crystal structures. The ground state stability of these D-A biradicals allows for detailed electronic studies as well as allow us to evaluate key electronic structure contributions to the magnitude of the electronic coupling matrix element (H_{ab}).

As described in the previous section, D-B-A biradicals are covalently linked nondisjoint heterospin biradicals which display strong intramolecular ferromagnetic coupling exchange between the spin carriers.[18,24,8] Previously, we recast the ferromagnetic contribution to exchange in these molecules in terms of D-A. Next we will show how exchange coupling can be related to ET and the electronic coupling matrix

element, H_{ab}. Finally we will use our new VBCI method to evaluate H_{ab} using magnetic susceptibility measurements.

V.1.A. Superexchange: relation between exchange coupling and electron transfer.

Superexchange is known to be an important mechanism for efficient electron transfer within biological processes.[15,22,25-27] Kramers and Anderson first used the term to describe the indirect exchange coupling of unpaired spins via orbitals having paired spins, which acquire paramagnetic character through mixing with charge transfer excited state configurations.[28,29] This occurs when the orbitals of metal ions, which have the unpaired electrons in them, overlap with filled orbitals, usually s and p, of bridging atoms and the unpaired electrons are delocalized in this manner. Later Goodenough and Kanamori developed rules that predict the signs of the individual magnetic interactions.[19,30]

As discussed in chapter 2, when the orbitals containing the unpaired electrons overlap, and according to Pauli exclusion principle, the spins must be aligned antiparallel giving an antiferromagnetic interaction. Anderson calls this the kinetic exchange, because it is "incipient" chemical bond formation. From this we get that the contribution of kinetic exchange, the antiferromagnetic contribution, to the total exchange coupling parameter is:

$$J_{kinetic,AFM} = -\frac{H_{ab}^{\ 2}}{U} \qquad (5.15)$$

where t is the transfer integral (t **a b**) between orbitals a and b and U is the energy difference between the ground state and the charge transfer state.

As discussed in chapter 2, when the orbitals containing the unpaired electrons are orthogonal, then according to Hund's rule, the spins must be aligned parallel giving a

ferromagnetic interaction. Anderson calls this the potential exchange. From this we get that the contribution of potential exchange, the ferromagnetic contribution, to the total exchange coupling parameter is:

$$J_{potential,FM} = \left\langle a(1)b(2)\left|\frac{e^2}{r_{12}}\right|a(2)b(1)\right\rangle \qquad (5.16)$$

This is the two center coulomb exchange integral, which we found to be $2k_{ab}$.

If the orthogonal orbitals are mixed with the orbitals of the bridging atom, the potential exchange ($\boldsymbol{J_{FM}}$) is determined by the amount of mixing between the metal orbitals and the bridging orbitals, and by the intra-atomic coupling on the bridge atom.

The contributions to the superexchange mechanism can be represented pictorially. If we consider two metal ions bridged by an atom, the spins can result in either a singlet state (Figure V.6 bottom) or a triplet state (Figure V.6 top).

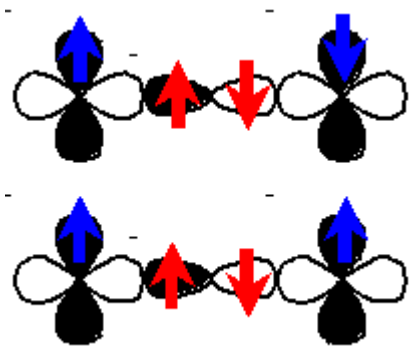

Figure V.6. Two metal ions connected via an bridge. Shown here are two metal d orbitals interacting through a p orbital. The top is representative of the triplet state, and the bottom is representative of the singlet state.

If we consider excited states where an electron is transferred from the bridging atom to one of the metal ions, a triplet state could result (Figure V.7 top) or a singlet state could result (Figure V.7).

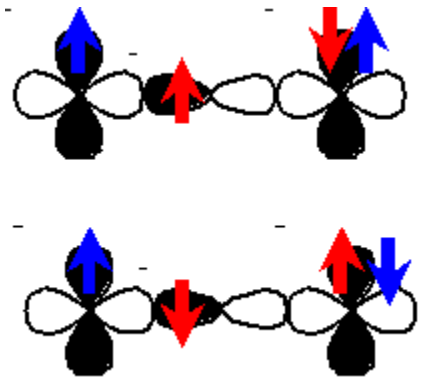

Figure V.7. Transfer of electron on bridge to metal ion resulting in a triplet state (top) and a singlet state (bottom).

If there is finite overlap between the orbitals of the metal and the bridge the major contribution to the total exchange coupling parameter will be from the antiferromagnetic portion, giving the singlet the lowest energy state. This gives an overall antiferromagnetic coupling. Mixing this excited state into the ground state (configuration interaction) leads to a stabilization of the ground state singlet. An analogous two electron two orbital treatment was given in chapter 2 in which we applied a second order perturbation (configuration interaction) to the exchange interaction.

ET occurs via superexchange, no charge ever actually resides on the bridge, and the states that the molecule occupies between the time when the electron leaves the donor and when it arrives at the acceptor are called virtual excitations. The quantity that dictates the probability of transmission of an electron from donor to acceptor in this way is the electronic donor-acceptor superexchange coupling, H_{DA}.[31] McConnell gives a perturbation theory-based expression for the magnitude of the H_{DA} in terms of individual resonance integrals between molecular subunits and the energy gap between the degenerate donor and acceptor and the bridge.[32]

The calculation of direct and indirect (superexchange) electronic coupling has been a theoretical challenge. It has been formulated through Generalized Mulliken-Hush (GMH) theory in terms of parameters that can be either derived from optical spectra in cases where the charge transfer state is emissive, or calculated using any method that yields excited state energies and dipole moments.[33] However, for some electron transfer systems, the charge transfer states from which H_{DA} can be obtained are not charge transfer states at all, but are radical ion pairs that can be several electron-volts above the neutral ground state and have vanishing transition moments. As a result, they display no emission upon charge recombination (CR) and acceptable determination of GMH parameters becomes very difficult. Wasielewski and coworkers used this fact to determine H_{AB}.[12-17,18] In these studies, magnetic field effects are used to experimentally determine the exchange parameter for the charge separated *excited state* biradical formed by photoinduced electron transfer (PET).

Wasielewski utilized the relationship that was originally proposed by Anderson to develop a method to evaluate the electron transfer in terms of exchange coupling. When the charge transfer process originates from a state in which the redox centers are also paramagnetic, *e.g.* charge recombination from a radical ion pair (RP), the electronic coupling that dictates electron transfer from the RP to energetically proximate electronic states is also that which facilitates the magnetic exchange interaction between the unpaired spins of the RP.[29] Sensitive measurement of exchange interactions within long-range radical ion pairs in electron transferring systems, most notably photosynthetic systems, using electron paramagnetic resonance and optically-detected magnetic resonance (magnetic field effects) has helped in acquiring a fundamental understanding of indirect exchange mechanisms and their contribution to the efficiency of long-range

charge and energy transfer processes.[12-17] In the magnetic superexchange coupling, 2***J***, between two unpaired spins, the singlet and triplet RP states are either stabilized or destabilized through virtual charge transfers via coupling of the orbitals on the paramagnetic centers to the bridge orbitals and to each other. Above we saw that Anderson used a perturbation approach to describe kinetic exchange between two magnetic centers separated by a nonmagnetic medium as the mixing between the ground state of the system and a charge transfer excited state via a virtual excitation.[29] More generally, the total perturbation to each RP state, ΔE_S or ΔE_T for the singlet and triplet, respectively, is a sum of pairwise interactions between the RP state and the state to which it couples via charge transfer such that 2***J***, the singlet-triplet splitting is (to lowest order)

$$2J = \Delta E_S - \Delta E_S = \sum_{n,S} \frac{\left|H_{RP-n,S}\right|^2}{\Delta E_{RP-n,S}} - \sum_{n,T} \frac{\left|H_{RP-n,T}\right|^2}{\Delta E_{RP-n,T}} \qquad (5.17)$$

where $H_{RP\text{-}n,S}$ and $H_{RP\text{-}n,T}$ are the electronic coupling matrix elements between the RP and proximate singlet and triplet electronic states, respectively and $\Delta E_{RP\text{-}n,S}$ and $\Delta E_{RP\text{-}n,T}$ are the energetic splittings between the RPs and these states. The work of Anderson and others led to the conclusion that the most important charge transfer in the kinetic exchange mechanism is that between half-filled orbitals of the magnetic pair, giving a contribution of $\frac{2t_{ab}{}^2}{U}$ to the magnitude of exchange.[29,32] Here *t* is the transfer integral between orbitals on magnetic centers *a* and *b* and *U* is the energy difference between the ground state and the charge transfer state. The transfer integral is equivalent to McConnell's superexchange coupling, H_{DA}; therefore, under certain assumptions, the magnitude of the magnetic interaction is directly proportional to $H_{DA}{}^2$. The relationship

between exchange coupling, $\boldsymbol{J}$, and electronic coupling, H_{DA}, has previously been described.[3,32]

We can now start to think about exchange coupling in terms of electron transfer. Within the two-electron two-orbital treatment in chapter 2 we found that the total exchange coupling parameter was found to be composed of both an antiferromagnetic and a ferromagnetic contribtion: $\boldsymbol{J_{TOT} = J_{FM} + J_{AFM}}$. If we look at this from a superexchange/electron transfer perspective we find that the ferromagnetic contribution is due to interelectron repulsion, just as in chapter 2, but the antiferromagnetic contribution can now be seen to arise from superexchange.

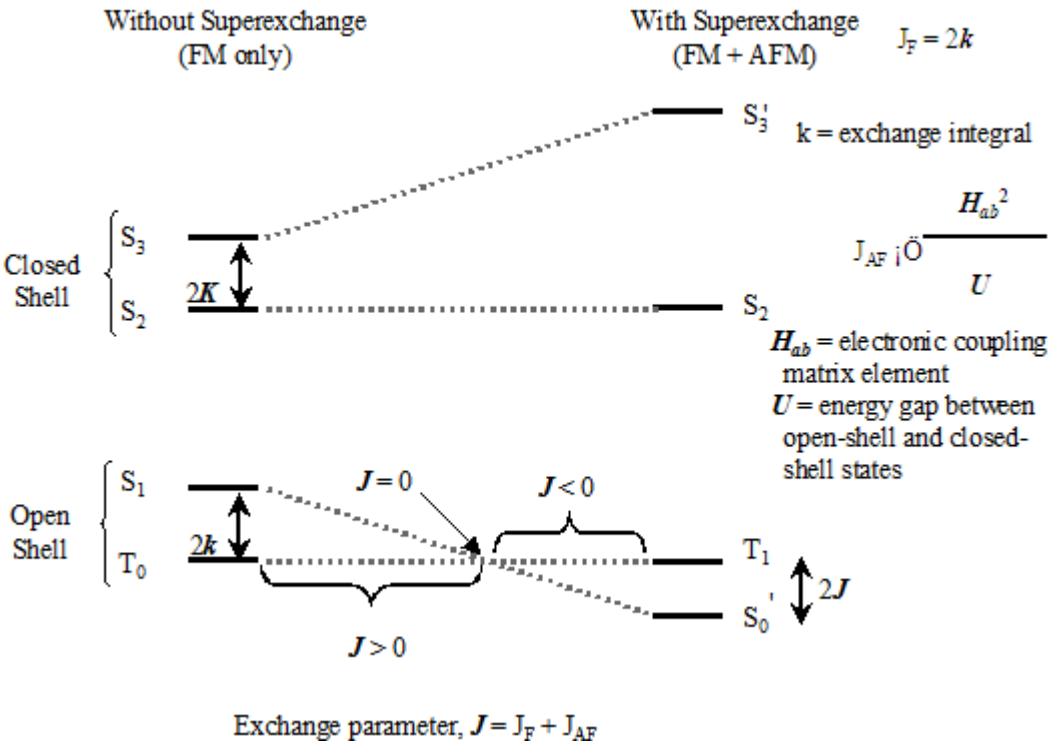

Figure V.8. Interelectron Repulsion and Electron Transfer: Two Principle Components of Exchange Coupling.

This method uses the magnetic field effect to determine singlet-triplet gap ($2J_{D^+BA^-}$) which is in turn correlated with H_{AB} via rate constants.

V.2. Using VBCI model to Evaluate Exchange Coupling in MSQNN Series.

We have developed a valence bond configuration interaction (VBCI) model in order to provide a framework for understanding the electronic origin of the strong ferromagnetic coupling in our nitronylnitroxide-semiquinone (SQNN) D-A biradical series, $Tp^{Cum,Me}M$(SQNN) ($Tp^{Cum,Me}$ = hydro-tris(3-cumenyl-5-methylpyrazolyl)borate; M = trasition metal ion and provides key design criteria for the synthesis of new *high-spin* biradicals.[10,18,24]

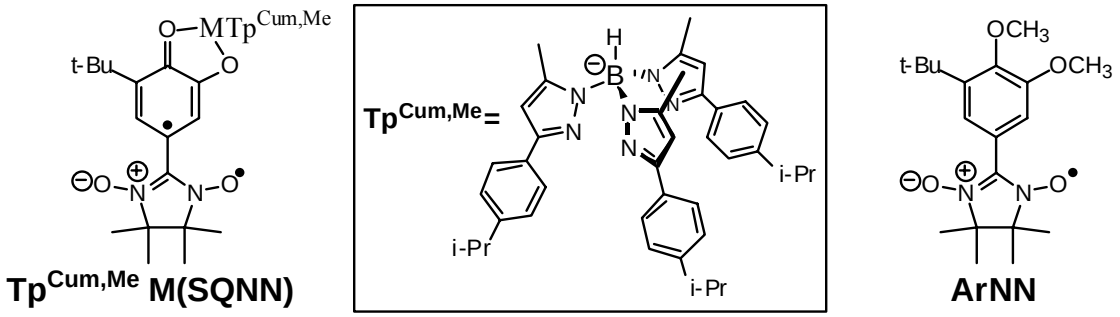

Figure V.9. $Tp^{Cum,Me}M(SQNN)$, $Tp^{Cum,Me}$, and ArNN.

The VBCI model differs from the more common MO model in that it provides a state, as opposed to orbital, description of the system. Thus, the VBCI approach is more amenable to spectroscopic investigations since electronic transitions occur between states. There is configurational mixing of charge transfer excited states into the ground state via the electronic coupling matrix element, H_{ab}. Since the biradical intra-ligand exchange interaction in $Tp^{Cum,Me}M(SQNN)$ is so strong, the donor and acceptor radicals may be covalently linked by various spacer (bridge) groups and maintain their strong ferromagnetic coupling. Expressions have been developed by us, and others, to relate the measured exchange coupling parameter, $\boldsymbol{J}$, with H_{ab}, which describes the efficiency of the transfer of an electron from donor to acceptor thru bridge, B.[12-18,24] Our D-B-A complexes are excellent systems for the study of orbital and pathway dependent electronic coupling contributions to electron transfer through the bridge fragment. If a crystal structure is known for the biradical, the magnetic susceptibility measurements are easily acquired in the solid state, therefore, H_{ab} may be determined *for single molecules in a known geometry*. D-B-A molecules are good candidates for probing electronic structure contributions to the design of potential molecular electronic/spintronic materials.[1,3,18,22,24]

V.2.A Results and discussion.

V.2.A.1. Spectroscopic Studies.

An overlay of the electronic absorption spectra for $Tp^{Cum,Me}Cu(SQNN)$ and $Tp^{Cum,Me}Zn(SQNN)$ is presented in Figure V.10.

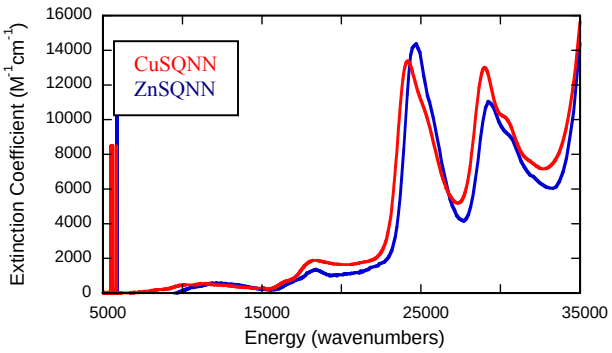

Figure V.10. Room temperature electronic absorption spectra of $Tp^{Cum,Me}Cu(SQNN)$ (red) and $Tp^{Cum,Me}Zn(SQNN)$ (blue).

The spectra look almost identical, they have the same spectral features. If we look at the Zn complex, the spectrum is slightly blue shifted in respect to that of the Cu spectrum. This is a good indication that the metal does not affect the electronic absorption spectra much.[9,18] The spectra of these, and other $Tp^{Cum,Me}M(SQNN)$ compounds, are virtually identical. From this it can be inferred that the observed spectral features are mainly due to SQNN intraligand based transitions with no significant band being derived from the ligand to the metal (LMCT) or vice-versa (MLCT). We can tentatively assign the bands in these spectra by comparing these to their constituent chromophore electronic absorption spectra.

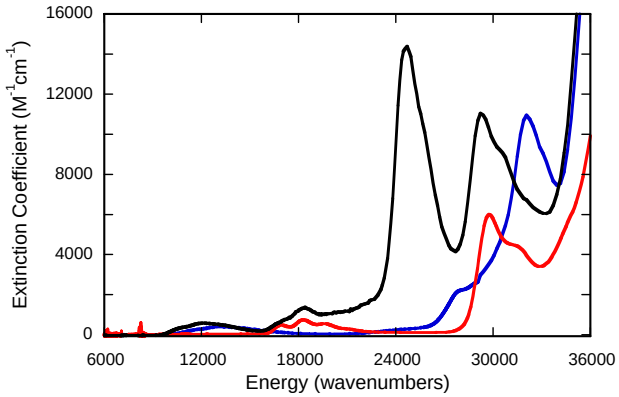

Figure V.11. Room temperature electronic absorption spectra of $Tp^{Cum,Me}Zn(SQNN)$ (black) ArNN (red) and $Tp^{Cum,Me}Zn(SQ)$ (blue).

For $Tp^{Cum,Me}Cu(SQNN)$, a broad low-energy absorption feature is found in the 10,000 – 15,000 cm^{-1} region (**e** ~ 625 $M^{-1}cm^{-1}$), assignable as an SQ n**Ø**p* transition by analogy with other SQ based chromophores. Similarly, the ~18,000 cm^{-1} (**e** ~ 1,875 $M^{-1}cm^{-1}$) band is assigned as an NN based n**Ø**p* transition based on the spectroscopic similarity with the aryl nitronylnitroxide, ArNN. Additional, higher energy transitions are observed at 24,500 cm^{-1} (**e** ~ 13,500 $M^{-1}cm^{-1}$), and 29,000 cm^{-1} (**e** ~ 13,000 $M^{-1}cm^{-1}$), with a shoulder on the latter at 30,300 cm^{-1} (**e** ~ 10,200 $M^{-1}cm^{-1}$). The 29,000 cm^{-1} band is assigned as the electronic origin of a NN based **p Øp** * transition, with an apparent ~1,300 cm^{-1} vibronic progression, based upon the spectra of similar ArNN.[9,34] Interestingly, the ~24,500cm^{-1} band is not present in absorption spectra of the constuent chromaphores of SQNN $Tp^{Cum,Me}Zn(SQ)$ or the aryl nitronylnitroxide, ArNN, indicating that this transition is unique to the SQNN chromophore.[9] This is the band that we believe to be the LLCT band.

This is not the only indication that the 25,000 cm^{-1} transition in SQNN is the LLCT band, additional support for the SQ**p Ø**NN**p*** assignment can be obtained from the resonance Raman (rR) spectroscopic studies on $Tp^{Cum,Me}Cu(SQNN)$.[18] In resonance Raman (rR) spectroscopy, the energy of the incoming laser is adjusted to coincide with

an electronic transition of the molecule. So, rather than exciting the molecule to a virtual energy state, it is excited to near one of its electronic transitions. When the frequency of the laser beam is tuned to be near an electronic transition (resonance), the vibrational modes associated with that particular transition exhibit a greatly increased Raman scattering intensity. This usually overwhelms Raman signals from all of the other transitions.

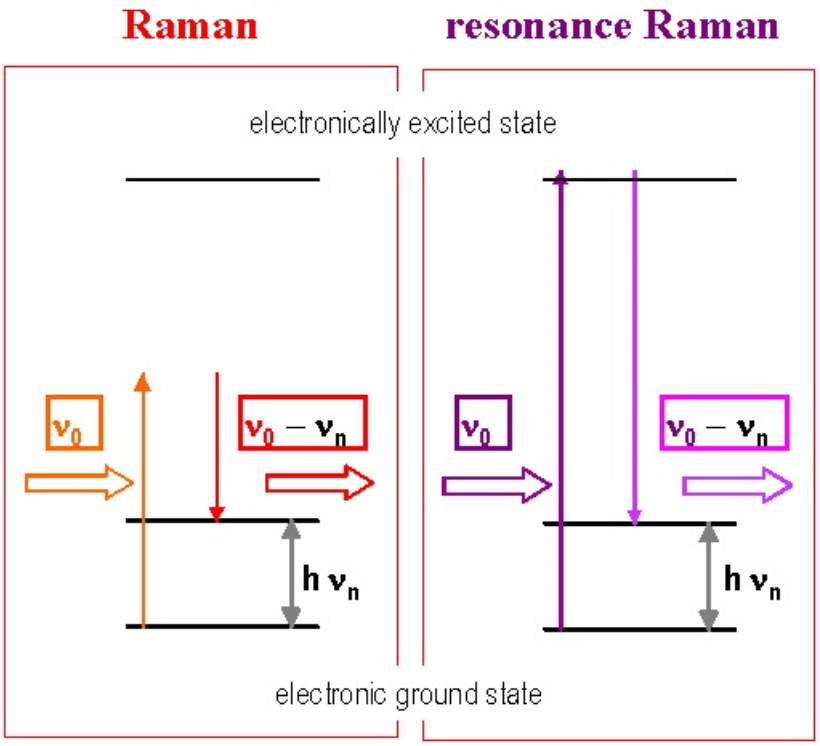

Figure V.12. Comparison of Raman and resonance Raman transitions.

Resonance Raman spectra collected at 413.7nm and 488nm for $Tp^{Cum,Me}Cu(SQNN)$ are shown in Figure V.13.

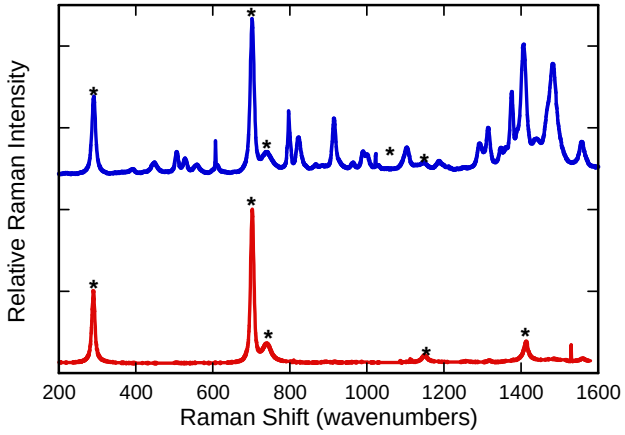

Figure V.13. Room temperature rR spectra of $Tp^{Cum,Me}Cu(SQNN)$ at 488nm (red) and 413.7nm (blue). Solvent modes are marked with an asterisk.

More than 20 vibration bands are found to be resonantly enhanced when pumping into the 24,500 cm^{-1} (408 nm) absorption band, and at least 11 vibrational bands are observed in the 1200 -1600 cm^{-1} region where the dominant in-plane SQNN ligand stretching vibrations are anticipated to occur. This is more vibrational modes than are expected for just one of the constituent chromaphores, again pointing to this band being an intraligand CT band. Vibrational frequencies and normal mode descriptions have been obtained from DFT frequency calculations and the results for the in-plane stretching region are compared with the experimental data and presented in Table 1.

Table V.1. Experimental Raman frequencies, calculated vibrational frequencies, and mode assignments for $Tp^{Cum,Me}Cu(SQNN)$.

Experimental $Tp^{Cum,Me}Cu(SQNN)$ rR frequency (cm^{-1})	Calculated SQNN rR frequency (cm^{-1})	Assignment (Dominant in-plane motion)
1000		SQ C_b-C_g stretch
1026	1025	NN C_a-N stretch
1106		SQ C_a-C_b stretch
1148	1147	NN N-C_a-N bend
1190	1185	NN N-C_β stretch
1291	1291	SQ C_b-C_a stretch
		NN N-C_β-N wag
1315	1299	SQ C-O stretch
		NN ring breathing
1348	1352	SQ C-O stretch
		NN N-O stretch
1375	1374	SQ C-O stretch
		NN C_a-N-C_β bend
1407	1401	SQ C_a-C_δ stretch
		NN C_α-N-C_β bend
1440	1423	SQ C-O stretch
		NN ring breathing
	1446	SQ C-O stretch
		NN ring breathing
1482	1460	SQ C-O stretch
		NN ring breathing
	1490	SQ C-Oσ stretch
		SQ C_α-C_b stretch
		NN C_α-N stretch
1557	1553	SQ C-O stretch
		NN ring breathing

The large number of observed in-plane vibrations, coupled with the fact that the vibrations are delocalized over the entire SQNN chromophore, are fully consistent with an assignment of the 24,500 cm^{-1} band as an intraligand SQ$\rightarrow$NN charge transfer, emphasizing the donor-acceptor nature of the SQNN ligand. Additionally, rR excitation profiles have been constructed for the 1407 cm^{-1} and 1482 cm^{-1} modes, which possess in-plane vibrational motions in both the NN and SQ fragments.[35,34]

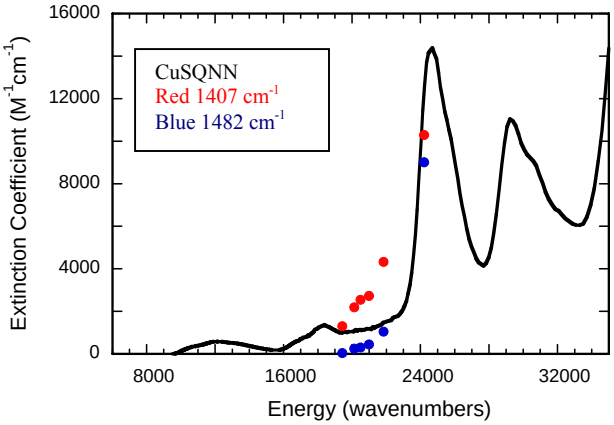

Figure V.14. rR excitation profiles of the 1407 cm^{-1} (closed red circles) and 1482 cm^{-1} (closed blue circles) modes of $Tp^{Cum,Me}Cu(SQNN)$.

The resonance Raman excitation profiles are consistent with the intraligand charge transfer nature of the 24,500 cm^{-1} band in $Tp^{Cum,Me}M(SQNN)$, as vibrations common to the coupled SQNN chromophore are resonantly enhanced. In summary, an intense intraligand SQ SQ $\pi \rightarrow$NN π^* CT transition is observed in $Tp^{Cum,Me}M(SQNN)$ that is unique to this composite chromophore.

V.2.A.2. Frontier molecular orbital description of biradical SQNN and evaluation of the singlet-triplet gap.

A frontier orbital description has already been presented for the SQNN biradicals. Here the relationship between the LLCT band observed in the electronic absorption spectra and frontier orbital model is to be made.

In order to explain the strong ferromagnetic coupling in the D-A biradicals from a MO perspective, a mixing of the $SOMO_{Donor}$ and the $LUMO_{Acceptor}$ must occur. This creates non-disjoint SOMOs that are a requirement in creating high-spin biradicals.

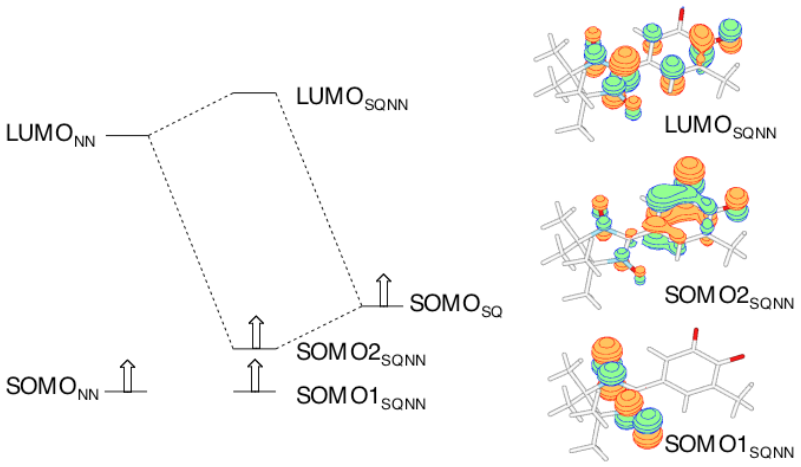

Figure V.15. MO mixing diagram (left) and frontier orbital wavefunctions for SQNN (right).

In Figure V.15. the mixing of the SOMOs is apparent in the SOMO2$_{SQNN}$ and LUMO$_{SQNN}$. The <LUMO$_{NN}$|SOMO$_{SQ}$> overlap integral is related to the intensity (I_{CT}) of the intraligand SOMO2$_{SQNN}$→LUMO$_{SQNN}$ charge transfer band according to:

$$I_{CT} \propto \left\langle \mathrm{LUMO}_{NN} \left| \mathrm{SOMO}_{SQ} \right\rangle^2 \right. \quad . \qquad (5.18)$$

Therefore, the high extinction coefficient (**e** ~ 13,500 $M^{-1}cm^{-1}$) for the SOMO2$_{SQNN}$**Ø**LUMO$_{SQNN}$ intraligand CT band confirms the large orbital mixing between the constituent LUMO$_{NN}$ and SOMO$_{SQ}$ basis functions in SQNN, and this is consistent with the bonding picture derived from DFT calculations as well as the simple MO picture.

V.2.A.3. The VBCI model.

We have described previously a VBCI method that extends beyond the typical active-electron approximation used to evaluate the exchange interactions in organic biradicals.[18] The important feature of the VBCI model is that it contains parameters that can be probed spectroscopically, allowing for an evaluation of excited state contributions to the ground state exchange. The intraligand SQ**Ø**NN charge transfer band that is

present in $Tp^{Cum,Me}M(SQNN)$ is the organic analogue of MMCT bands observed in transition metal dimers for which VBCI is commonly used.[36] One advantageous feature of these donor-acceptor biradicals over their inorganic counterparts is that there is a single dominant superexchange pathway, and this allows for a straightforward determination of H_{12} within the VBCI formalism.[36] A state energy diagram for $Tp^{Cum,Me}Zn(SQNN)$ is constructed from electron occupation of the a_1 ($SOMO_{NN}$), b_1 ($SOMO_{SQ}$), and a_2 ($LUMO_{NN}$) basis functions, is presented in Figure V.16.

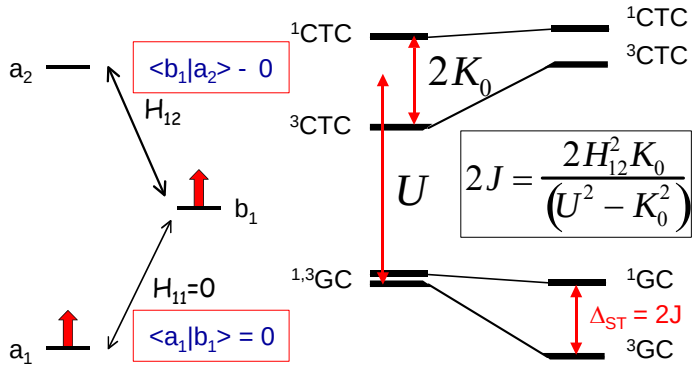

Figure V.16. The VBCI model. Simplified orbital diagram using $SOMO_{NN}$ (a_1), $LUMO_{NN}$ (a_2), and $SOMO_{SQ}$ (b_1) basis functions (left), and a state diagram (right) deriving from $\overline{a}_1\overline{b}_1$ (^{3}GC), $a_1\overline{b}_1$ (^{1}GC), $\overline{a}_1\overline{a}_2$ (^{3}EC), and $a_1\overline{a}_2$ (^{1}EC) configurations (note that the singlets are multi-determinantal wavefunctions). a and b are not irreducible representations.

We have already shown that within the active electron approximation H_{11} is zero and the ^{1,3}GC are degenerate and $J_{SQNN} = 0$, in contradiction with experiment.

According to Figure V.16, the experimental observation of an intense SQ**Ø**NN CT transition requires a large value for H_{12} (H_{AB} **a** HAD), the electronic coupling matrix element that connects $SOMO_{SQ}$ and $LUMO_{NN}$. Furthermore, the extent to which the ^{3}CTC configuration mixes into the ^{3}GC ground configuration will result in an energetic stabilization of ^{3}GC and a high-spin triplet ground state, as derived earlier. In order to

determine the magnitude of the ^{3}GC state stabilization relative to the ^{1}GC (i.e. $2J_{SQ\text{-}NN}$) in $Tp^{Cum,Me}Zn$(SQNN), we use a perturbative expression (Eq. 4) which has already been derived within this three-orbital model.

$$2J_{SQNN} = \frac{2H_{12}^2 K^0}{U^2 - K^{0^2}} \tag{5.19}$$

Here, K^0 is a single-site exchange integral that splits the $a_1\bar{a}_2$ singlet and $\bar{a}_1\bar{a}_2$ triplet excited state configurations (Hund's rule). Equation 5.19 shows that the ferromagnetic interaction is maximized in heterospin D-A biradicals when 1) the electronic coupling matrix element that connects one fragment SOMO and the other fragment LUMO is maximized, 2) the single-site exchange integral is large, and 3) the intramolecular CT energy ($U - K^0$) is low. These represent key design criteria for the synthesis of Donor-Acceptor heterospin biradicals with high-spin ground states. Stabilization of the ^{3}GC is strongly dependent on the magnitude of the electronic coupling matrix element, H_{12}, which describes the efficiency of "electron transfer" from the SQ donor to the NN acceptor. A determination of H_{12} for D-A biradicals may be made from a combination of magnetic susceptibility and/or EPR measurements (J) and optical spectroscopy (U and K^0). As discussed in previous sections, Wasielewski and coworkers have recently reported an elegant method for determining H_{ab} in the weakly-coupled nonadiabatic regime.[12-17] In these studies, magnetic field effects are used to experimentally determine the exchange parameter for the charge separated *excited state* biradical formed by PET. Donor-acceptor biradicals, like the ligand SQNN are ground-state analogs of excited state charge-separated species formed by PET. This allows for the accurate calculation of the exchange coupling parmeter through magnetic studies. The exchange coupling parameter for a biradical can be evaluated over ca. 6 orders of magnitude, H_{ab} for adiabatic and

nonadiabatic cases can be probed using a variety of bridges, provided the crystal structure is known. A major problem in determining H_{12} in the adiabatic limit is the evaluation of K^0. This requires the observation of the spin-forbidden ^{3}GC**Ø**^{1}CTC intraligand CT in order to determine the ^{3}CTC-^{1}CTC splitting.

V.2.A.4. Analysis of Hot Bands.

The incorporation of an S = 1 Ni(II) center in $Tp^{Cum,Me}$Ni(SQNN) leads to *antiferromagnetic* exchange between the Ni(II) ion and the S = 1 SQNN D-A biradical ligand.[9] This results in a diamagnetic S = 0 ground state with a low-lying triplet at 160 cm^{-1} (**2*J*)** above the ground state singlet. Since **2*J*** is on the order of kT, variable temperature electronic absorption spectroscopy may be used to probe transitions originating from both the S = 0 and S = 1 ground state spin manifolds within the ^{3}GC of $Tp^{Cum,Me}$Ni(SQNN). At low temperatures only the S = 0 ground state component of the ^{3}GC is populated and optical transitions to the S = 1 component of the ^{1}CTC are spin-forbidden. However, upon warming the system the S = 1 component of the ^{3}GC is populated allowing the observation of the formerly spin forbidden $^3GC \rightarrow {}^1CTC$ intraligand CT transition. The intensity gaining mechanism occurs through intensity borrowing from the fully spin allowed S=1 $^3GC \rightarrow$ S=1 ^{3}CTC intraligand CT at lower energy.

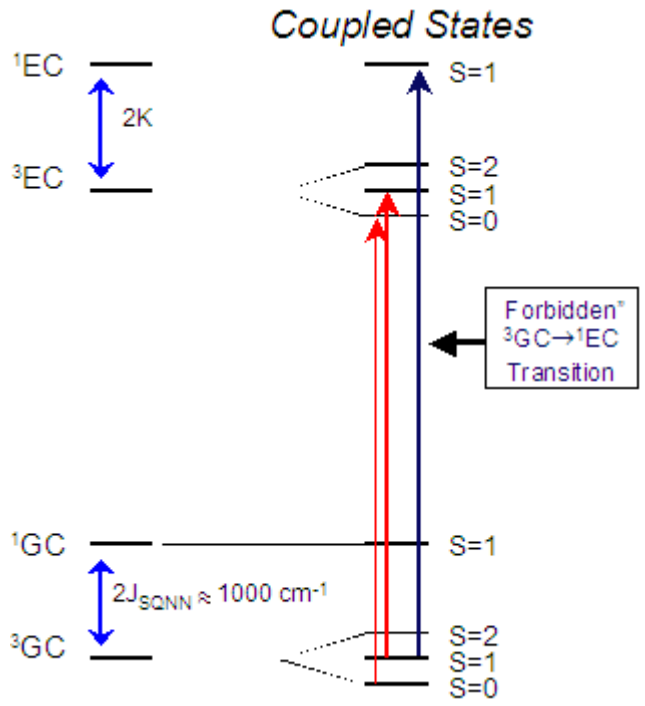

Figure V.17. Energy diagram for SQNN (left) and $Tp^{Cum,Me}Ni$(SQNN) (right). Note that Ni^{II} (S=1) – SQNN (S=1) antiferromagnetic exchange provides a means for accessing the "forbidden" ^{1}CTC at 29,500 cm^{-1}.

The 4 K electronic absorption spectrum of $Tp^{Cum,Me}Ni$(SQNN) in Figure V.18 displays broad low-energy absorption features in the 10,000 - 15,000 cm^{-1} and 16,000 - 21,000 cm^{-1} regions, with additional bands centered at 25,100 cm^{-1}, 29,000 cm^{-1}, and 29,900 cm^{-1} similar the those observed for $Tp^{Cum,Me}Zn$(SQNN) and $Tp^{Cum,Me}Cu$(SQNN) with similar assignment of the bands.

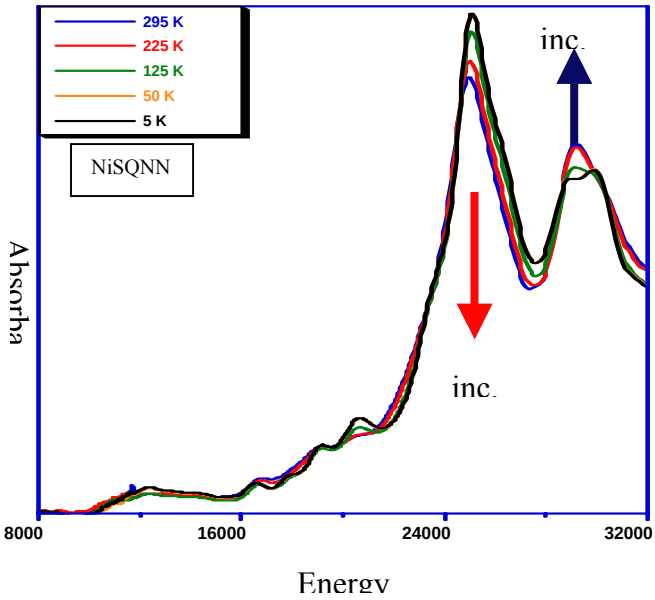

Figure V.18. Variable Temperature electronic absorption spectrum of $Tp^{Cum,Me}Ni(SQNN)$ in a polystyrene film.

As predicted from Figure V.17, when the temperature is increased a decrease in the 25,100 cm^{-1} band is observed with a parallel increase in absorption intensity at 29,200 cm^{-1}. This is consistent with the population of the S=1 magnetic component of the exchange coupled ^3GC and the appearance of the "forbidden" S=1 ^3GC Ø S=1 ^1CTC intraligand CT transition. The ^3CTC-^1CTC energy gap is ~4,000 cm^{-1}, which is equal to $2K^0$ in the VBCI model, and U is equal to 27,000 cm^{-1}. The intensities of the 25,100 cm^{-1} and 29,200 cm^{-1} bands in $Tp^{Cum.Me}Ni(SQNN)$ can be plotted as a function of temperature, and this is displayed in Figure V.19 along with the Boltzmann population of the S=0 and S=1 magnetic sublevels determined from magnetic susceptibility measurements on $Tp^{Cum.Me}Ni(SQNN)$.[9]

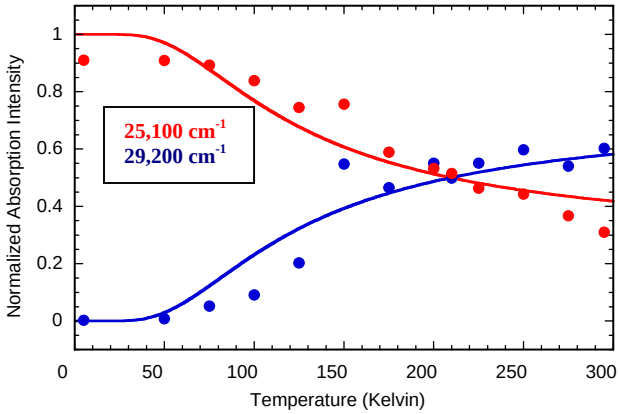

Figure V.19. Normalized electronic absorption intensity changes as a function of temperature for the 25,100 cm^{-1} (red solid circles) and 29,200 cm^{-1} (blue solid circles) of $Tp^{Cum,Me}Ni(SQNN)$. The solid lines are the Boltzmann populations for the S=0 (red) and S=1 (blue) magnetic sublevels of determined from solid state magnetic susceptibility measurements on $Tp^{Cum,Me}Ni(SQNN)$.

The good agreement between the variable temperature electronic absorption and the magnetic susceptibility data strongly suggest that the $Tp^{Cum.Me}Ni(SQNN)$ SQ-NN ring torsion angle remains unchanged when dissolved in a polymer matrix, since this torsion is expected to affect SQNN exchange coupling.[9,37,38]

Since J, K^0, and U have now been determined experimentally, the magnitude of the electronic coupling matrix element can be calculated directly from equation 5.19 and it is found to be H_{12} = 13,700 cm^{-1}. Under the assumption that K^0, the single-site exchange integral, is unchanged by the nature of the bridge fragment, equation 5.19 can be used to determine the electronic matrix element for any SQ-bridge-NN system given the magnitude of the exchange coupling, J, and the energy of the ^{3}GC Ø ^{3}CTC intraligand CT transition. The electronic absorption spectrum of the phenyl-bridged analogue looks similar to the other SQNN complexes with the LLCT band being around 24,000 cm^{-1}.

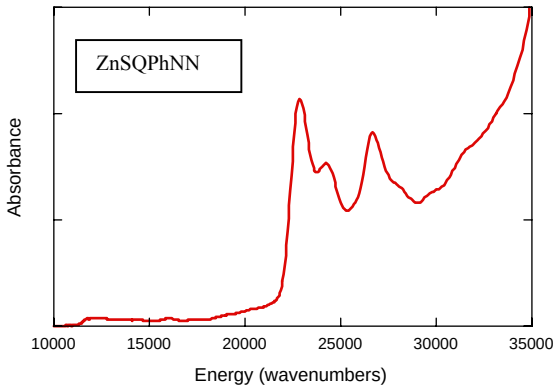

Figure V.20. Electronic absorption spectrum $Tp^{Cum.Me}Zn(SQ\text{-}Ph\text{-}NN)$

The rR spectrum is comparable with $Tp^{Cum.Me}Zn(SQ\text{-}NN)$ parent. In addition to the SQNN modes there are additional modes present that are attributable to the bridge fragment.

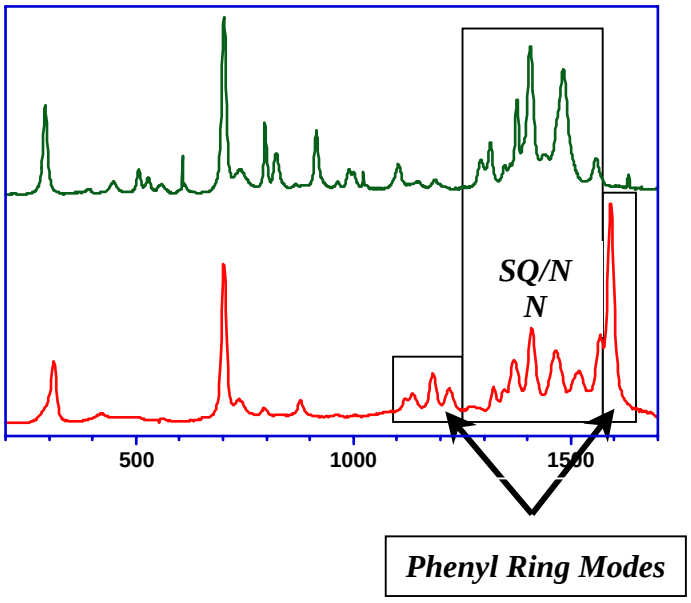

Figure V.21. Resonance Raman spectra of $Tp^{Cum.Me}Zn(SQ\text{-}Ph\text{-}NN)$ and $Tp^{Cum.Me}Zn(SQ\text{-}NN)$.

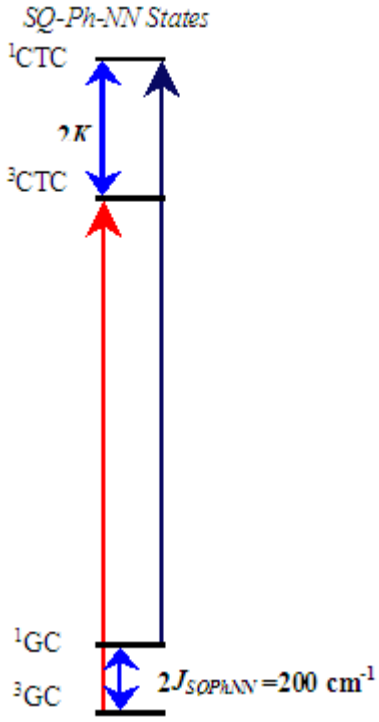

Figure V.22. Energy diagram for $Tp^{Cum,Me}Zn$(SQ-Ph-NN). Accessing excited states via "hotband" analysis.

When the temperature is increased a decrease in the 24,00 cm^{-1} band is observed with a parallel increase in absorption intensity at 26,000 cm^{-1}.

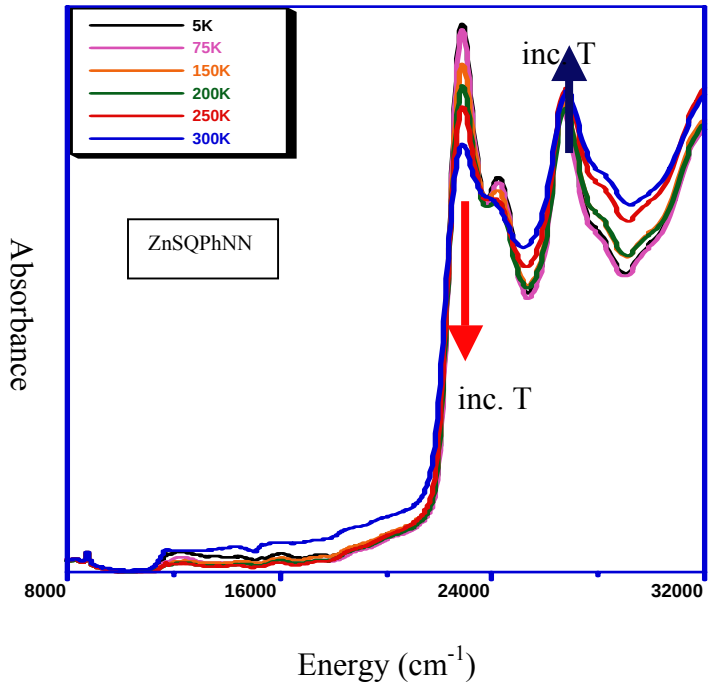

Figure V.23. Variable temperature electronic absorption spectrum of $Tp^{Cum.Me}Zn$(SQ-Ph-NN).

The ^{3}GC **Ø** ^{3}CTC intraligand CT transition energy and the magnetic exchange parameter for phenyl-bridged $Tp^{Cum.Me}Zn$(SQ-Ph-NN) have been determined to be U = 25,500 cm^{-1} and $\mathbf{2}J$ = +200cm^{-1}, respectively.[9] The intensities of the 24,000 cm^{-1} and 26,000 cm^{-1} bands in $Tp^{Cum.Me}Zn$(SQ-Ph-NN) can be plotted as a function of temperature, and this is displayed in Figure V.24 along with the Boltzmann population of the S=1 and S=0 magnetic sublevels determined from magnetic susceptibility measurements on $Tp^{Cum.Me}Zn$(SQ-Ph-NN).[9] This results in H_{12} = 5685 cm^{-1} for $Tp^{Cum.Me}Zn$(SQ-Ph-NN); an ~41% decrease compared with $Tp^{Cum.Me}Zn$(SQNN).

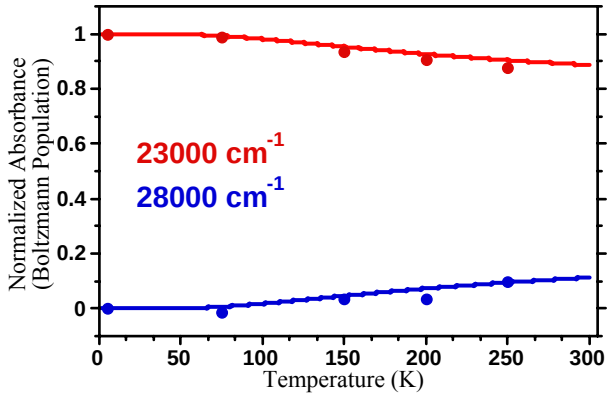

Figure V.24. Normalized electronic absorption intensity changes as a function of temperature for the 23,000 cm^{-1} (red solid circles) and 28,000 cm^{-1} (blue solid circles) of $Tp^{Cum,Me}Zn$(SQ-Ph-NN). The solid lines are the Boltzmann populations for the S=1 (red) and S=0 (blue) magnetic sublevels determined from solid state magnetic susceptibility measurements on $Tp^{Cum,Me}Zn$(SQ-Ph-NN).

V.2.A.5. VBCI Model is Most Useful for D-A Heterospin Biradicals.

The above analysis is best suited for the heterospin D-A biradicals. If we try to use this analysis for our bis-SQ series, for example, of biradicals it looses utility. Due to **p**-connectivity within the bis-SQ biradicals a charge transfer from the $SOMO_{SQ(1)}$ to the $LUMO_{SQ(2)}$ would be a weak transition; since no conjugated pathway exists to create the dipole. Although the D-A heterospin biradicals are cross conjugated, the **p**-connectivity allows the dipole to be created from transfer of an electron from SQ to NN, Figure V.25.

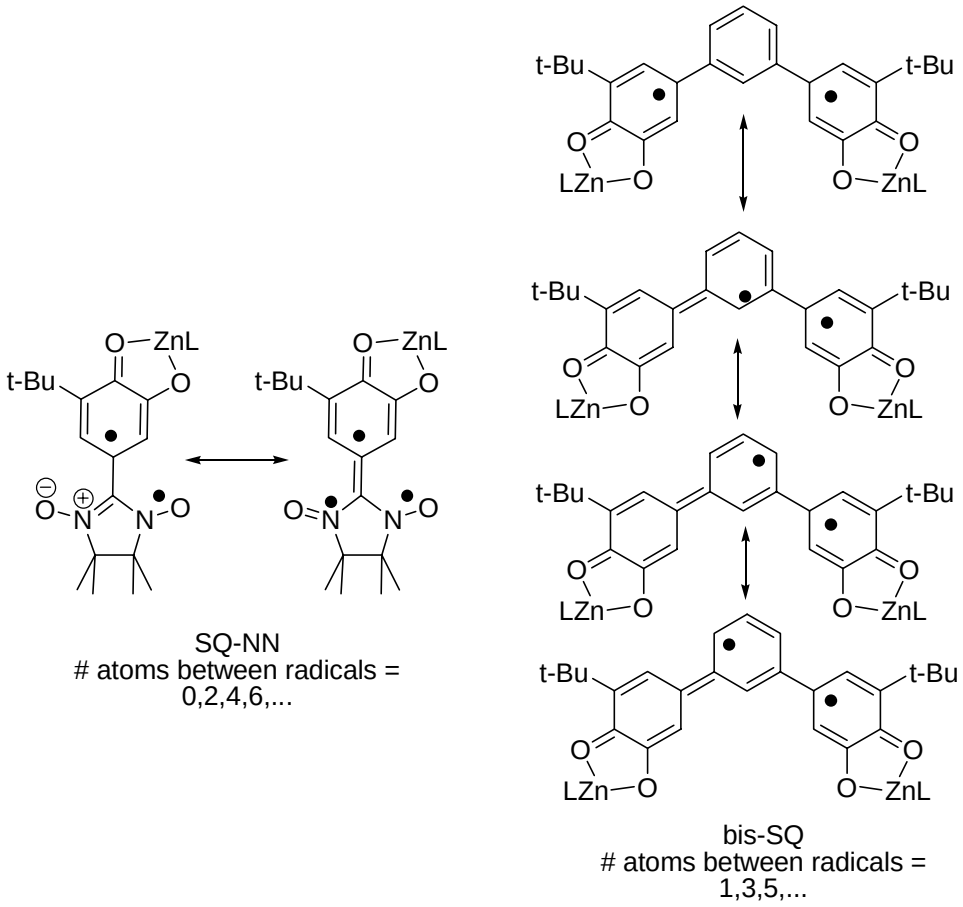

Figure V.25. Contributing resonance structures when a CT occurs from: (left) $SOMO_{SQ}$ to $LUMO_{NN}$ and (right) $SOMO_{SQ1}$ to $LUMO_{SQ2}$. When there are an even number of atoms between D-A then get stronger dipole than when there is odd number of atoms between D-A.

Above it is clear that when there are an even number of atoms between the D-A the unpaired electron can be delocalized into the A fragment. Thereby allowing a stronger transition, and possibly a stronger CT band. On the other hand, when there are an odd number of atoms between the D-A the unpaired electron cannot be delocalized onto the A fragment, it can only be delocalized onto the bridge. This would result in a weaker transition. We can observe the lack of an obvious CT band if we look at the electronic absorption spectra of the substituted MPH coupled bis(SQ), FigureV.26. Therfore, we reserve the VBCI for D-A heterospin biradicals.

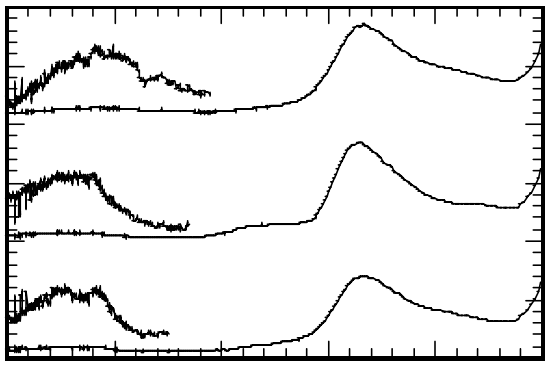

Figure V.26. Electronic absorption spectra of MPH bis-SQ with substituents on the 4 positon of the MPH from top to bottom: dimethyl amine, tert-butyl and nitro, structures are given in chapter 1.

V.2.A.6. Conclusions about VBCI and Exchange Coupling.

In summary, utilization of a VBCI model as applied to organic biradicals provides key design criteria for the synthesis of new high-spin organic and hybrid metal-organic molecular materials, which can be monitored conveniently by optical spectroscopies. Stabilization of the ^{3}GC is strongly dependent on the magnitude of the electron transfer matrix element, H_{12}, that describes the efficiency of electron transfer from the SQ donor to the NN acceptor.

Donor-acceptor biradicals, like the ligand SQNN, are ground-state analogs of excited state charge-separated species formed by PET. Since the exchange parameter for a biradical can be evaluated over ca. 6 orders of magnitude, H_{12}'s can be probed using a variety of bridges. In addition, the angular and distance dependence of H_{12} can be evaluated in a straightforward manner. The magnitude of the electronic coupling matrix element can be related to the ground and excited state electronic structure of the donor, bridge, and acceptor, allowing the determination of electronic structure contributions to electron transfer. Future efforts will include evaluating the effects of different bridge fragments on the electronic coupling matrix element, and exploring the angular

dependance of H_{12} in various SQ-bridge-NN donor-acceptor biradical complexes via strained bridges.

.

V.3. References

(1) Lahti, P. M., Ed. *Magnetic Properties of Organic Materials*; Marcel Dekker: New York, 1999.

(2) Hatfield, W. E. In *Theory and applications of molecular paramagnetism*; Boudreaux, E. A., Mulay, L. N., Eds.; Wiley Interscience: New York, 1976, pp 381-385.

(3) Kahn, O. *Molecular Magnetism*; VCH: New York, 1993.

(4) Wolfsberg, M.; Helmholtz, L. *J. Chem. Phys.* **1952**, *20*, 837-843.

(5) Hay, P. J.; Thibeault, J. C.; Hoffmann, R. *J. Am. Chem. Soc.* **1975**, *97*, 4884-4899.

(6) Whangbo, M.-H.; Koo, H.-J. *Inorg. Chem.* **2002**, *41*, 3570-3577.

(7) Rajca, A. *Chem. Rev.* **1994**, *94*, 871-893.

(8) Borden, W. T.; Davidson, E. R. *J. Am. Chem. Soc.* **1977**, *99*, 4587-4594.

(9) Shultz, D. A.; Vostrikova, K. E.; Bodnar, S. H.; Koo, H.-J.; Whangbo, M.-H.; Kirk, M. L.; Depperman, E. C.; Kampf, J. W. *J. Am. Chem. Soc.* **2003**, *125*, 1607-1617.

(10) Shultz, D. A. *Polyhedron* **2003**, *22*, 2423-2426.

(11) Shultz, D. A.; Farmer, G. T. *J. Org. Chem.* **1998**, *63*, 6254-6257.

(12) Weiss, E. A., Tauber, M. J., Ratner, M. A., and Wasielewski, M. R. *J. AM. CHEM. SOC.* **2005**, *127*.

(13) Weiss, E. A.; Ratner, M. A.; Wasielewski, M. R. *J. Phys. Chem. A* **2003**, *107*, 3639-3647.

(14) Weiss, E. A. T., M. J.; Kelley, R. F.; Ahrens, M. J.; Ratner, M. A.; Wasielewski, M. R. *J. Am. Chem. Soc.* **2005**, *127*, 11842.

(15) Lukas, A. S. B., P. J.; Wasielewski, M. R. *J. Phys. Chem. A* **2002**, *106*, 2074.

(16) Lukas, A. S. B., P. J.; Weiss, E. A.; Wasielewski, M. R. *J. Am. Chem. Soc.* **2003**, *125*, 3921-3930.

(17) Miller, S. L., A.; Marsh, E.; Bushard, P.; Wasielewski, M *J. Am. Chem. Soc.* **2000**, *122*, 7802-7810.

(18) Kirk, M. T., Shultz, D. A., Depperman, E.C. *Polyhedron* **2005**, *24*, 2880.

(19) Goodenough, J. B. *Physical Review* **1955**, *100*, 564-573.

(20) Astruc, D.; Ruiz, J.; Lacoste, M.; Gloaguen, B.; Ardoin, N.; Linares, J.; Varret, F. *J. Chem. Soc., Chem. Commun.* **1995**, 1565.

(21) Marcus, R. A. *Chem. Phys. Lett.* **1988**, *146*, 13-22.

(22) Astruc, D. *Electron Transfer and Radical Processes in Transition-Metal Chemistry*; Wiley-VCH: New York, 1995.

(23) LAMBERT, C., NÖLL, GILBERT, and SCHELTER, JÜRGEN *nature materials* **2002**, *1*, 69-73.

(24) Shultz, D. A.; Vostrikova, K. E.; Bodnar, S. H.; Koo, H. J.; Whangbo, M. H.; Kirk, M. L.; Depperman, E. C.; Kampf, J. W. *J. Am. Chem. Soc.* **2003**, *125*, 1607-1617.

(25) Giese, B. L.-d. c. t. i. D. T. h. m. *Acc. Chem. Res.* **2000**, *33*, 631-636.

(26) Kilsa, K. K., J.; Macpherson, A. N.; Martensson, J.; Albinsson, B. *J. Am. Chem. Soc.* **2001**, *123*, 3069.

(27) Lukas, A. S.; Bushard, P. J.; Weiss, E. A.; Wasielewski, M. R. *J. Am. Chem. Soc.* **2003**, *125*, 3921-3930.

(28) Kramers, H. A. *Physica* **1934**, *1*, 182-192.

(29) Anderson, P. W. *Phys. Rev.* **1959**, *115*, 2-13.

(30) Kanamori, J. *J. Phys. Chem. Solids* **1959**, *10*, 87.

(31) Marcus, R. A. *J. Chem. Phys.* **1965**, *43*, 679.

(32) McConnell, H. M. *J. Chem. Phys.* **1961**, *35*, 508-515.

(33) Creutz, C. *Prog. Inorg. Chem.* **1983**, *30*, 1-73.

(34) Xiao, C.; Feng, K.; Mo, Y.; Meng , Q.; Zhang , M.; Wan , M.; Zhao, J. *Chem. Phys.* **1998**, *237*, 73–79.

(35) Lynch, M. W.; Valentine, M.; Hendrickson, D. N. *J. Am. Chem. Soc.* **1982**, *104*, 6982.

(36) Brunold, T. C.; Gamelin, D. R.; Solomon, E. I. *J. Am. Chem. Soc.* **2000**, *122*, 8511-8523.

(37) Shultz, D. A.; Fico, R. M., Jr.; Bodnar, S. H.; Kumar, R. K.; Vostrikova, K. E.; Kampf, J. W.; Boyle, P. D. *J. Am. Chem. Soc.* **2003**, *125*, 11761-11771.

(38) Shultz, D. A., Fico,Rosario M., Lee,Hyoyoung, Kampf,Jeff W., Kirschbaum,Jeff W., Pinkerton, A. Alan, and Boyle, Paul D. *J. Am. Chem. Soc.* **2003**, *125*, 15426-15432.